# RECONSTRUCTING LONG TERM SEDIMENT FLUX FROM THE BROOKS RANGE, ALASKA USING SHELF EDGE CLINOFORMS.

by

Christina Marie Kaba

B.A., University of Pennsylvania, 2002

Submitted in partial fulfillment of the requirements of the degree of
Master of Science

at the
Massachusetts Institute of Technology
and the
Woods Hole Oceanographic Institution

June 2004





Signature of Author Christina Kaba
Joint Program in Oceanography / Applied Ocean Science and Engineering
Massachusetts Institute of Technology and
Woods Hole Oceanographic Institution
June 2004

Certified by David Mohrig
David Mohrig
Assistant Professor
Thesis Supervisor

Accepted by Jim Hirth
Greg Hirth
Chair, Joint Committee for Marine Geology and Geophysics
Massachusetts Institute of Technology /
Woods Hole Oceanographic Institution

## Table of Contents

**Reconstructing long-term sediment flux from the Brooks Range, Alaska using shelf edge clinoforms.**

By Christina M. Kaba

Submitted to the Department of Earth, Atmospheric, and Planetary Sciences on May 20th, 2004, in partial fulfillment of the requirements for the degree of Master of Science in Marine Geology.

## Abstract

Laterally extensive, well-developed clinoforms have been mapped in Early Cretaceous deposits located in the northeastern 27,000 $km^2$ of the Colville Basin, North Slope of Alaska. Using public domain 2-D seismic data, well logs, core photographs, and grain size data, depositional geometries within the Nanushuk and Torok formations were interpreted in order to constrain the transport conditions associated with progradation of the shoreline and construction of the continental margin out of detritus shed from the ancestral Brooks Range. Using STRATA, a synthetic stratigraphic modeling package, constructional clinoform geometries similar to those preserved in the North Slope clinoform volume (32,400 $km^3$) were simulated. Sediment flux, marine and nonmarine diffusivities, and basin subsidence were systematically varied until a match was found for the foreset and topset slopes, as well as progradation rates over a 6 million year period. The ability of STRATA to match the seismically interpreted geometries allows us to constrain measures of possible water and sediment discharges consistent with the observed development of the Early Cretaceous clinoform suite. Simulations indicate that, in order to reproduce observed geometries and trends using constant input parameters, the subsidence rate must be very small, only a fraction of the most likely rate calculated from the seismic data. Constant sediment transport parameters can successfully describe the evolution of the prograding margin only in the absence of tectonic subsidence. However, further work is needed to constrain the absolute magnitude of these values and determine a unique solution for the NPR-A clinoforms.

Thesis Supervisor: David Mohrig
Title: Assistant Professor, Dept. of Earth, Atmospheric, and Planetary Sciences.

## Introduction

Since 1944, and more recently with the discovery of the Prudhoe Bay oil field in 1967, the Coleville Basin, North Slope of Alaska has been an international, commercial center for petroleum and natural gas production. Due to intense exploration by the U.S. Navy, U.S. Geological Survey, and private enterprise, an extensive data set covering the regional outcrop and subsurface geology has been compiled. This archive is in the public domain, available through the USGS National Petroleum Reserve, Alaska (NPR-A) Legacy Data Archive (USGS, 2002), and includes over 12,000 line miles of 2-D seismic data, 64 widely spaced test and exploration wells, and countless geologic and reservoir characterizations. Reports available through the USGS and related publications focus on the Brookian sequence (late Aptian to Cenomanian in age) within the Coleville Basin due to its present and potential future commercial hydrocarbon accumulations and large-scale clinoform suites (Bird and Molenaar, 1992; Houseknecht and Schenk, 2002; Houseknecht, 2002a; Burns et al., 2004).

This project takes advantage of the Legacy Data Archive's seismic data to identify regional-scale geometric and volumetric trends in the clinoform structure within Early Cretaceous formations on the North Slope of Alaska (NPR-A). Regional mapping shows a west to east migration of the clinoform rollover point with a north-south translating shoreline. Using seismically interpreted depositional patterns of basin slope geometries, the characteristics and kinematics necessary to produce the average clinoform surface were quantified for the NPR-A seismic data interpreted over a 150 km by 180 km area and from 1000 - 1500 meters in thickness. This volume of approximately 32,400 $km^3$ represents some fraction of the detritus shed from the Brooks Range during the Early Cretaceous. From these clinoforms, the period of deposition, the foreset angle, the topset angles, the foreset height, the ratio of topset thickness to foreset height, and the translation of the topset to foreset break, were interpreted and used to ask the simple question whether these parameters can be described by constant feed rates, or must it be time-varying.

In STRATA, a diffusion-based stratigraphic modeling package, these reconstructed values for sediment transport conditions were used to constrain the erosional history of the Lower Cretaceous Brooks Range. As a final exercise, these simulations quantify the first-order implications of constant sediment transport conditions over long temporal and spatial scales on the building of basin-scale clinoforms. In order to complete these simulations, input model parameters were varied and iterative simulations run in STRATA until a final, geometric match of the seismically interpreted geometric parameters was produced. The final model output for Lines R13 and R14 best replicated the rotated foreset slopes, the rotated topset slopes, and the total distance traveled in the time of the study period. Once these solutions were found, the clinoform suite, with input parameters held constant over space and time, was prograded across the simulated length of our focus region (200 km) and the seismically- interpreted basal topography.

A basic question of this study is whether a package as large as the NPR-A clinoforms can prograde with constant transport parameters for six million years without little seismically resolvable changes in clinoform architecture. The answer to this question has important implications as to how we interpret the long-term production of sediment from uplifting mountain belts and the subsequent filling of basins with this detritus.

## Terminology

In order to understand the effects of transport conditions on slope architecture, it is important to first give meaning and application to the volumes of terminology within this field of stratigraphy.

Clinoform geometries

As sediment is deposited into standing water, such as an ocean basin or lake, a characteristic sigmoidal profile forms on the depositional front, known as a clinoform (Figure 1). This shape, usually associated with continental slopes and deltas, can be produced when diffusional slope transport processes vary in space. The final geometry

is influenced by the balance of sediment flux, base level, and basin subsidence (Mitchum, 1977; Van Wagoner, 1995; Milton and Bertram, 1995). Clinoforms developing at the end of terrestrial transport systems are present at all scales, ranging in height from well below 24 m (1937 Lake Mead Delta) to more than 1140 m (NPR-A) (Pirmez et al., 1998; Houseknecht and Schenk, 2002).

In seismic data, clinoforms are identified by their characteristic sigmoidal shape. In this study, the clinoform surfaces interpreted in the NPR-A seismic data are employed as indicators not only of the direction of sediment transport from the ancestral Brooks Range, but recorders of sediment flux and diffusivity, as well.

The clinoform surface is broken down into three named sections, the topset, foreset, and bottomset, each distinct in depositional process and deposit characteristics (Figure 1). The initial building of clinoform deposits occurs on the nearly horizontal topset beds. Within this portion of the clinoform, most sediment is moved as part of a fluvial transport regime (Bates and Jackson, 1987). The topset deposits of the NPR-A clinoforms represent a transition of depositional environments from fluvial to marine shelf (Vail, 1990). Houseknecht and Schenk (2002) identify topsets in the NPR-A seismic data as moderate to high amplitude reflections that display a basinward inflection point at their distal end.

This inflection point, commonly referred to as the rollover or the off lap break, represents the highest curvature along the clinoform surface (Vail et al. 1990; Milton and Bertram, 1995; Pirmez et al., 1998). The rollover marks the transition either from a shallow marine or nonmarine environment into greater water depths (Swenson et al., 2000). Regular transport of a coarse fraction into deeper water does occur by mass wasting and turbidity currents (Milton and Bertram, 1995; Pirmez et al, 1998).

The rollover is also the transition point from the nearly horizontal topset beds to the inclined foreset beds on the clinoform front. These beds, particularly the ones located on the upper foreset, are the primary locations of sediment accumulation in the clinoform system. Fine-grained sediment, that bypasses the topsets, is deposited along

the upper foreset due to the spatial decrease in near-bed shear stresses as the clinoform surface enters deeper water (Bates and Jackson, 1987; Pirmez et al., 1998). Along with preferential deposition, slope processes and turbidity currents drive the advancing clinoform suite forward.

Within the NPR-A, the upper foreset slopes are composed of laminated mudstones with thin, interbedded sands containing evidence of slumping, as seen in the cores: Drew Point 1 Cores #1 and #3, J.W. Dalton 1 Core # 2, and North Kalikpik 1 Core # 3 (Appendix 1) (Zihlman and Oliver, 1999; Zihlman et al., 2000). These sandstones, along with the more distal sandstones on the lower foreset slope, are the depositional markings of small-scale turbidity currents. This deposition creates an easily identifiable, regular interlamination of fine to medium-grained sandstones and mudstones, and supports the assumption of advective processes occurring along the NPR-A clinoforms (Houseknecht and Schenk, 2002).

Farther along the clinoform surface, a second inflection point, known as the bottomset transition point, separates the foreset beds from the nearly horizontal bottomset beds. Following the lead of Pirmez et al. (1998), the foreset-bottomset transition point was defined as the location along the clinoform surface where the change in surface slope reaches a local maximum. On the distal side of the bottomset transition point lie the bottomset strata, deposited at the tail of the clinoform as the foreset sediment moves forward, or progrades. Within this section along the clinoform surface, sedimentation rates are extremely low, equivalent to the background sedimentation of deep water zones, with intervals of large-scale clastic deposition by the distal tails of turbidites and slope failures (Swenson et al., 2000). These processes generate laminated mudstones with thin, repetitive planar laminated sandstone banding (Bates and Jackson, 1987).

Transport parameters

The mechanics of sediment transport, as they relate to basin filling and clinoform development, are based on the assumption that rate sediment is moved along a clinoform surface is a function of slope. From this assumption, this driving force can be united with conservation of mass into a simplified equation of diffusion, which states that

erosion and deposition on a surface are functions of the surface gradient and a transportation coefficient (K), herein called the diffusivity. In the equation below, h is the elevation of the point on the clinoform, *t* is any given time, and *x* is the horizontal position of the point (Jordan and Flemings, 1991; Paola et al., 1992).

$$\frac{\partial h}{\partial t} = K \frac{\partial^2 h}{\partial x^2}$$

The magnitude of K is related to the ability of the ambient water to carry sediment over a given length. The main controls on the value of K are the time-averaged water discharge and the transport channel conditions, whether the channel is meandering or braided in the fluvial case (Jordan and Flemings, 1991; Paola et al, 1992). Reasonable values of K in the nonmarine realm range from 15,000 $m^2 y^{-1}$ to 600,000 $m^2 y^{-1}$ (Jordan and Flemings, 1991), while reasonable values of K in marine systems range from 1,000 $m^2 y^{-1}$ to 10,000 $m^2 y^{-1}$ (Flemings and Grotzinger, 1996). While important to the final modeling effort of this paper, the details of the derivation of these parameters will not be discussed; for further discussion, the reader is referred to Paola et al. (1992) and Jordan and Flemings (1991), or the more general paper by Flemings and Grotzinger (1996).

However, to draw conclusions from these diffusion-based models, such as STRATA, the relationships between key input factors in basin development: sediment flux, basin subsidence, and eustasy, must be qualitatively understood. An important combination of these factors occurs when an increase in the subsidence rate and/or a rise in base level create an open area of water above the active depositional surface. This area, known as accommodation space, is where later sediment may be deposited. The volume of this space is controlled by the relative rates of base level change, subsidence, sediment flux and topset area (Van Wagoner, 1995; Milton and Bertram, 1995). The proportion of this space to the sediment flux will determine the style of clinoform suite that is deposited.

Clinoform Suite Architecture

The overall shape and character of clinoform suites fill a continuous spectrum between two end-member categories, aggradational and progradational sets (Figure 2). Their position along the spectrum depends on the relative magnitudes of eustasy, sediment flux, and subsidence.

An aggradational sequence, or aggradational clinoforms, is a series of vertically stacked clinoform surfaces in which the rollover point experiences minimal lateral shifting (Mitchum, 1977; Van Wagoner, 1995) (Figure 2). Clinoforms aggrade when the volume of the accommodation space made by base level rise or seafloor subsidence is equal to or larger than the sediment flux can fill at a given time. In this instance, the relative impact of the sediment flux is attenuated, the advance of the clinoform system stalls, and the strata vertically accumulate.

When the ratio of accommodation volume to sediment flux is reversed, the sediment flux is able to fill the space created in the accommodation volume. In this scenario, fine-grained sediment begins to bypass the fluvial topsets, due to an increase in the near-bed shear stresses of the shallow environment. This sediment is transported past the rollover point and onto the clinoform foresets; here, the system is said to prograde. In seismic and outcrop data, progradational clinoforms are seen as a series of sigmoidal surfaces in which the rollover point builds out basinward with little vertical accumulation (Gary et al., 1974; Van Wagoner, 1995; Milton and Bertram, 1995).

Figure 3 illustrates these two architectural styles of clinoform development within a single delta front unit, in which an initially progradational clinoform suite translates into a strongly aggradational suite. As the clinoform suite builds basinward, the area of the topset and foresets increase, which increases the overall accommodation volume. With the increased volume of available depositional space, the constant flux from the source area is unable to maintain forward motion of the clinoform rollover point. At the point where accommodation space is equal to sediment flux, the clinoform suite stalls and begins to fill to sea level, creating an aggradational suite. Like in Figure 3, dominant

within the NPR-A, is this transition between progradational suites of clinoforms and intervals of aggradational packages at smaller scales.

Within this study, we also refer briefly to an architectural style category termed, "mixed". Clinoforms that are members of the mixed category are not solely aggradational or progradation, but are transitional between the two end member categories. Although we identify the existence of clinoforms within this category, we will not treat them any further than to provide their geometric statistics.

## Background Information

The clinoform suites described in this paper were interpreted on USGS public domain 2-D seismic data of the North Slope Coleville Basin. The Coleville Basin is a late Mesozoic-Cenozoic foreland basin that extends 240,000 square kilometers across the North Slope of Alaska (Figure 4). The basin is well delineated by major physical features on all sides: to its north by a subsurface remnant rift shoulder, the Barrow Arch, to its south by the thrust belt of the present-day Brooks Range, to its east by the fill of the Mackenzie Delta, and to its west by the Herald Arch near the United States - Russian sea line (Bird and Molenaar, 1992).

Beginning in the early Mesozoic, the Arctic Alaska microplate, upon which the present Coleville Basin was created, was a southwest-facing passive margin attached to North America north of the Canadian Arctic Islands. During the Jurassic through earliest Cretaceous (135 Ma), rifting occurred along the plate's eastern boundary in the present location of the Barrow Arch, separating the land mass from the larger continent (Mayfield et al., 1988 ; Blythe et al, 1996). The small plate rotated counter clockwise, opening the Canada Basin (Figure 5). During this rotation of the western margin, the eastern and southern margins collided with an oceanic island arc, creating the new south-southeastern boundary of the plate, the ancestral Brooks Range (Bird and Molenaar, 1992; Houseknecht and Schenk, 2002).

The fill of the Coleville Basin is predominately marine shales and mudstones with intervals of shallow marine-fluvial sandstones deposited during the Middle Jurassic through later Tertiary (Bird and Molenaar, 1992; Houseknecht, 2003). The basin fill is divided into two main sequences: the Beaufortian Megasequence and the Brookian Megasequence, on which this study will focus (Figure 6). Some researchers divide the Beaufortian Megasequence into two sections, the earlier Beaufortian Sequence and the overlying Ellesmerian Sequence (Lerand, 1973; Hubbard et al., 1987; Bird and Molenaar, 1992; Houseknecht, 2003). For simplicity, this paper will consider the Beaufortian Sequence and Ellesmerian Sequence as a single entity.

The Beaufortian strata date from Middle Jurassic through the earliest Cretaceous and are the current focus of major oil exploration to the northeast of the NPR-A (Figure 6). The Beaufortian fill are south-dipping, northern-sourced clinoforms associated with the uplift of the Barrow Arch and the opening of the Arctic Ocean (Bird and Molenaar, 1992; Houseknecht, 2002). Core interpretation of the thickest Beaufortian unit, the Kingak Shale, by Houseknecht (2002a), identified continental margin stratigraphic features, such as wave-influenced bedforms and intense bioturbation, which thin and deepen to the south. Houseknecht (2002a) identified, within this stratigraphy, a transition in the depositional regime from an offshore shelf environment through several small-scale marine regressions.

Following these regressions in the Neocomian, subsidence of the Arctic margin forced a northward transgression of the Arctic sea, and deposited the aptly named, Pebble Shale unit, unconformably on top of the Kingak Shale. This unit is approximately 60 to 90 m thick, containing dark grey, silty, non-calcareous shale that supports few, rounded, quartz grains throughout the deposit (Bird and Molenaar, 1992; Zihlman and Oliver, 1999; Houseknecht and Schenk, 2002). The Pebble Shale is the capping unit of the Beaufortian Megasequence (Figure 6). After the depositional of the Pebble Shale, the region experienced a period of very low sedimentation, during which the overlying condensed Gamma Ray Zone (GRZ), this study's basal datum, was deposited (Bird and Molenaar, 1992; Zihlman and Oliver, 1999).

While maximum thrusting in the Brooks Range continued through the Early Cretaceous, relative sediment flux increased in the Aptian stimulating renewed deposition (Mayfield et al, 1988; Blythe et al, 1996). Derived from the Brooks Range to the south, and a postulated source area to the west of the Herald Arch (Houseknecht and Schenk, 2002; Bird and Molenaar, 1992), the Lower Cretaceous sediment of the Nanushuk and Torok formations (Figure 6) forms a thick, laterally extensive suite of delta-front clinoforms prograding to the north-northeast (Figures 7-9). These formations lay conformably atop the Pebble Shale and GRZ.

The Nanushuk Formation comprises the topsets of seismically resolvable clinoforms, and consists of non-marine pro-delta to marine shelf deposits, including coal and peat deposits that indicate local subaerial deposition (Magoon and Byrd, 1988). The underlying Torok Formation defines the clinoform foresets and bottomsets (Bird and Molenaar, 1992; Houseknecht and Schenk, 2002), and is the deeper water equivalent of the Nanushuk Formation (Figure 10). The Torok Formation is composed almost entirely of mud-rich marine slope and outer basin deposits. The transition from one unit to the other lies 150 to 300 meters above the rollover point separating the topset from the foreset (Molenaar, 1988; Houseknecht, 1999; Houseknecht and Schenk, 2002) (Figure 10). Deformation and uplift in the western NPR-A begins to wane concurrently with the deposition of the upper Nanushuk Formation (Mayfield et al, 1988; Blythe et al, 1996). The end of the Nanushuk Formation, and the Brookian Megasequence, occurs with the Cenomanian-age Seabee Formation, a condensed section deposited during a marine transgression (Bird and Molenaar, 1992; Houseknecht, 2002) (Figure 6).

During the deposition of the early Cretaceous deposits, the region experienced preferential uplift in the western portion of the NPR-A (Mayfield et al, 1988; Blythe et al, 1996). Evidence for this post-depositional uplift and tilting of the clinoform geometries is seen in the vitrinite reflectance ($R_o$) data collected at the base and top of the Torok Formation (Figures 7b and 8b). Vitrinite is a type of coal in which the ability of the surface to reflect light increases with increasing environmental temperature. Vitrinite, in essence, records the maximum temperature, and thus, the thermal maturity, reached by

a unit. It is often used as a proxy for the burial or subsidence history of the rock. $R_o$ is often related to the reservoir potential of hydrocarbon bearing rocks. In order to be considered "mature", or having experienced substantial thermal conditions, the value of $R_o$ must be greater than 0.6 percent (Bayliss and Magoon, 1988).

Within the NPR-A vitrinite reflectance data, several trends are evident. First, within the Torok Formation, the samples taken along the northeast coastline, at the South Barrow wells, have $R_o$ values between 0.4 and 0.52 and are considered immature. The thermal maturity of the unit increases to the south and west where it reaches a maximum $R_o$ value of 1.85 within the unit at the Tunalik 1 and Seabee 1 wells (Figure 7b). Within the Nanushuk Formation, $R_o$ values also decrease to the northeast following contours similar to those representing the depositional thickness of the clinoforms (Figure 8a and 8b) (Magoon and Bird, 1988). This trend indicates that the Torok and Nanushuk formations matured first in the south and west due to their proximal location to the source area and greater depositional thicknesses, and supports our assertion of a southwest to northeast progradation direction.

Second, within the westernmost portion of the NPR-A, the $R_o$ values in the Nanushuk Formation increase more rapidly to the west than do the depositional thickness contours (Magoon and Bird, 1988). This pattern suggests that preferential uplift occurred during or after the deposition of the Nanushuk Formation (Bird and Molenaar, 1992; Houseknecht and Schenk, 2002). This uplift caused post-depositional tilting of the clinoform geometries within the underlying succession (Mayfield et al, 1988; Bayliss and Magoon, 1988; Blythe et al, 1996).

## Research Methods

Using a seismic and geologic modeling package, Seismic Micro-Technology Kingdom Suites (TKS), and the data available on the USGS Data Legacy Archive (USGS, 2002), 140 2-D seismic lines across the NPRA were loaded for interpretation (Figure 11). This seismic data was reprocessed, migrated, and stacked by the USGS before being placed into the public domain. Other data loaded onto the computer included digital core

photos and well logs from 25 boreholes, which characterize the subsurface sedimentary deposits and constrain the time-depth relationship of the stratigraphy and the seismic data (Zihlman and Oliver, 1999; Zihlman et al., 2000; USGS, 2002).

In order to better identify important depositional events away from direct structural influence of the Brooks Range thrust belt and foredeep, a focus area (29,800 sq. km) was identified in the northeast corner of the NPR-A. This region includes 51 regional and local seismic survey lines and seven exploration wells. This region is delineated to the south by USGS regional seismic line R-15, to the west by USGS fill line 46-75, and to the north and east by slope-break canyons (Figure 11). Within this region, the focus of this interpretation is on the Lower Cretaceous units, the Nanushuk and the Torok formations, as they contain the most well-defined and laterally extensive clinoform suite on the North Slope (Bird and Molenaar, 1992; Molenaar, 1998; Houseknecht and Schenk, 2002; Houseknecht, 2003). In addition, due to varying degrees of quality within the seismic data, this paper will focus on the clinoform interpretations along Regional Lines 13 and 14 (Lines R-13 and R-14) (Figure 11).

In this study, the base of the Torok-Nanushuk clinoform succession was chosen as the highly reflective, and easily identifiable, Gamma Ray Zone (GRZ). The GRZ is a 30-45 m thick, condensed section of late Aptian-Albian (116 - 95 Ma) distal marine deposits resting conformably above the Pebble Shale of the Beaufortian Megasequence (Houseknecht, 2002a; Burns et al, 2004). This basal horizon is an important datum used in many of the following measurements (Figure 12).

Latest data from the USGS constrain the time evolution of the Gamma Ray Zone and the Upper Torok and Nanushuk deposits within the focus area to have been deposited beginning at 103 Ma and 94 Ma, respectively (Burns et al., 2004). These ages were used in the STRATA simulations to constrain maximum sediment flux off the Brooks Range in the Early Cretaceous.

Core descriptions

Listed on the Legacy Data Archive are 64 wells with drill records, well logs, and other core information within the NPR-A. Within the focus region of this study, 11 cores in seven of these wells (Drew Point 1, East Simpson 1, Ikpikpuk 1, Inigok 1, JW Dalton 1, North Kalikpik 1, and North Inigok 1) are located above the determined basal datum, the GRZ (Figure 11).

In order to correlate these cores and well logs with the seismic grid and published reports, TKS was used to create a synthetic seismogram for each well (Appendix 2). Through each well's synthetic seismogram, cores located along the clinoform surface were coupled with the relevant seismically defined geometry, so that lithology and depositional shape could be correlated. By examining this correlation, one can gain a better sense of the depositional patterns and mechanics that constructed the NPR-A clinoforms.

Core descriptions were compiled from drilling reports and published core descriptions, along with interpretation of composition and structural elements from high quality core photographs available on the NPR-A Data Legacy Archive (Zihlman and Oliver, 1999; Zihlman et al., 2000; Houseknecht and Schenk, 2002; USGS, 2002; Houseknecht, 2002b). Cores were described and classified by location along the depositional surface, dominant lithology, existence of sedimentary structures (laminations, burrowing, slumping, ripples), and the amount and organization of sand bodies (Appendix 1).

The dominant lithology across all cores is laminated mudstone with varying levels of bioturbation and percentage of interbedded sandstone layers. Throughout all 11 cores, two main trends in the Torok Formation can be deciphered. First, the number, thickness, and organization of sandstone laminations increases with depth and distance along the clinoform surface. This is particularly applicable as the depositional environment transitions off the shelf (topsets) onto the clinoform foresets. Within the sand laminations, two styles of deposit are evident in the interbedded cores. In samples taken from the topset and upper foresets, interlaminated sandstones are scarce and thin (Drew Point Core # 1, Ikpikpuk Core #2, Inigok Core # 1, J.W. Dalton Cores # 2 and

#3). Preserved within these sandstones are primary sedimentary structures including ripples and cross stratification. In the lower cores (Drew Point Cores # 2 and # 3, East Simpson Core # 4, North Inigok Core # 1, and North Kalikpik Cores # 2 and # 3) located along the clinoform foresets and bottomsets, laminations are more frequent and thicker with planar bedding. The lithology of these deposits is fine to medium-grained sandstone with rounded to sub-rounded grains.

From the grain size data, sedimentary structures, and their location at the distal end of steepened foreset slopes, these repetitive interbeds seen in the lower cores can be interpreted as turbidite deposits. In addition, these small-scale, repetitive turbidites are interpreted as, over the course of the Albian, the main factor in the construction of the large, seismically resolvable scale clinoforms of the Torok-Nanushuk succession (Hoyal et al., 2001; Houseknecht and Schenk, 2002).

In relation to later modeling efforts, the presence of these turbidite deposits allows the application of a sloped-based transport mechanism to be applied. This justifies the use of a diffusion model, such as STRATA, to simulate similar clinoform geometries to the NPR-A, despite the fact that our model does not explicitly model turbidite deposition.

An interesting discussion point from these core descriptions is the origin of the anomalous quartz grains supported within the matrix of the Pebble Shale. From interpretation of the core photographs, as well as drilling reports available at the USGS Legacy Data Archive (USGS 2002), the Pebble Shale can be classified as a distal toe-of-slope deposit, composed of laminated fine-grained mudstone. Within the mudstone, intervals of coarser-grained, more lithic deposits with no obvious stratification can be identified. It is within these intervals that the quartz grains are supported. These intervals are interpreted as discrete debris flow or slide deposits that came to rest within the condensed section along the low slopes of the clinoform bottomsets, bringing with them the rounded quartz grains.

Interpretation and definition of patterns in clinoforms

Clinoform interpretation within the NPR-A seismic grid was central to this project. In order to define the vertical region of interpretation on the 2D seismic lines, the top of the Torok- Nanushuk succession was identified as the onlapping Seabee Formation (Bird and Molenaar, 1992). Due to loss of seismic resolution in the upper portion of the 2D grid (above 0.2 seconds), this bounding horizon is unable to be interpreted. Within this study, the top of the seismic lines was used as the capping surface. Next, we defined the basal datum, the GRZ, on the seismic grid. The GRZ is the large, high-amplitude reflection located at depths ranging from 1,500 to 3,000 meters (Figure 12). This reflection was traced as a seismic horizon throughout the NPR-A to give insight to the basal topography onto which the Lower Cretaceous clinoforms were deposited.

The topography of the GRZ mimics that of the Coleville tectonic foredeep (Figure 13) upon which an east-dipping ramp of sediment was deposited by the progradation of the Lower Cretaceous clinoform succession. The focus region is located on a south-dipping limb of the basal topography (Figure 14). During the deposition of the clinoform package in the Aptian-Albian, this region experienced slight southeastward basal tilting, evident in the oversteepened slopes of the clinoform topsets (Bird and Molenaar, 1992; Houseknecht and Schenk, 2002; Burns et al., 2004).

Above the GRZ, clinoforms geometries were identified by their high-amplitude bounding reflections and sigmoidal shape (Figure 15), and interpreted on regional and fill lines throughout the focus region. Within this interpretation, three main styles of clinoform packaging were observed; two were classified as progradational architecture and one as aggradational architecture. These geometries include:

- Complete preservation of underlying clinoform, with large progradation of the overlying clinoform surface (Progradational).
- No preservation of underlying topset, with a large progradation of rollover, foreset and bottomset of the overlying clinoform surface (Progradational).
- Aggradation of topset of overlying clinoform surface with erosion along the rollover/foreset of the underlying clinoform (Aggradational).

Clinoform suites were defined as a group of two to three clinoform surfaces that represent an independent area laterally along Profiles R13 or R14. Each suite was termed either aggradational or progradational, depending on its relative location to the proximal clinoform suite to its west, according to the defined geometries above (Figure 15). Within each suite, the individual clinoform surfaces were also termed aggradational, progradational, or "mixed" depending on the length of the lateral and vertical shift of the rollover throughout the suite (Chart 1).

| | R13 | R14 |
|---|---|---|
| **Progradational Clinoforms** | 8 | 12 |
| **Aggradational Clinoforms** | 6 | 6 |
| **Mixed Clinoforms** | 7 | 4 |

**Chart 1:** Clinoform architectural classification along regional seismic lines R13 and R14 within the NPR-A focus area. Chart indicates the number of clinoform surfaces interpreted along R13 and R14.

These seismic interpretations were correlated with depth profiles, published interpretations, and core data through previously created synthetic seismograms. Clinoform geometries were then exported, depth converted, and normalized for comparison following the method of Pirmez et al. (1998).

Next, the topset and foreset slopes of the interpreted clinoforms surfaces were calculated. The topset slope was defined as the slope between the first interpreted point along the clinoform surface and the rollover transition point. The foreset slope was defined as the slope between the rollover transition point and the bottomset transition point. If the bottomset transition point was not interpreted on the clinoform surface, due to erosion or slumping on the lower foreset, the depth of the last interpreted point was used in its place.

In order to visualize and compare the depositional profiles along Lines R13 and R14, interpreted clinoforms geometries were normalized by their maximum height (H) as in

Pirmez et al. (1998). Determination of H from the point which the topsets and bottomsets become conformable (Pirmez et al., 1998) was not possible in this study due to the limited resolution of the seismic data and the preservation of a complicated stratigraphy associated with slumping and substantial erosion on the lower foreset and bottomset slopes. In this study, H was defined as the total elevation difference between the first interpreted topset point and the last interpreted bottomset point.

The normalized clinoforms are presented in two ways. First, the changes in the unrotated clinoform geometries west to east along the interpreted seismic lines R13 and R14 are shown in Figures 16 and 19, respectively. In order to create these graphs, the values of the x-axis remained as the x-locations of the clinoforms interpreted along Lines R13 and R14. These values were then rotated using denudation data available from the USGS (Figures 17 and 20) to reduce the affect of post depositional uplift of the rollover depth (Burns et al., 2004). In order to normalize the clinoform heights and allow for a simpler comparison among the different clinoform topset and foreset geometries, the y-axis values were divided by H. Next, the resulting y-value of the rollover transition point was defined and subtracted from each subsequent y-value along the clinoform surface. This shifted the rollover point of the clinoform to zero on the graphs (Figures 18 and 21).

Second, in order to compare the relative geometries within the progradational and aggradational architectural styles, the clinoforms were normalize in the y-axis, following the method stated above, as well as in the x-axis. The x-axis was normalized by H and the rollover shifted to the origin (Figures 22 and 23). This normalization stacked the resulting clinoform surfaces on top of each other and allowed for a better comparison of the geometries and slopes.

Another way of viewing the seismically interpreted clinoform surfaces along Lines R13 and R14 is as lines of constant time through the Aptian to Albian. In this manner, the progradation of a single delta slope break can be traced through the focus area and the regional patterns in deposition can be determined. The trajectory of the rollover point

was mapped as a seismic horizon along Lines R13 and R14 as it prograded west to east and along the fill lines as it translated south to north through the focus region (Figure 24). This process was repeated, interpreting the trajectory of the bottomset transition point through the seismic grid (Figure 26). The interpreted horizons were converted into gridded surfaces, which show the depth to the rollover (Figure 25) and the depth to the bottomset transition point (Figure 27) through the focus region. Differencing these maps gives insight on the spatial and temporal changes of clinoform thickness across the NPR-A (Figure 28).

Time-Depth conversion

Seismic data is projected onto a time-horizontal distance (X-Y) grid. The X-horizon is the time (seconds) that a sound reflector takes to penetrate the subsurface to that horizon and return (two-way travel time) (Figure 12). In order to generate meaningful surface topographies and clinoform geometries, the seismic interpretations were converted from time-space into depth-space.

To do this, a synthetic seismogram (synthetic) was created for each well. These synthetics are simulated responses of seismic waves from velocity data in the wells' downhole geophysical logs. For the NPR-A data, velocity profiles were created in TKS SynPak from published sonic logs of the seven wells in the focus area (Zihlman and Oliver, 1999; Zihlman et al., 2000). From this data, a synthetic was created with a depth profile for the time-space in each seismogram. This profile was then culled, reducing noise in the data, to every 0.01 seconds. The seven individual depth profiles were then related to the time-space of each well and combined into a shared time-depth chart interpolated throughout the study area (Lee et al., 1999). For a more detailed discussion on the creation of synthetic seismic profiles in TKS, see a copy of the TKS Help section in Appendix 2 (SMT, 2004).

Time-depth charts, such as that shown in Appendix 3, allow the conversion of interpreted geometries in the seismic sections into realistic depths. Clinoform geometries and rollover and bottomset progradation maps were interpreted in TKS and depth-converted using the synthetic shared time-depth chart. Due to sparse well control

within the focus section of the NPR-A, and a comparison of this data with previous studies (Houseknecht, 2002a; Houseknecht and Schenk, 2002), the depth conversion of the seismic data can be assumed to be within 12 percent of the true depth.

Decompaction

Decompaction is the process in which layers of sediment are backstripped, removing the overburden that causes compaction on underlying layers, allowing the calculation of original depositional thicknesses (Van Hinte, 1978). Within this study, decompaction on the rollover (Figures 25a and 25b) and bottomset transition (Figures 27a and 27b) maps were used to determine the original thickness of the Torok-Nanushuk clinoform suite (Figure 27).

For a general, first approximation of the depositional thicknesses of the NPR-A clinoforms, the simple porosity expansion model originated by Van Hinte (1978) and presented in Angevine et al. (1990) was applied to the rollover an bottomset transition maps. This model predicts that porosity ($\Phi$) decreases exponentially with depth (z) with respect to a lithographic constant (c). The key assumptions of this model are that the volume of rock within the formation is constant, and negative changes in porosity are due solely to compaction. Within the NPR-A these assumptions are valid, as core from the wells in the focus region indicates little evidence of major secondary chemical alteration, namely cementation of the sediment. Since the composition of the strata is predominately shale with interbedded sand stringers, the average lithology constant and original porosity, $\Phi_o = 0.45$ and $c = 4.0 \times 10^{-4}\ m^{-1}$ (Angevine et al, 1990) were assigned.

To complete the decompaction of the NPR-A Torok-Nanushuk clinoforms succession, the depth to rollover transition map was converted into a grid using TKS. The gridded surface was considered to represent a single stratigraphic unit with the values in each grid cell the present depth to the rollover from the surface ($T_o$), which is assumed to be at seal level. An initial decompaction was applied at each grid point (Figure 25a).

$$T_o = (1 - \phi_N) * \frac{T_N}{(1 - \phi_o)}$$

$$\phi_N = \phi_o^{(-cz)}$$

This process was repeated for the bottomset transition map (Figure 27a). These maps give a minimum estimate of the depositional thickness of the Torok-Nanushuk succession.

However, since the NPR-A clinoform suite within the focus area is a thick deposit (approximately 1000 to 3000 m) (Figure 28), this simple model of porosity expansion is limited in its ability to predict the depositional thicknesses suggested by Houseknecht and Schenk (2002) and Bird and Molenaar (1992). To assign thicknesses that are more realistic in relatively thick layers (> 100 m), an iterative decompaction process with the same assumptions as the above, simplified equation is suggested by Angevine et al. (1990).

$$\int_{d_o}^{d_o + T_o} (1 - \phi)\mathrm{dz} = \int_{d_N}^{d_N + T_N} (1 - \phi)\mathrm{dz}$$

Which, analytically becomes,

$$T_o = -\frac{\phi_o}{c}\exp(-c d_o)[\exp(-c T_o) - 1] + T_n +$$

$$\frac{\phi_N}{c}\exp(-c d_N)[\exp(-c T_N) - 1]$$

To complete this iterative porosity expansion within the NPR-A data, the above analytical model was applied to the original gridded surface of the rollover transition map. For this run, the value of $T_o$ in each grid cell was set to the interpreted, present depth of the rollover transition point below sea level. After the first run, a new $T_o$ was produced ($T_{oN}$) for each grid cell. This process was continued until the values of $T_{oN}$ converged to within 0.1% of $T_{oN-1}$. This process was then repeated to decompact the original bottomset transition map. The results of the iterative decompactions of the rollover and bottomset transition points are seen in Figures 25b and 27b, respectively.

Rigid Body Rotation

| | TOPSET SLOPE | FORESET SLOPE |
|---|---|---|
| **Line R13** | **0.015 (± 0.002)** | **0.065 (± 0.011)** |
| **Line R14** | **0.012 (± 0.003)** | **0.044 (± 0.020)** |

**Chart 2:** Slope values for originally interpreted clinoforms surfaces along R13 and R14. Values in parentheses are standard deviations.

Though consistent between lines R13 and R14, the values of the topset and foreset slopes for the seismically-interpreted clinoforms are high for this type of system (Chart 2). Jordan and Flemings (1991) calculate maximum topset slopes of 1° for their diffusion-based models of clinoform geometries, while Pirmez et al. (1998) found natural foreset slope ranging from less than 0.5° up to 6.3°. As is evident in Figures 16 and 19, the most proximal point of each clinoform, as well as the rollover point, decreases in depth as the system progrades west to east. This trend, combined with the vitrinite reflectance data introduced in the previous section (Magoon and Bird, 1988), are interpreted as the signatures of Early Cretaceous post-depositional tilting in the western NPR-A. This tilting overprinted a 0.002 % increase in slope on the proximal clinoforms in the west, which was then propagated through the system into the focus region of this study.

Using denudation amounts calculated by Burns et al. (2004), a linear decrease in the magnitude of the uplift (in m) can be calculated across the focus region using the equation y = - 0.00024x + 1091. In order to rotate the clinoform system to its pre-uplift orientation, the amount of denudation for each x-location along the clinoform surface was calculated using the above equation. Next, the sum of this value and the depth value of the point was taken, and applied as the new depth. This rigidly rotated the clinoform surfaces, so the most proximal point along the clinoform surface sees little to no increase in depth as the system progrades west to east (Figures 17 and 20). The new slope values are seen in Chart 3 and have decreased approximately 0.5 degree.

| | TOPSET SLOPE | FORESET SLOPE |
|---|---|---|
| **Line R13** | **0.012 (± 0.003)** | **0.067 (± 0.020)** |
| **Line R14** | **0.010 (± 0.002)** | **0.042 (± 0.011)** |

**Chart 3:** Rotated topset and foreset slope values along Lines R13 and R14. Values in parentheses are standard deviation of the data.

## Trends in patterns of clinoforms

In order to quantify what similarities and differences exist among the NPR-A clinoforms, the structure of the bottomset transition and rollover trajectory maps will be examined to determine the large-scale motion of the clinoform system. The bottomset transition map, shown in Figure 27b, indicates that the lower foreset of the clinoforms in this region begins at approximately 1250 m of depth along the western edge of the focus region. As the system prograded eastward, the bottomset transition point plunged into deeper water and was preserved at a maximum depth of 2650 m. This downward progression of the bottomset transition points with eastward progradation is best seen on Lines R13 and R14 on Figures 16 and 19.

The bottomset transition points are deposited upon an east-dipping wedge of sediment in the southern half of the focus region, seen on the bottomset transition map. This

wedge is also seen in the seismic line data as the base of the Torok Formation, and more specifically, as distal clinoform bottomsets and turbidites deposited at the far western edge of the focus region (Houseknecht and Schenk, 2002). This geometry is similar in magnitude and extent to that of the basal GRZ (Figure 14); however, the obvious linearity of the GRZ structure is tapered by the overlying toe-of-slope deposits. The depth to rollover trajectory map mimics the topography of the bottomset transition map with the magnitude of the GRZ linearity attenuated further by a second east dipping wedge of sediment. This wedge has widened and thickened in the western and central portions of the focus region through the deposition of the Torok Formation.

Differencing the bottomset transition and the rollover trajectory maps creates a map of clinoform foreset thickness through the focus region (Figure 28). This map indicates general consistency is maintained in the clinoform thicknesses throughout the focus region (ranging from 500-700 m in thickness). This map supports that, within the NPR-A clinoform system, the first order depositional scheme is one of persistent progradation with superimposed intervals of aggradation throughout the late Aptian to Albian. A large-scale departure from this depositional style is evident near Ikpikpuk well 1, as a long, narrow depositional high running perpendicular to the present day Brooks Range (Figure 29). This event, along with a smaller one to its east, is regional in extent with deposition orthogonal to the direction of transport. These large events help provide continuity of interpretation throughout the 2D seismic grid and allow us to view the progradational lobes of the clinoforms in nearly three dimensions. More importantly, these events provide another piece of evidence of the north to northeast transport direction of the Early Cretaceous sediment in the NPR-A.

Having determined the general progradational trend of the NPR-A clinoform suite, the geometries of the individual clinoforms deposited along Lines R13 and R14 can be explored. The most obvious difference between the interpreted clinoforms on Lines R13 and those interpreted on Line R14 is their length. The clinoforms interpreted on R13 are, on average, longer with the bottomset transition point and bottomset surfaces interpreted with an average interpreted length of 45.9 km (Figure 17). With an average

interpreted length of 35.0 km, the clinoforms on Line R14 (Figure 20) are usually truncated in the upper to mid foreset due to complicated stratigraphy associated with slumping and turbidity currents.

Also evident in both Figures 17 and 20 is the stepped progradation characteristic of the NPR-A clinoform suite. The clinoform surfaces on both seismic lines are bundled into suites of two to three surfaces that show variations in rollover depth and clinoform architecture among the suites. However, among the clinoform suites, little variation in the slopes or clinoform length is evident. Figures 18 and 21 show the clinoform geometries, normalized in height and shifted rollover depth, as they prograde west to east across Lines R13 and R14, respectively. In these figures, it is straightforward to compare the relative topset and foreset slopes (Chart 3). Again, little variation is evident between Lines R13 and R14 in the qualitative geometries of the clinoform surfaces.

Lastly, the clinoforms interpreted on Lines R13 and R14 were categorized into three architectural classes, progradational, aggradational, and mixed. A simple comparison of the spatially-averaged slopes of the topsets and foresets (Chart 4) through the NPR-A focus region shows similarities across all architectural categories. In order to better illustrate the extent of the similarities among members of each architectural class, the clinoforms were normalized and stacked following the procedure outlined in the above sections (Figures 22 and 23).

| | TOPSET SLOPE | FORESET SLOPE |
|---|---|---|
| **Progradational clinoforms** | 0.015 (± 0.010) | 0.055 (± 0.017) |
| **Aggradational clinoforms** | 0.011 (± 0.003) | 0.058 (± 0.024) |
| **Mixed clinoforms** | 0.013 (± 0.004) | 0.042 (± 0.018) |

**Chart 4:** Spatially averaged slope values within the NPR-A focus area for each architectural style. Values within the parentheses are the standard deviations within

Figures 22 and 23 illustrate similarities within and among the architectural styles throughout the NPR-A. First, the rollover shape within both clinoform styles is rounded. Adams (2001) suggests this geometry is caused by small-scale variations in base level due to storms and larger scale events controlled by tectonic eustasy. Second, the stacked graphs show the least variation in slope in the lower topset and upper foreset regions nearest the rollover transition point. This region along the clinoform surface is dominated by the characteristics of the fluid and sediment fields, without complications from mass wasting or sediment storage. It is not surprising that within the same depositional system, this region maintains similar slope values. The similarities in the clinoform geometries, both qualitative and those characterized by the spatially averaged slopes, are striking across both seismic lines and all architectural styles.

The most obvious trend in the clinoform geometries is the consistency of the clinoform rollover profiles as they prograde west to east across the NPR-A. From examining this consistency in the NPR-A clinoforms at all scales, no observable differences can be made in the rollover position, foreset or topset slopes along Line R13, Line R14, or between the architectural classes. From this result, the geometries of the NPR-A clinoforms seem independent of the original depositional kinematics, and most likely, a function of larger scale events associated with variability in the detritus shed off the Brooks Range and post-depositional tilting.

## STRATA Modeling

Basin geometries have been simulated at every scale from large geodynamic models to single basin synthetic models. Within this range of models, few replicate the natural sigmoidal shape of prograding clinoforms without using pre-defined equilibrium profiles. Pirmez et al. (1998) recognized three types of stratigraphic models and gave the following examples to satisfy each category: geometric models (Jervey, 1988; Reynolds et al. 1991), process based models (Tezlaff and Harbaugh, 1989), and diffusion models (Kenyon and Turcotte, 1985; Jordan and Flemings, 1991; Paola et al., 1992).

Geometric models define set depositional profiles at the onset of the simulation, which are then modified by the competing effects of subsidence and erosion. Though powerful at the basin scale, these models are unable to describe the physical processes that determine the small-scale stratal geometries that we are interested in modeling (Pirmez et al., 1998; Jordan and Flemings, 1991). In a second category of models, process-based models are powerful tools that also allow the user to understand the larger scale workings of a basin system. These models are derived from the equations of fluid flow, and thus can utilize a wide range of input parameters to simulate natural processes. However, the sheer amount of required input parameters can over-constrain the system. Simpler process based models, like geometric rule-based models, also pre-define equilibrium profiles of sediment distribution (Pirmez et al, 1998). Using seismic scale heterogeneities as the basis for these simulations, does not permit sufficient detail to successfully model clinoform geometries using this in-depth method.

One of the simplest and least constrained approaches to simulating clinoform geometries is a diffusion model (Jordan and Flemings, 1991; Paola et al., 1992; Flemings and Grotzinger, 1996). Based on the equations of slope-driven motion and conservation of mass, as mentioned in the terminology section of this paper, these models successfully produce a wide range of realistic depositional slope, including clinoforms (Figure 3). In addition, these models allow the user to maintain control of a few simple equations and assumptions within the model for easy output interpretation.

One particular diffusion-based model is STRATA, created at the Massachusetts Institute of Technology (MIT) by Peter Flemings and John Grotzinger (1996). The motivation behind STRATA was to forward-model stratigraphic geometries interpreted in seismic and outcrop work, and illustrate straightforward suggestions of the background sediment transport conditions. The simple outputs of STRATA allow the user to determine the relative importance of various transport conditions in determining the geometries of their subaqueous clinoforms with few rule-based assumptions.

STRATA has been used in many contexts to better visualize the interplay of subsidence, sediment flux, and eustasy. In Adams (2001), STRATA was used to

determine the factors in creating a rounded shelf break point (rollover). In this examination, STRATA was used to relate the seismically interpreted geometric and volumetric data from the NPR-A seismic data to simulated STRATA clinoform surfaces. The purpose of this investigation was to determine if the volumetrics and kinematics interpreted in the NPR-A seismic data are consistent with invariant flux conditions off the Brooks Range through the Early Cretaceous , or if they suggest a more complicated time history of basin development.

Methods

After the deposition of the Pebble Shale and overlying GRZ, the provenance of the sediment shifted from the northern Barrow Arch to the southern Brooks Range. This change in provenance was partnered with an adjustment in clinoform progradation direction toward the east-northeast (Houseknecht 2002a; Bird and Molenaar, 1992). Depositional thicknesses of the Torok and Nanushuk formations were mapped by Houseknecht and Schenk (2002) to illustrate the source locations of the clastic influx through the Albian (Figures 7a and 8a). Dipmeter data from Bird and Molenaar (1992) reinforces the idea that although the majority of sediment is derived from the southern Brooks Range and transported to the north, a secondary sediment source is located along the western margin of the Coleville Basin through the Lower Cretaceous (Figure 9). This data from subsurface seismic data and outcrop data, respectively, reinforces the idea that sediment is being transported from the southwest to the northwest with a substantial longitudinal component of sediment transport parallel to the Brooks Range through the late Aptian to Albian. Within the focus area, a significant portion of the sediment is transported along R13 and R14. Using this trend, the 2D transport conditions along R13 and R14 will be modeled assuming sediment flux is coming only from the west.

Within STRATA, the main parameters of sediment flux, subsidence, sea level, and diffusivities were used to model the North Slope clinoforms along Lines R13 and R14 (Flemings and Grotzinger, 1996). The initial input parameter values were based on previous work on clinoform development (Jordan and Flemings, 1991; Paola et al.,

1992; Pirmez et al., 1998), as well as from the seismically-defined clinoform geometries. A fuller discussion of each parameter follows.

In order to quantify the average impact of constant parameters on depositional geometries, the values were first fit for the above named parameters to match the geometries of the western clinoforms of Lines R13 and R14, according to three measures: foreset slope, topset thickness to clinoform height ratio, and distance traveled in the time of the study period. Input parameters were varied and iterative simulations run until a final geometric match was produced. Once a suitable simulation was created, the constant input parameters were prograded across the focus region.

Time and Length

The average depositional ages of the GRZ and upper Nanushuk Formation deposits across the NPR-A constrain the model simulation time to 6 million years (Burns et al., 2004). In order to examine the clinoforms in a fully developed state, the simulation period was extended to $T = 9 \times 10^6$ years. This allowed the clinoforms to establish their shape and fill the initial accommodation space in the far western edge of the run before entering the focus region.

The maximum progradation distance of the NPR-A clinoforms is 200 km along Line R14. Within this distance, the clinoform rollover translated 164 km along Line R14 and 145.3 km along Line R13. The maximum distance (200 km) was the length of the simulation in STRATA. In order to remove an initial blanking distance (10% of total length) at the proximal end of the model which STRATA automatically creates, and the residual boundary effects at the distal end from the simulated results, the length was padded on both sides by 200 km (X = 600 km).

Subsidence

Subsidence was modeled in STRATA with a cratonic basal topography and a spatially and temporally averaged subsidence rate. In order to create a single subsidence rate each for Lines R13 and R14, the depth of the basal topography was assumed to be at its present, interpreted depth at the end of the Nanushuk deposition in the Albian.

Second, the subsidence rate was assumed constant over the 6 million year depositional period (t). The height of the clinoforms, interpreted as the difference in elevation between the clinoform rollover point and the basal topography of the GRZ, was divided by t. The spatial average was then taken to obtain a maximum subsidence rate of 0.0001905 m/yr on Line R13 and 0.0002445 m/yr on Line R14.

Flux

Initial sediment flux rates were set by previously published values by Paola et al. (1992) and Jordan and Flemings (1991). For flux in a system with subsidence rates averaging 0.0001 m $yr^{-1}$, sediment flux was initially set to the order of 100 $m^2$ $yr^{-1}$.

Using the most current age estimations for the NPR-A clinoform package (Burns et al., 2004), the value of the sediment flux can be further constrained by calculating a time-averaged rate of progradation for the seismically-interpreted clinoforms on NPR-A Lines R13 and R14. The progradation along Line R14 covered 164 km over the course of 6 million years, while the clinoforms on Line R13 moved 145.3 km, giving transport rates of 0.0275 m/yr and 0.0242 m/yr respectively. Using these limitations, the sediment flux can be adjusted in each simulation to allow for replicated progradation rates.

The magnitude of the sediment flux parameter has a direct effect on the size and progradation distance of the clinoforms produced. The larger the sediment flux, the faster the clinoforms fill the available accommodation space and begin to prograde. This causes faster translation of the rollover position, larger topset areas, and longer horizontal distances between equal time lines (Figure 3). This rate of progradation was calculated in the NPR-A seismic data simply as the x distance along Lines R13 and R14 that the first interpretable clinoform rollover prograded over t. This resulted in a progradation rate for the clinoform package on R13 of 0.0242 m/yr (145.3km / 6 million years) and a rate of 0.0273 for the clinoform package on R14 (164km / 6 million years). This rate is quantified in the first of our model fitting parameters as the distance the first clinoform rollover point translates over the course of t (6 million years).

Diffusivities

The diffusivities input into STRATA are the transportation or efficiency coefficients for the nonmarine and marine scenarios of the coupled diffusion equation ($K_n$ and $K_m$). For the NPR-A clinoform system, the simulation was initiated with the minimum suggested values from Jordan and Flemings (1991) of 1000 $m^2\,yr^{-1}$ for $K_m$ and 10,000 $m^2\,yr^{-1}$ for $K_n$. These results were modified in subsequent runs to better simulate the average foreset slopes and topset thickness to clinoform height ratios seen in the NPR-A seismic data.

The effects of changing the nonmarine diffusivity have direct implications for the second of the main fitting parameters, the ratio of topset thickness to clinoform height. This ratio was measured in the seismic data as the thickness of the total topset package divided by the thickness of the average clinoform height of the clinoform suite. The thickness of the topset package on both the seismic data and STRATA simulations was measured perpendicular to the topset slope, 50 km updip of the rollover location. This distance removed any topography or thickening associated with the rollover transition point from the measurements. The clinoform height was measured as the difference in elevation between the rollover transition point and the bottomset transition point of each clinoform surface. If the bottomset transition point was not interpreted, the depth of the last interpreted point was used. By matching this ratio on the NPR-A seismically-interpreted clinoforms and the STRATA simulations, there is assurance that the simulations are modeling the entire depositional package, instead of just the foreset progradation.

The final fitting parameter of the model to the seismically-interpreted data is the foreset and topset slope measurements. Within the seismic data, the slopes were calculated for the clinoforms along R13 and R14 (Chart 4 and Chart 5) as the spatially-averaged values between most proximal clinoform point and the rollover transition point, and the rollover transition point and the bottomset transition point. In STRATA, for every simulation run, the slopes were calculated as the spatial average of the slope of each timeline between the most proximal clinoforms point and the rollover point as well as the rollover transition point and the bottomset transition point. These values were

compared and iterative simulations run until the seismically-interpreted slope values were matched.

Results

The output simulations in STRATA show the clinoform geometries bounded by lines of equal time (Figures 30 - 35). The simulation area of this study is defined as the area on the output screen containing all clinoform deposits between x = 200 km and x = 400 km.

Using the maximum subsidence rate defined by the seismically-interpreted clinoform geometries and with sea level set to zero, the amount of space required to build the clinoforms to their seismically-interpreted heights can be created. Simulations using this upper limit of subsidence rate for the NPR-A created clinoform profiles in which the position of the rollover continually climbed in space with distance along the simulation area, following an exponential curve with respect to t (Figures 30 and 31). This profile indicates that the maximum subsidence rate creates a large enough volume for the foreset and topsets to fill that, eventually, the sediment flux is overwhelmed. At this point, the clinoform architecture transitions from progradational to strongly aggradational. This change in rollover location is inconsistent with the trends interpreted in the seismic data, and limits the solution set of our simulation parameters to those with substantially lower subsidence rates.

One way to force the system to respond with no rollover climb is to turn off the tectonic subsidence altogether. In this scenario, sea level is adjusted so that water depth equals the average height of the seismically-defined clinoforms. This set of parameters produces the desired constant clinoform height and rollover position as the clinoforms prograde across the simulation area (Figures 32 and 33).

Imposing a subsidence rate of zero on the basin is unrealistic. Within the depositional period of the Torok-Nanushuk succession, the Brooks Range is interpreted as undergoing intense thrusting and uplift (Mayfield et al., 1988; Blythe et al., 1996). These

processes lead to uplift in the western portion of the NPR-A, along with enhanced subsidence due to sediment loading in the distal portions of the NPR-A. However, these simulations give valuable insight into the minimum flux values required to prograde the clinoform system the distances focused on in the seismic analysis. A sediment flux value of about 55 $m^2/y$ is necessary to prograde the clinoforms 165 km along Line R14 and 34 $m^2/y$ is required to prograde the clinoforms 143 km along Line R13.

| R14 STRATA Run | | Average | North Slope Values |
|---|---|---|---|
| Vertical scale in m (1 cm: ) | 357.143 | | |
| Horizontal Scale in m (1 cm: ) | 16949.153 | | |
| $K_{marine}$ ($m^2$ / year) | 750 | | |
| $K_{nonmarine}$ ($m^2$ / year) | 15000 | | |
| Sediment Flux ($m^2$ / year ) | 300 | | |
| Subsidence rate (m / year) | 0.0000611 | | |
| Sea level datum (m) | 978 | | |
| T (years) | 9000000 | | |
| X (km) | 600 | | |
| **Topset Slope** | | **0.011** | **0.010** |
| **Foreset Slope** | | **0.045** | **0.042** |
| **Progradation Distance over T (km)** | **161.0** | | **164.0** |
| **Minimum flux required to prograde ($m^2$ / year)** | **55.0** | | |

**Chart 5**: Model parameters and matching North Slope seismic values for R14.

Subsidence must be lowered during the interval of interest to a fraction (1/4) of the maximum value in order to reproduce the observed trajectory of the rollover point. Along with the lowered subsidence, the sea level is also set to a fraction (2/3) of the calculated clinoform height, creating enough initial space for the clinoforms to begin to develop. These reported values of reduced subsidence and sea level are not the only solutions for this system, but rather are good approximations of the magnitudes for the reductions necessary to produce a nearly constant rollover depth. This solution also reproduces the topset and foreset slopes measured for the rotated clinoform geometries (Figures 34 and 35). Chart 5 gives the model parameters and matching statistics for the simulation for Line R14 and Chart 6 lists the values for Line R13.

| R13 STRATA Run | | Average | North Slope Values |
|---|---|---|---|
| Vertical scale in m (1 cm: ) | 357.143 | | |
| Horizontal Scale in m (1 cm: ) | 16949.153 | | |
| $K_{marine}$ ($m^2$ / year) | 300 | | |
| $K_{nonmarine}$ ($m^2$ / year) | 15000 | | |
| Sediment Flux ($m^2$ / year ) | 500 | | |
| Subsidence rate (m / year) | 0.0000611 | | |
| Sea level datum (m) | 978 | | |
| T (years) | 9000000 | | |
| X (km) | 600 | | |
| **Topset Slope** | | **0.016** | **0.012** |
| **Foreset Slope** | | **0.065** | **0.060** |
| **Progradation Distance over T (km)** | **149.3** | | **145.3** |
| **Minimum flux required to prograde ($m^2$ / year)** | **34** | | |

**Chart 6:** Model parameters and matching North Slope seismic values for R13.

## Implications for sediment flux derived from the Early Cretaceous Brooks Range

The extensive seismic mapping of the NPR-A subsurface reveals many interesting details that are not directly relevant to the regional-scale development of the system but worthy of mention here. First, core from NPR-A wells can be combined with section sections to define the position of the shoreline relative to the clinoform rollover point. This core analysis and that of Houseknecht and Schenk (2002), reveals shoreline positions located updip from clinoform rollover points. A shallow marine environment is associated with the rollover position. Second, individual delta lobes can be mapped using the grid of 2-D seismic lines. This allows the interpreter to trace the changing delta front through time and space. As sea level drops along a coastline, focused incision along isolated channels occurs, increasing the degree of curvature and shifting the shoreline position. Changes in degree of shoreline curvature have been correlated with changes in base level (Heller et al., 2001; Plink-Bjorklund and Steel, 2002) and if compared to known sea level curves (Haq et al., 1988), one could gain a better sense for the signal of eustasy in sedimentary deposits of the NPR-A.

At the regional scale, the seismically interpreted clinoforms show no discernable change in geometry across the NPR-A focus region. Slopes of topsets and foresets and the vertical position or elevation of the rollover point remained approximately constant. Surprisingly, these properties where not systematically affected by local variation in the aggradational versus progradational character of clinoform sets. This constancy in form places a substantial constraint on the transport conditions building the Torok-Nanushuk clinoforms. STRATA runs point at two possible scenarios. In one case, the clinoforms build out into a pre-existing body of water about 1 km in depth. In this scenario, clinoform progradation is associated with no tectonic subsidence and the translation represents a post-orogenic phase of basin filling. In the second case, a very low subsidence rate must be coupled to a high input sediment flux. Both of these scenarios satisfy the field data by producing little vertical climb in the rollover point with time. These two runs demonstrate that the necessary magnitude of the sediment flux is very sensitive to change in the rate of subsidence within the basin. By increasing the subsidence rate from zero to a low value equivalent to ¼ of the maximum possible rate, the input sediment flux must be increased by a factor of 6 in order to preserve the observed clinoform geometry.

The low subsidence rates and high values for input sediment flux required by STRATA to recreate clinoform geometries run counter to the thermal uplift data presented in the regional geology section of this thesis. These simulations provide a future opportunity to look back to the exhumation history of the region and predict the volume and rate of detritus shed off the Brooks Range during the Early Cretaceous. Additional analysis of thermal records from the Brooks Range and the Coleville Basin (Mayfield et al., 1988; Magoon and Bird, 1988; Blythe et al., 1996; Burns et al., 2004) can be used to further constrain the magnitudes of subsidence and sediment flux. These values, in turn, can be used to refine simulations using STRATA and further constrain transport conditions associated with production of the NPR-A clinoforms.

## Resources:


Adams, E.W. 2001. Subaquatic slope curvature and its relation to sedimentary processes ad sediment composition. PhD thesis: Vrije Universiteit, Amsterdam. pp.135.

Angevine, C.L., Heller, P.L., and Paola, C. 1990. Quantitative Sedimentary Basin Modeling. AAPG Course Note Series # 32.

Bates and Jackson 1987. Glossary of Geology. American Geological Institute, Alexandria, VA.

Bayliss, G.S. and Magoon, L.B. 1988. Organic facies and thermal maturity of sedimentary rocks in the National Petroleum Reserve in Alaska *in* Gryc, G., ed. Geology and exploration of the National Petroleum Reserve in Alaska, 1974 to 1982, U. S. Geological Survey Professional Paper, p. 381-450.

Bird, K.J., and Molenaar, C.M. 1992. The North Slope foreland basin, Alaska *in* Macqueen, R.W. and Leckie, D.A., eds. Foreland basins and fold belts. Memoir 55: American Association of Petroleum Geologists, p. 363-393.

Blythe, A.E., Bird, J.M., Omar, G.I. 1996. Deformation history of the central Brooks Range, Alaska: Results from fission-track and (super 40) Ar/ (super 39) Ar analyses, Tectonics 15 (2).

Burns, W.M., Hayba, D.O., Rowan, E.L., and Houseknecht, D.W. 2004. Reducing uncertainty in burial and thermal history modeling of the Coleville Basin, Alaska, North Slope. American Association of Petroleum Geologists Abstract Book.

Flemings, P.B. and Grotzinger, J.P. 1996. STRATA: Freeware for analyzing classic stratigraphic problems. GSA Today, v.6 (12), p.1-7.

Gary, M., and McAfee Jr., R. 1974. Glossary of Geology. American Geological Institute, Washington D.C. 805 pp.

Haq, B.U., Hardenbol, J., and Vail, P.R. 1988. Mesozoic and Cenozoic chronostratigraphy and cycles of sea level change, *in* Wilgus, C.K., Hastings, B.S., Posamentier, H., Van Wagoner, J., Ross, C.A., and Kendall, C.G.S.C., eds. Sea-Level Changes: An Integrated Approach. SEPM Special Publication 42, p.71-108.

Heller, P.L., Paola, C., Hwang, I., John, B., Steel, R. 2001. Geomorphology and sequence stratigraphy due to slow and rapid base-level changes in an experimental subsiding basin (XES 96-1), AAPG Bulletin. 85 (5), p. 817-838.

Houseknecht, D.W. 2003. Beaufortian stratigraphic plays in the National Petroleum Reserve - Alaska (NPRA). USGS Open File Report 03-40.

Houseknecht, D.W. 2002a. Beaufortian (Jurassic – Lower Cretaceous) sequence stratigraphy and Sedimentology in the National Petroleum reserve – Alaska (NPR-A), *in* Houseknecht, D.W. 2002. Alaska North Slope Core Workshop notes. Pacific Section SEPM Workshop, Book 92.

Houseknecht, D.W. ed. 2002b. NPRA core images and well data, USGS digital data series 75.

Houseknecht, D.W., and Schenk, C. 2002. Depositional sequences and facies in the Torok formation, National Petroleum Reserve – Alaska, *in* Houseknecht, D.W. 2002. Alaska North Slope Core Workshop notes. Pacific Section SEPM Workshop, Book 92.

Hoyal, D., Mohrig, D., Pirmez, D., Foreman, L., and Patterson, P. 2001. Manuscript. Controls on turbidite deposition using forward numerical flow models: a sedimentary-event-scale approach to reservoir characterization and prediction.

Hubbard, R.J., Edrich, S.P., and Rattey, R.P. 1987. Geologic evolution and hydrocarbon habitat of the "Arctic Alaska microplate", *in* Tailleur, I., and Weimer, P., eds. Alaskan North Slope geology. SEPM, Pacific Section, Book 50, v.2. p.797-830.

Jordan, T.E., and Flemings, P.B. 1991. Large-scale stratigraphic architecture, eustatic variation, and unsteady tectonism: A theoretical evaluation, Journal of Geophysical Research, B, Solid Earth and Planets, 96 (4), p.6681- 6699.

Kenyon, P.M., and Turcotte, D.L. 1985. Morphology of a delta prograding by bulk sediment transport. GSA Bulletin, 96 (11), p. 1457-1465.

Lee, M.W., Agena, W.F., Grow, J.A., and Miller, J.J. 1999. Seismic Processing and velocity assessments, *in* The oil and gas resource potential of the 1002 Area, Arctic National Wildlife Refuge, Alaska. U.S. Geological Survey Open File Report 98-34.

Lerand, M. 1973. Beaufort Sea, *in* McCrossan, ed. The future petroleum provinces of Canada – their geology and potential: Canadian Society of Petroleum Geologists Memoir 1. p. 315-386 .

Magoon, L.B. and Bird, K.J. 1988. Evaluation of petroleum source rocks in the National Petroleum Reserve in Alaska, using organic-carbon content, hydrocarbon content, visual kerogen, and vitrinite reflectance *in* Gryc, G., ed. Geology and exploration of the National Petroleum Reserve in Alaska, 1974 to 1982, U. S. Geological Survey Professional Paper, p. 381-450.

Mayfield et al., 1988 *in* Gryc, G., ed. Geology and exploration of the National Petroleum Reserve in Alaska, 1974 to 1982, U. S. Geological Survey Professional Paper, p. 381-450.

Milton, N.J., and Bertram, G.T. 1995. Topset play types and their controls stratigraphy *in* Sequence stratigraphy of foreland basin deposits: Outcrop and subsurface examples from the Cretaceous of North America. Memoir 64: The American Association of Petroleum Geologists, Tulsa. p. 1-9.

Mitchum, R.M., Vail, P.R., and Thompson, S. 1977. Seismic stratigraphy and global changes in sea level, Part 2: The depositional sequence as a basic unit for stratigraphic analysis, in Payton, C.E., ed., Seismic stratigraphy applications to hydrocarbon exploration: AAPG Memoir 26, p. 53-62.

Molenaar, C.M. 1988. Depositional history and seismic stratigraphy of lower Cretaceous rocks in the National Petroleum Reserve in Alaska and adjacent areas, *in* Gryc, G., ed. Geology and exploration of the National Petroleum Reserve in Alaska, 1974 to 1982. U.S. Geological Survey Professional Paper 1399. p. 593-621.

Paola, C., Heller, P.L., and Angevine, C.L. 1992. The large-scale dynamics of grain-size variation in alluvial basins, 1: Theory. Basin Research, 4 (2), p. 73-90.

Pirmez, C., Pratson, L.F., and Steckler, M.S. 1998. Clinoform development by advection-diffusion of suspended sediment; modeling and comparison to natural systems, Journal of Geophysical Research, B, Solid Earth and Planets, 103 (10), p. 24,141-24,157

Plink-Bjorklund, P., Steel, R. 2002. Sea level fall below the shelf edge, without basin-floor fans, Geology. 30 (2), p. 115-118.

Seismic Micro Technologies. 2004. The Kingdom Suites 7.2 software and help files.

Swenson, J.B., Voller, V.R., Paola, C., Parker, G., and Marr, J.G. 2000. Fluvio-deltaic sedimentation: A generalized Stefan problem. European Journal of Applied Mathematics, 11, p. 433-452.

Tezlaff, D.M. and Harbaugh, J.W. 1989. Simulating clastic sedimentation. Van Nostrand Reinhold, New York, pp. 202.

U.S.G.S. 2002. Central Region Energy Resource Team. National Petroleum Reserve, Alaska. Legacy Data Archive. Available: http://nerslweb.cr.usgs.gov.

Vail, P.R., Audemard, F., Bowman, S.A., Eisner, P.N., and Perez-Cruz, C. 1991 Stratigraphic Signatures of Tectonics, Eustasy, and Sedimentology – an Overview *in* Einsele, G., Ricken, W. & Seilacher, A., eds. Cycles and Events in Stratigraphy. Springer-Verlag, Berlin.

Van Hinte, J.E. 1978. Geohistory analysis – Application of micropaleontology in exploration geology: American Association of Petroleum Geologists Bulletin (62), p.201-222 *in* Angevine, C.L., Heller, P.L., and Paola, C. 1990. Quantitative Sedimentary Basin Modeling. AAPG Course Note Series # 32.

Van Wagoner, J.C. 1995. Overview of sequence stratigraphy of foreland basin deposits: Terminology, summary of papers, and glossary of sequence stratigraphy *in* Sequence stratigraphy of foreland basin deposits: Outcrop and subsurface examples from the Cretaceous of North America. Memoir 64: The American Association of Petroleum Geologists, Tulsa. p. ix-xxi.

Zihlman, FN, and Oliver, HL. 1999. Selected data from eleven wildcat wells in the NPR-A, USGS Open File Report 99-015.

Zihlman, FN, Oliver, HL, Nelson, PH, and Kibler JE. 2000. Selected data from fourteen wildcat wells in the NPR-A, USGS Open File Report 00-200.

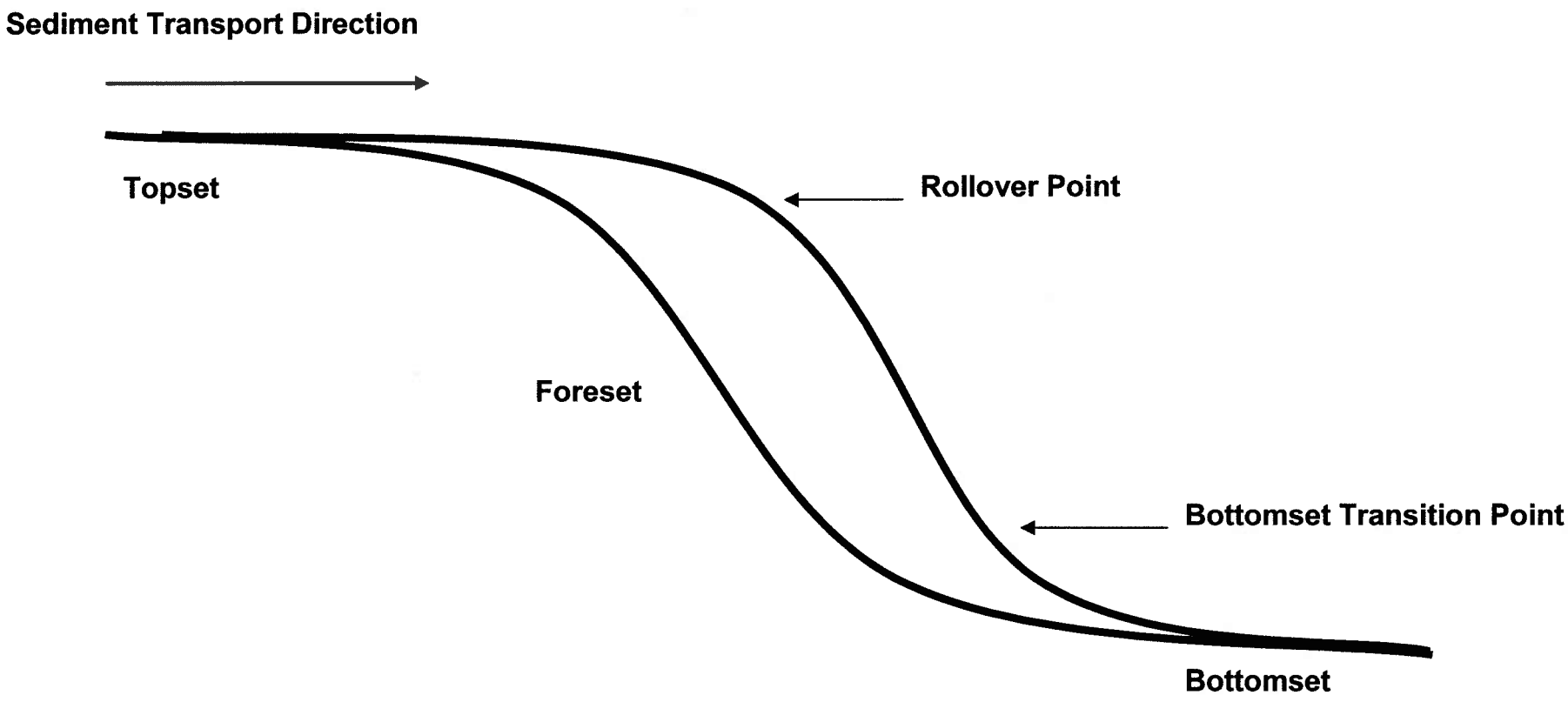


**Figure 1:** Clinoform geometry and terminology.

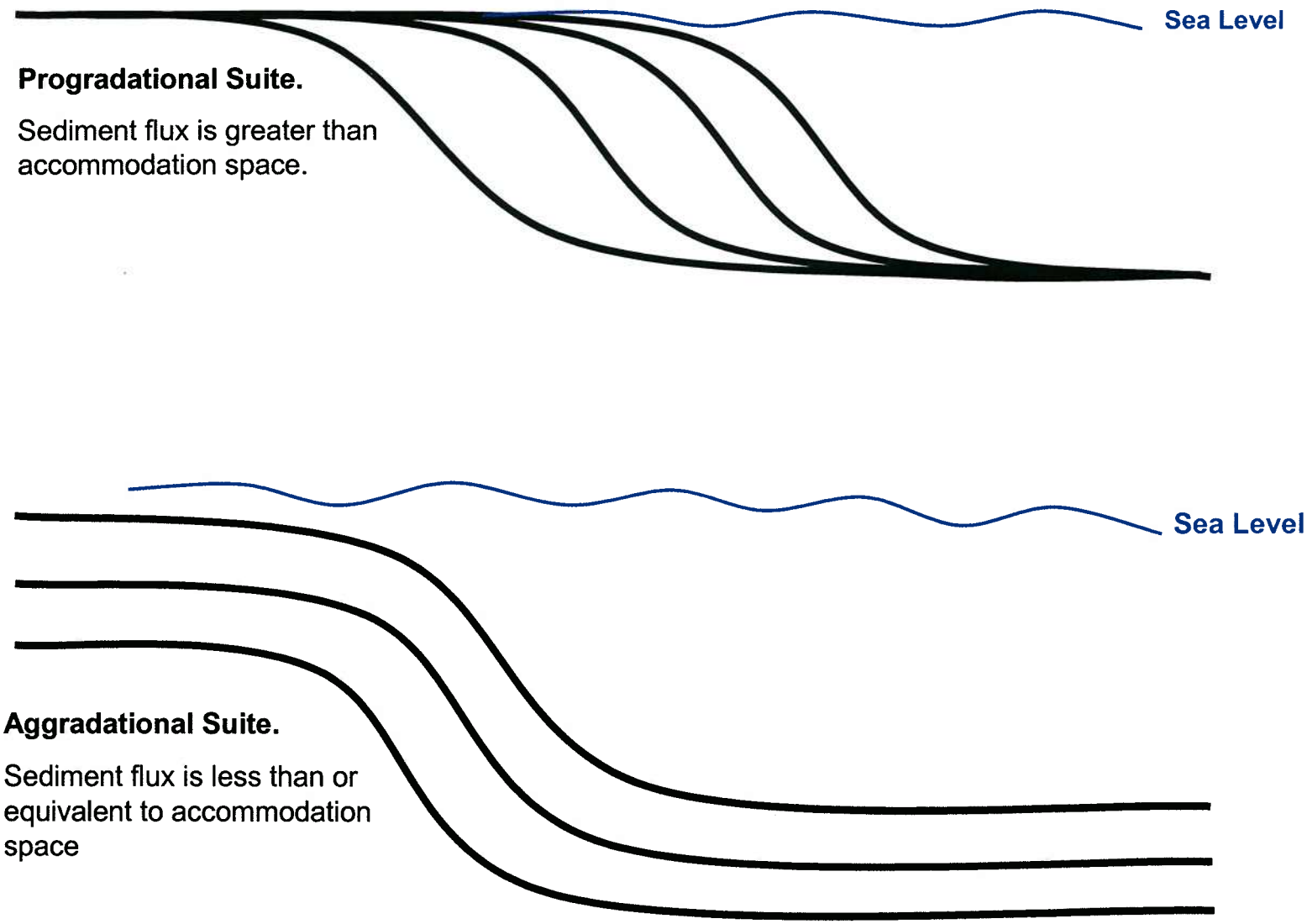


**Figure 2:** Clinoform architectural styles.

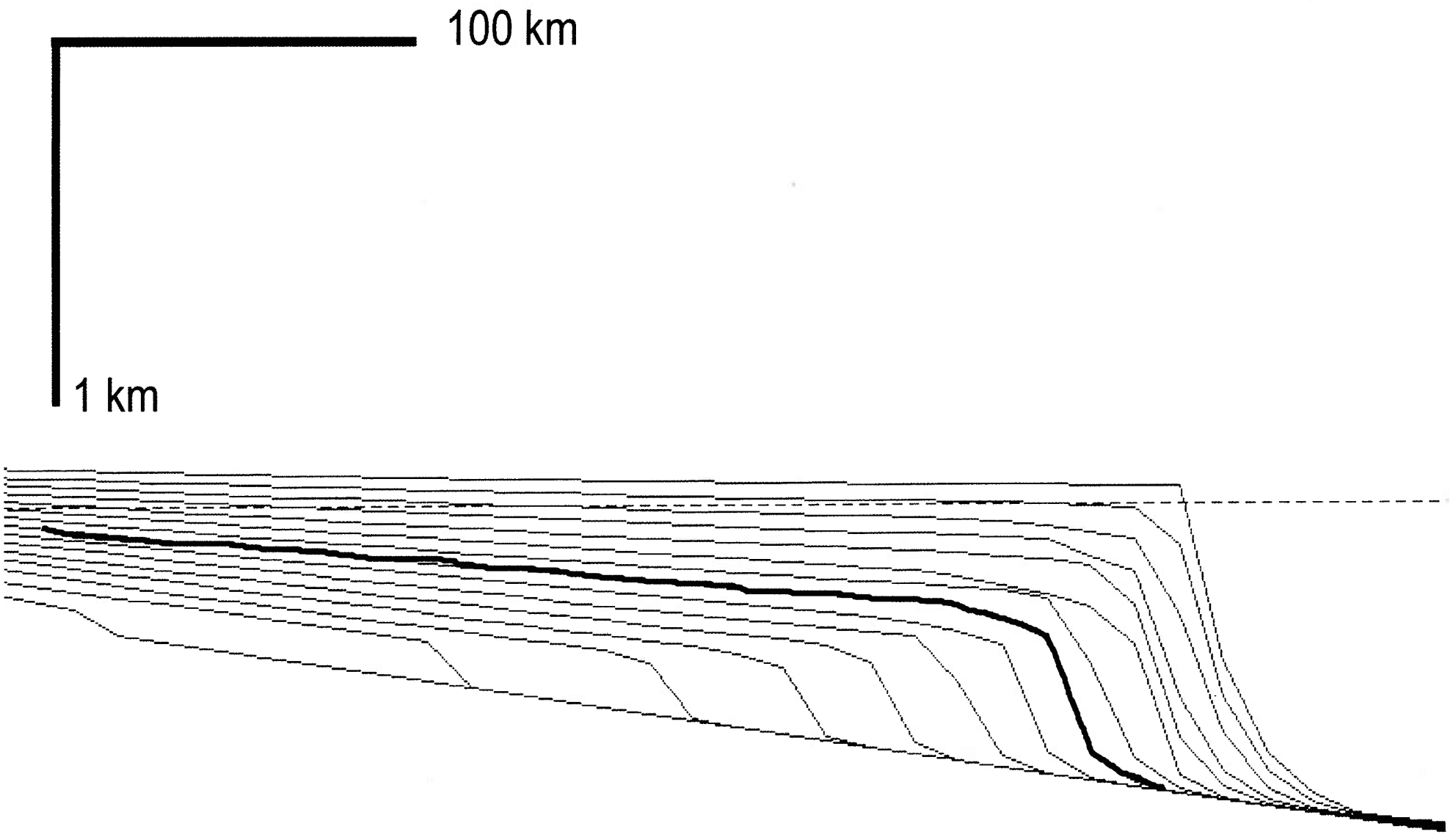


**Figure 3:** Simulated clinoform suite in STRATA. Clinoform architecture change from strongly progradation to strongly aggradational at bold line. This line marks the transition where sediment flux = accommodation space.

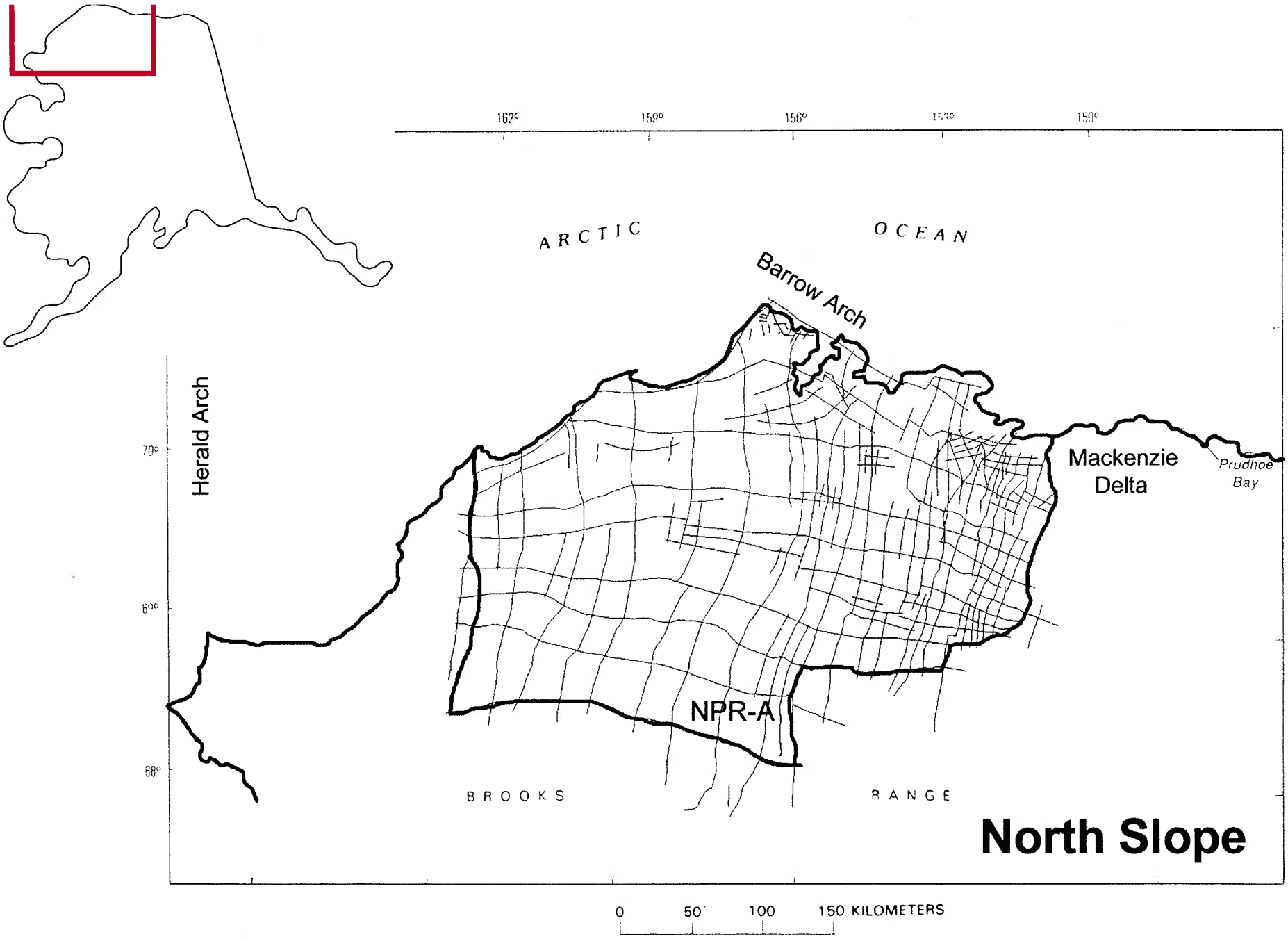


**Figure 4:** Map of the North Slope of Alaska, including seismic 2D grid in NPR-A. Modified from Bird and Molenaar (1992)

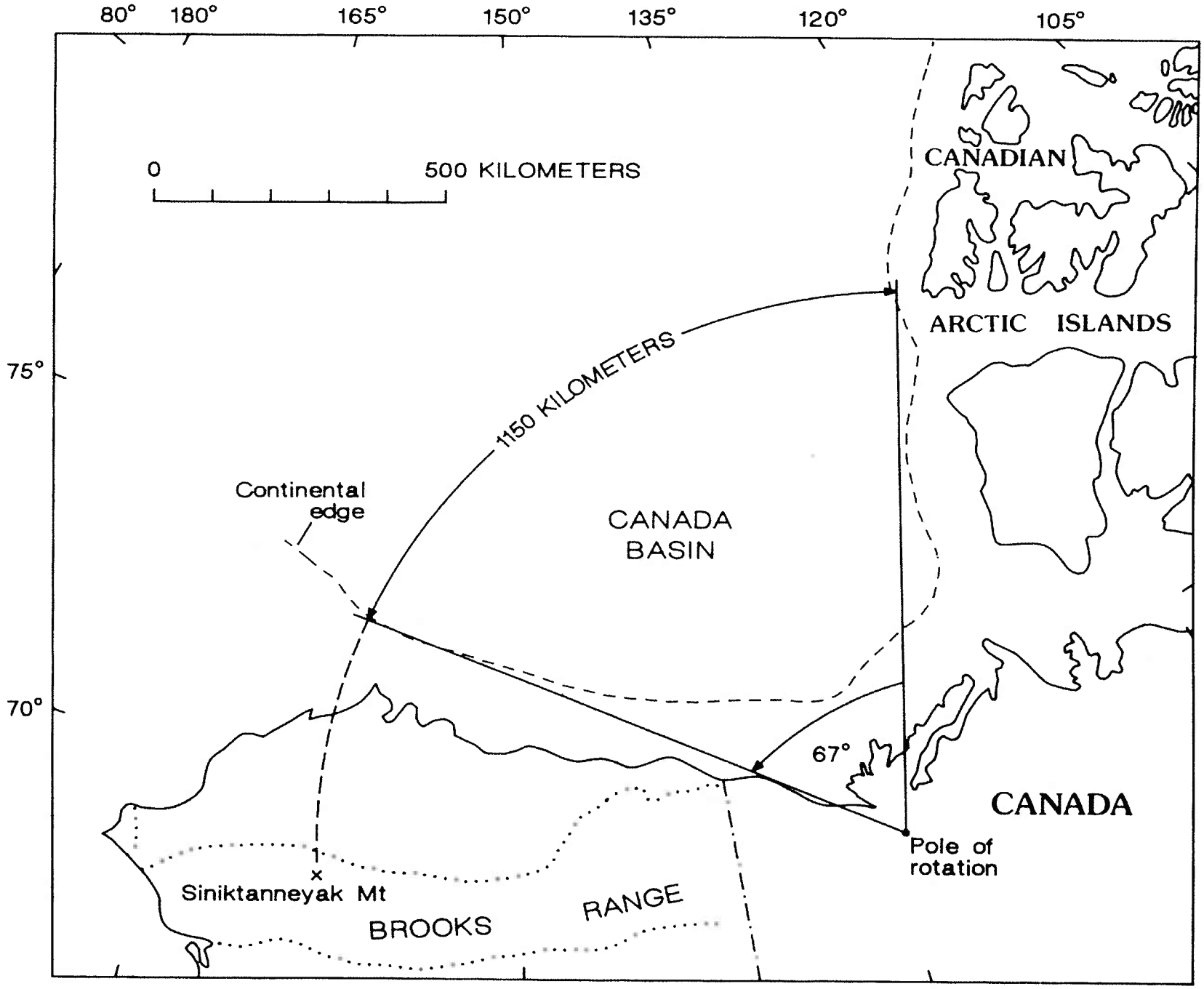


**Figure 5:** Representation of the tectonic events that created the North Slope. Modified from Gryc (1988)

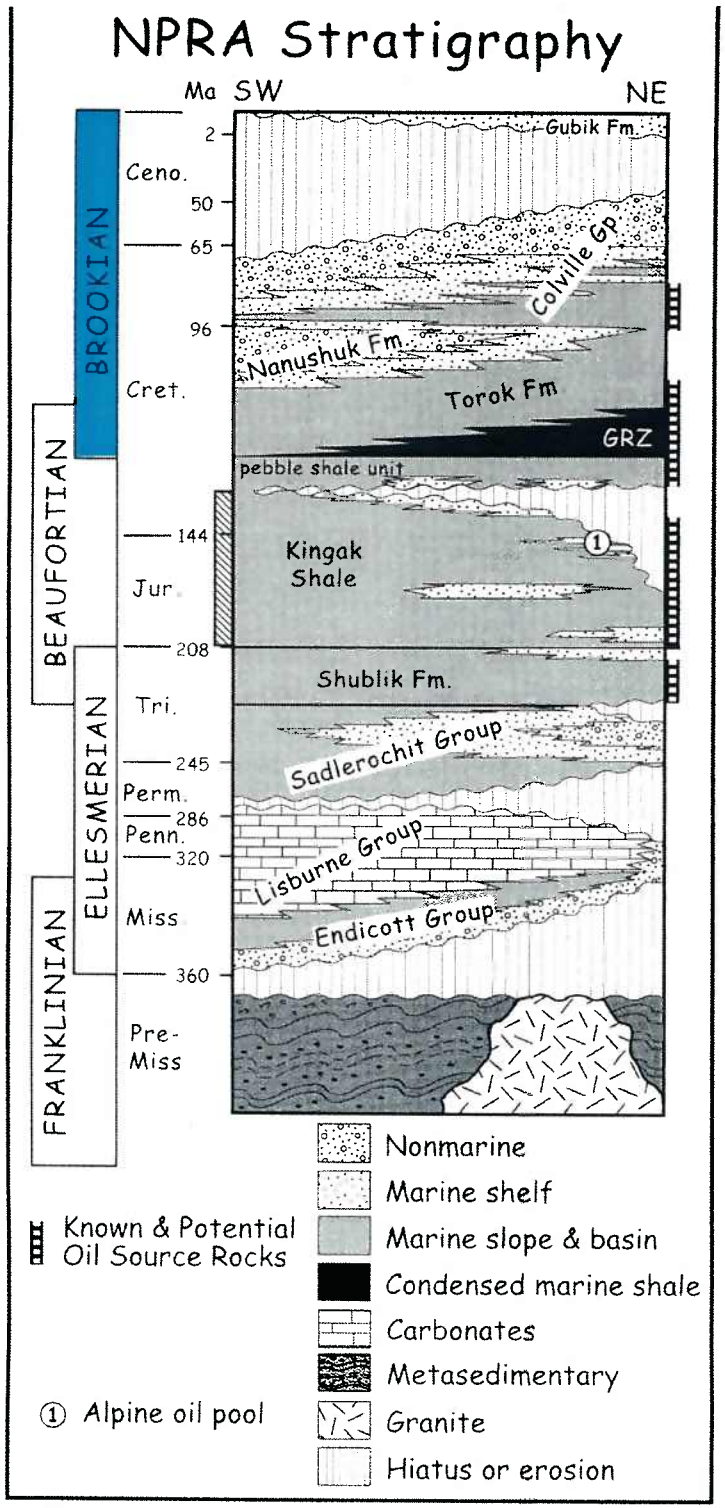


**Figure 6:** Stratigraphic column for the NPR-A. Adapted from Houseknecht and Schenk (2002).

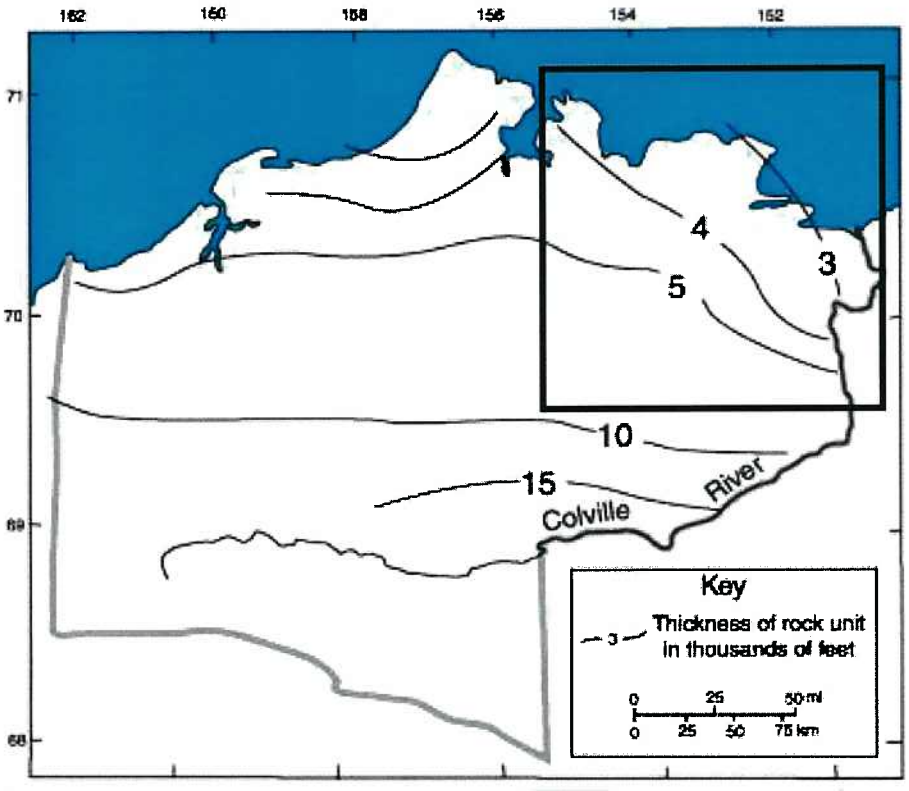


**Figure 7a:** Thickness contours of Torok (left) and Nanushuk Formations (right) through the NPR-A. Figure taken from USC (2002) after Montgomery (1998) and Bird (1988).

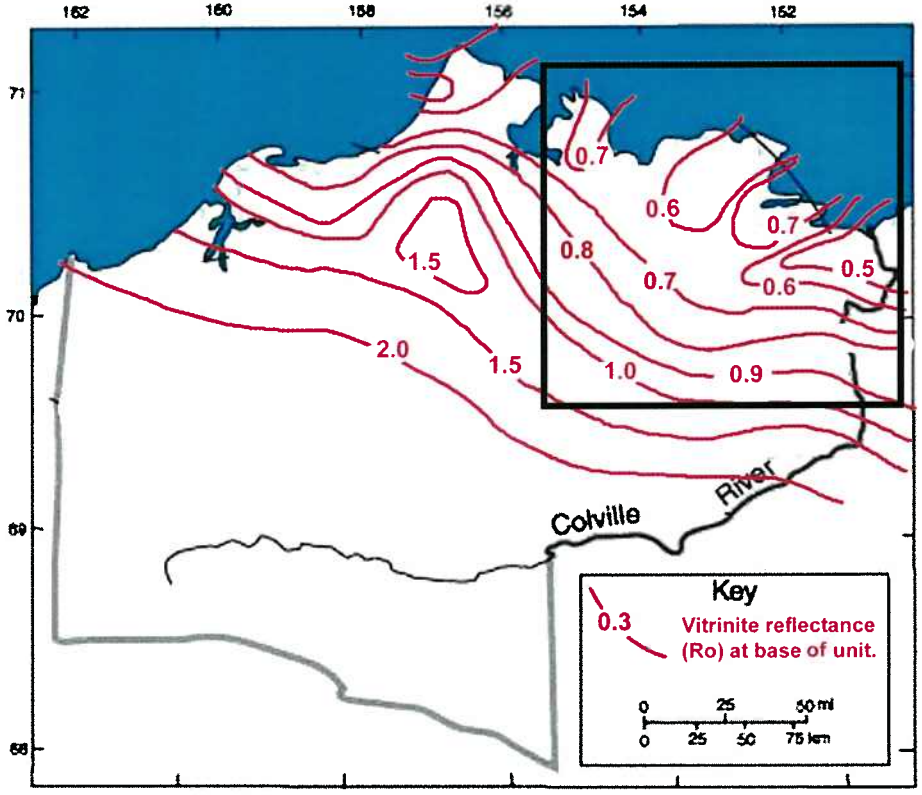


**Figure 7b:** Vitrinite reflectance contours along the base of the Torok. Modified after USC (2002) and Magoon and Bird (1998).

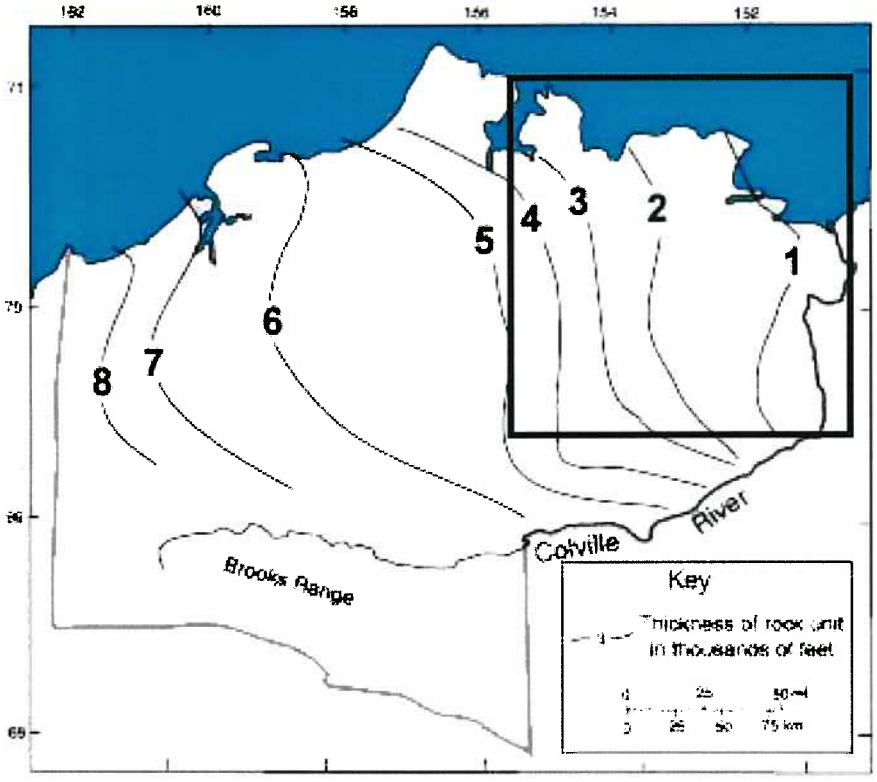


**Figure 8a:** Thickness contours of Nanushuk Formations through the NPR-A. Focus area is highlighted in black. Figure modified from USC (2002) after Montgomery (1998) and Bird (1988).

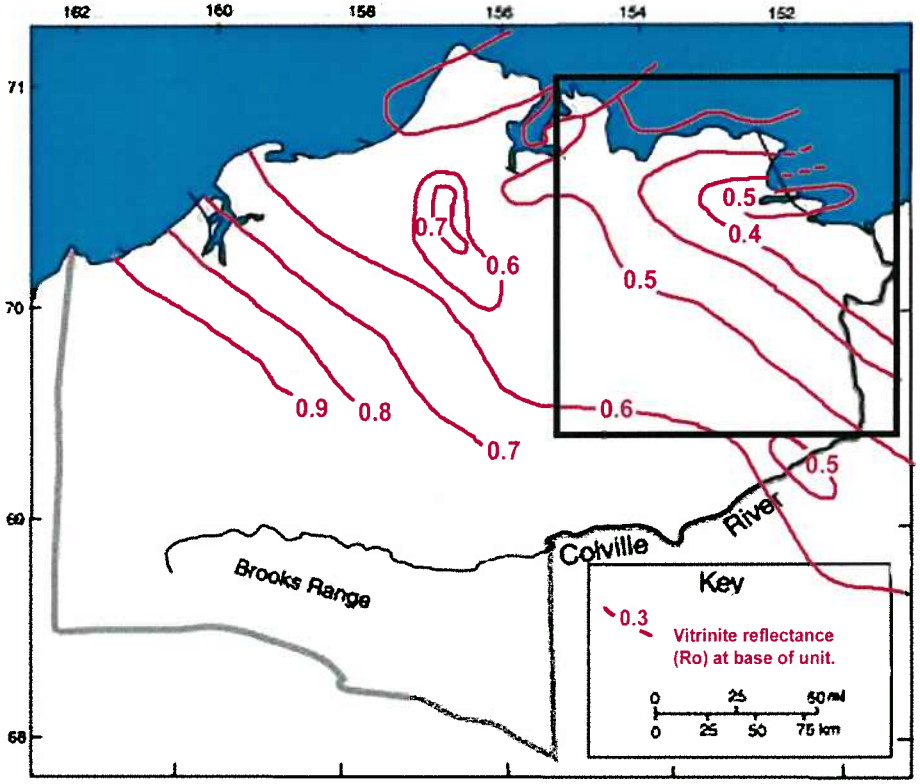


**Figure 8b:** Vitrinite reflectance contours along the base of the Nanushuk. Modified from Magoon and Bird (1998) and USC (2002).

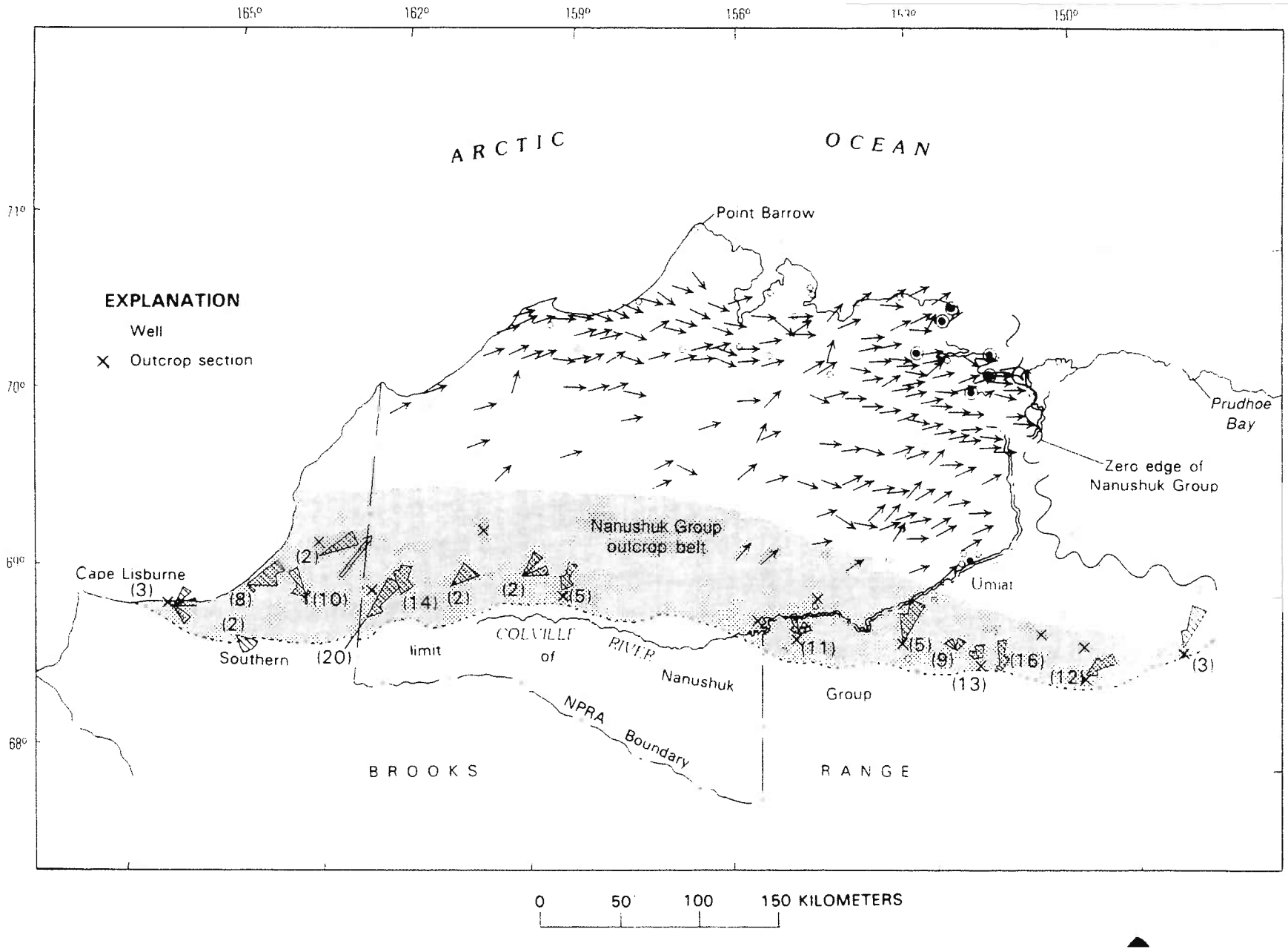


**Figure 9:** Clinoform dip directions of Torok Formation clinoforms. Modified from Bird and Molenaar (1992).

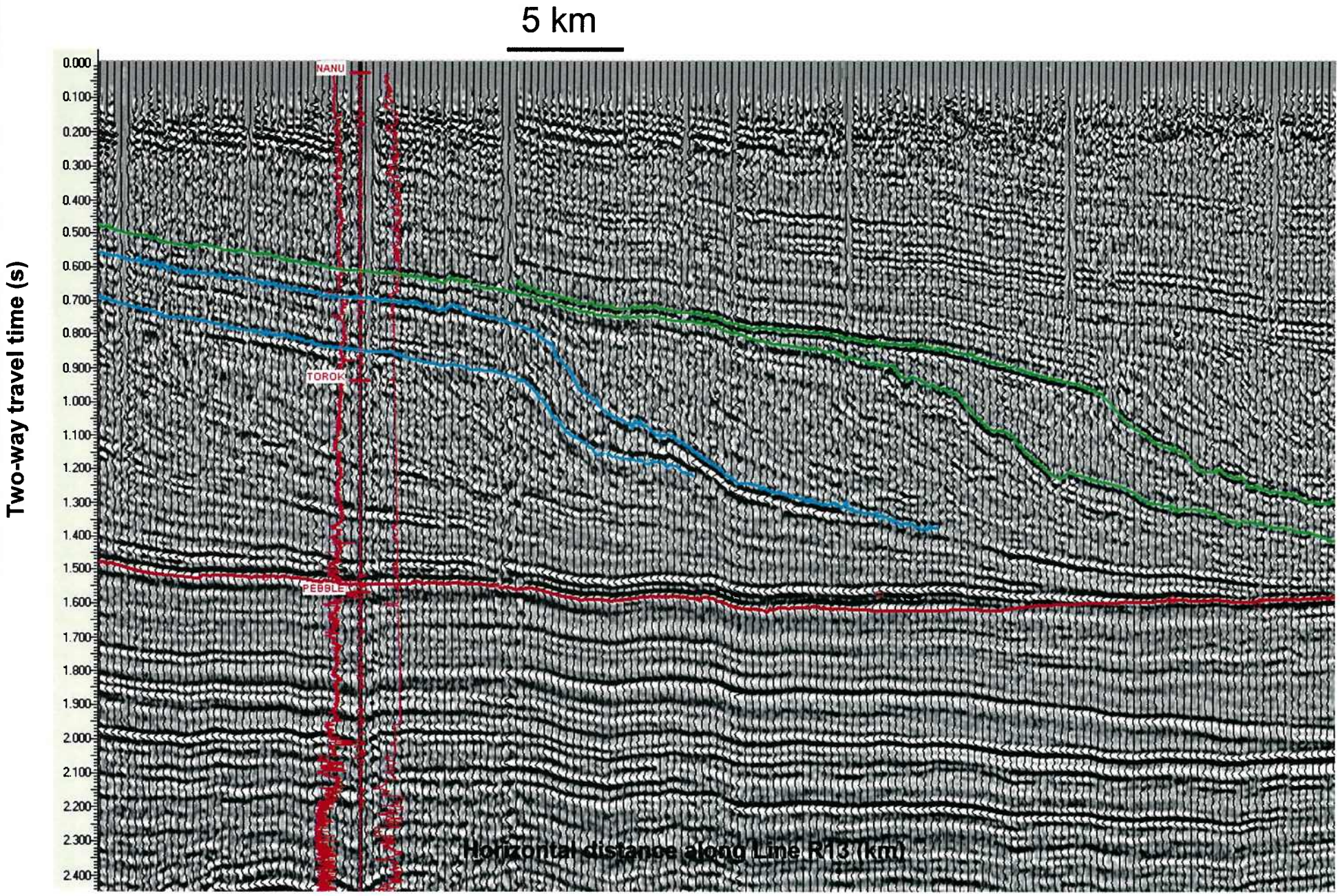


**Figure 10:** R13 line with Ikpikpuk well. Formation tops indicate the Torok to Nanushuk Formation transition located at or near the clinoforms rollover position.

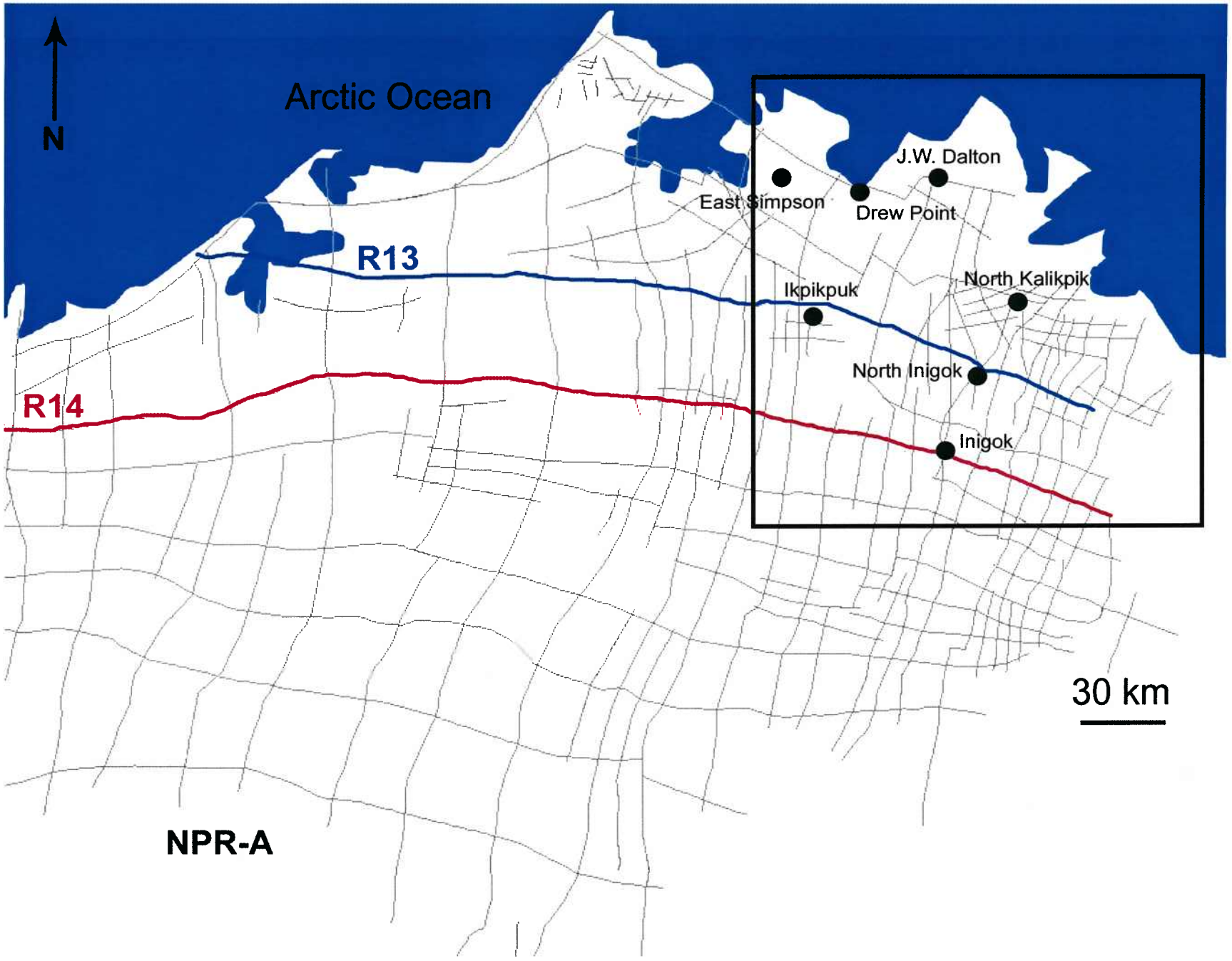


**Figure 11:** 2D seismic grid of the NPR-A, including seven wells in focus area and seismic lines R13 and R14. Focus region of this study outlined in black.

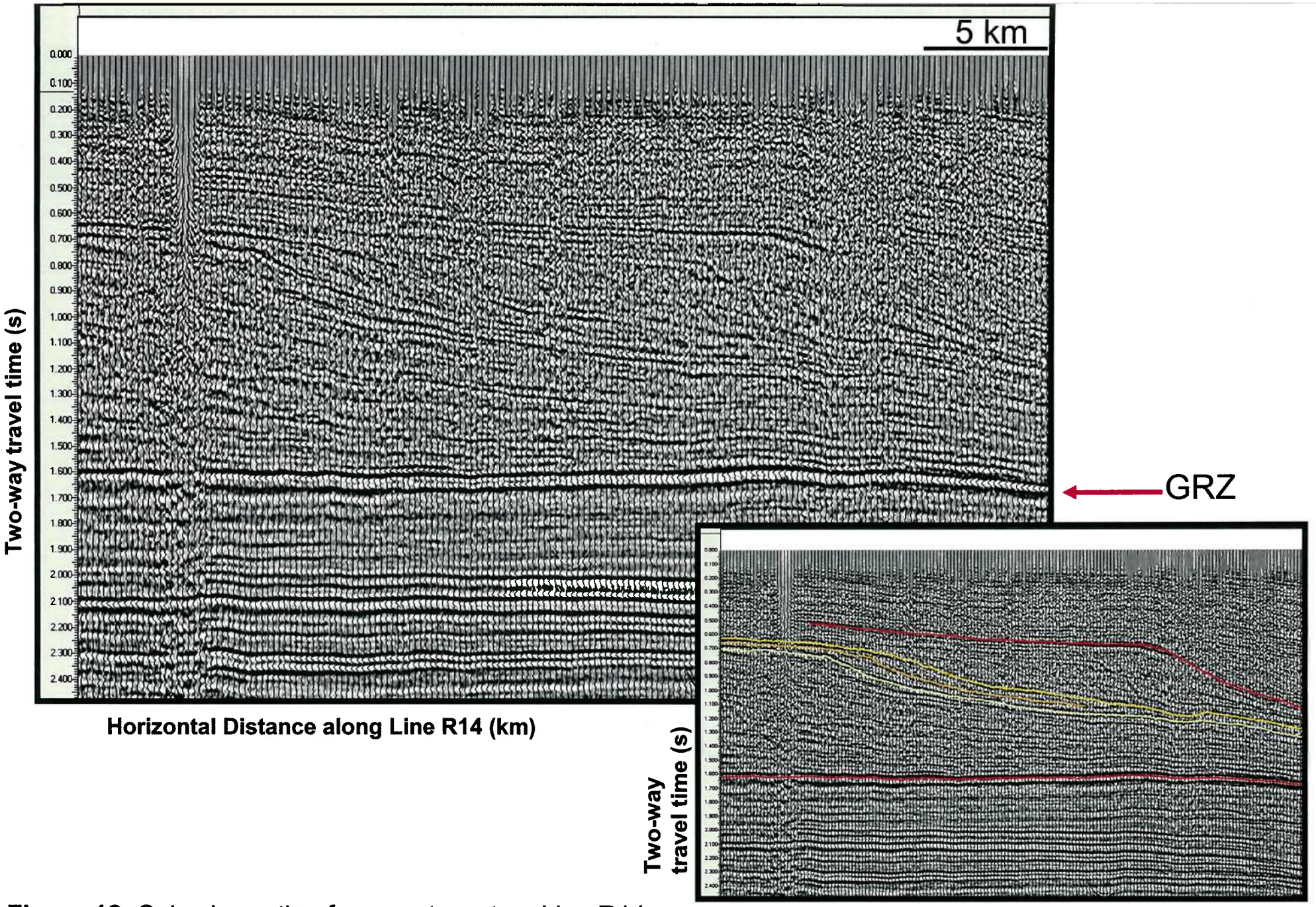


**Figure 12:** Seismic section from east-west on Line R14. Inset image is the interpreted version of the clinoform suite and GRZ.

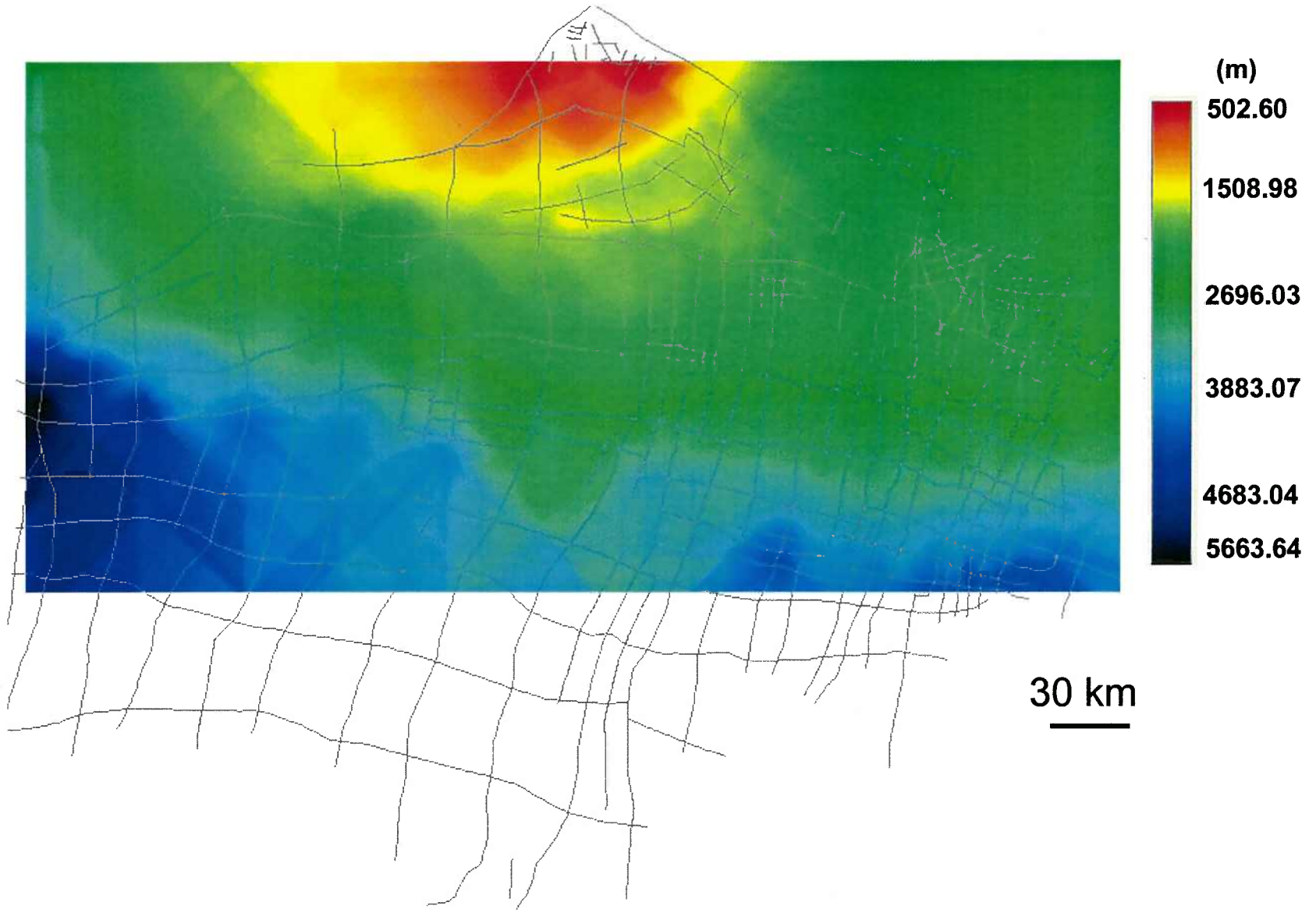


**Figure 13:** Map of depth to GRZ through NPR-A.

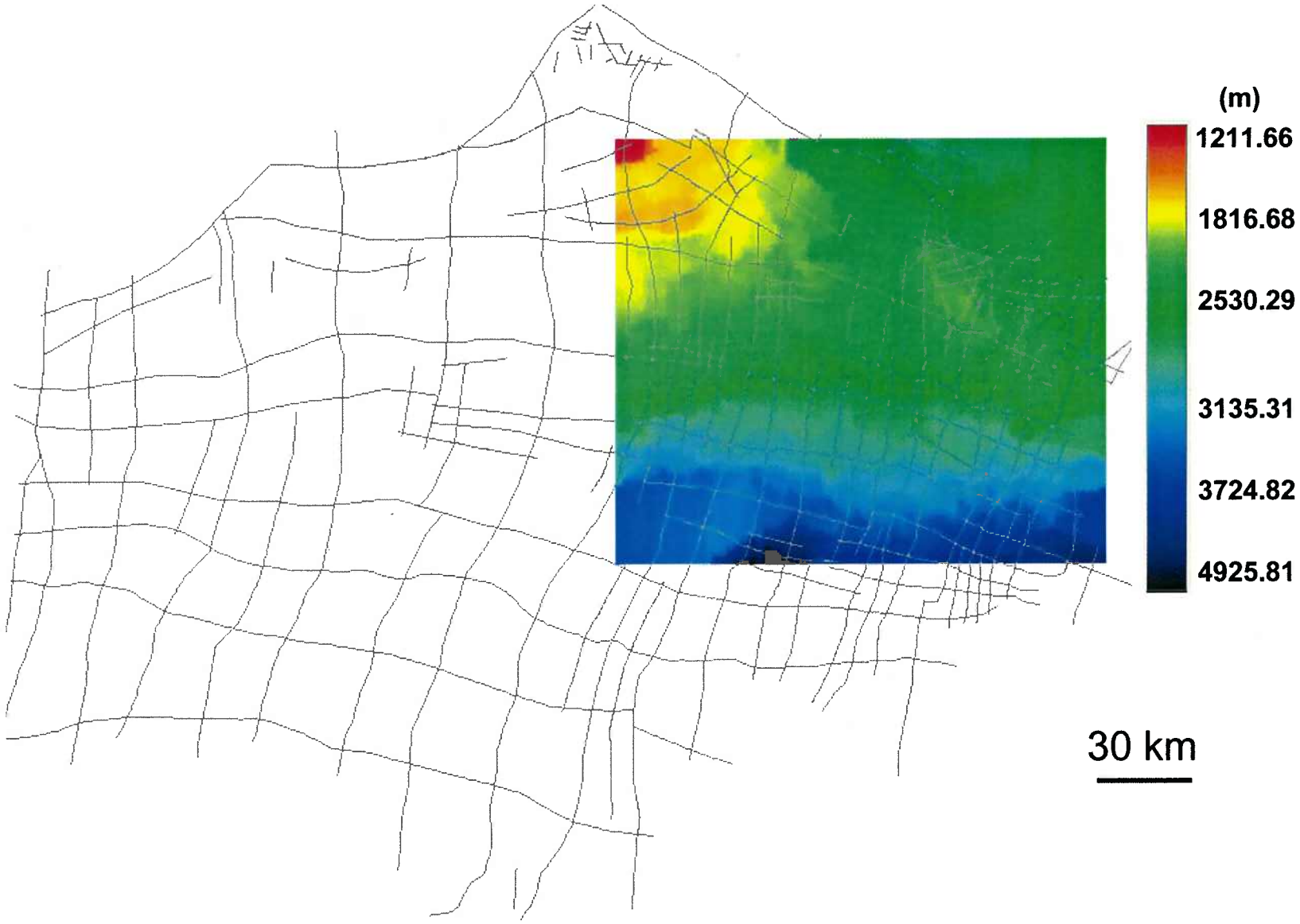


**Figure 14:** Depth to GRZ within focus region.

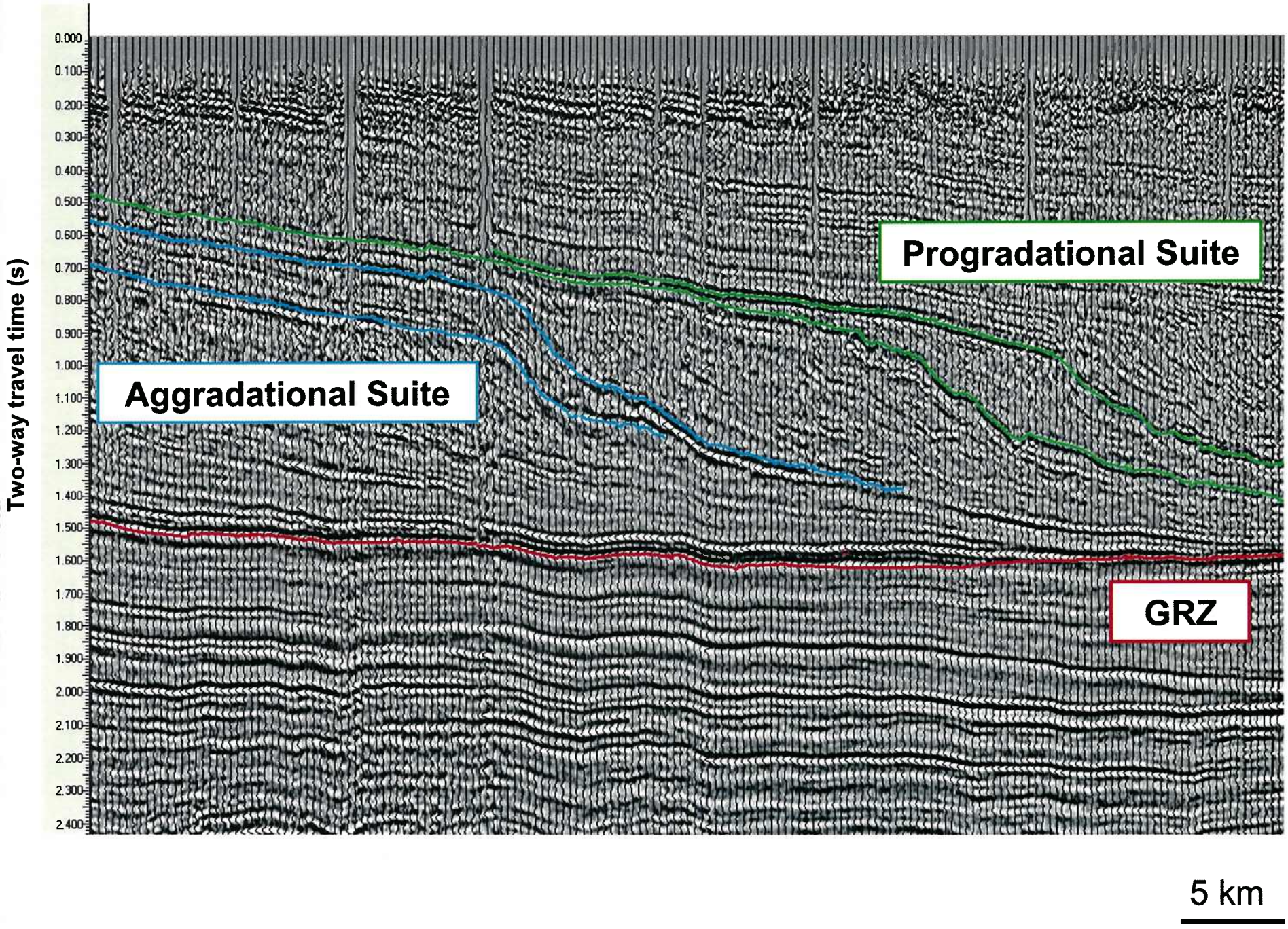


**Figure 15:** Seismic line R13 near the Ikpikpuk well with interpreted aggradational (blue) and progradational (green) suites above the GRZ.

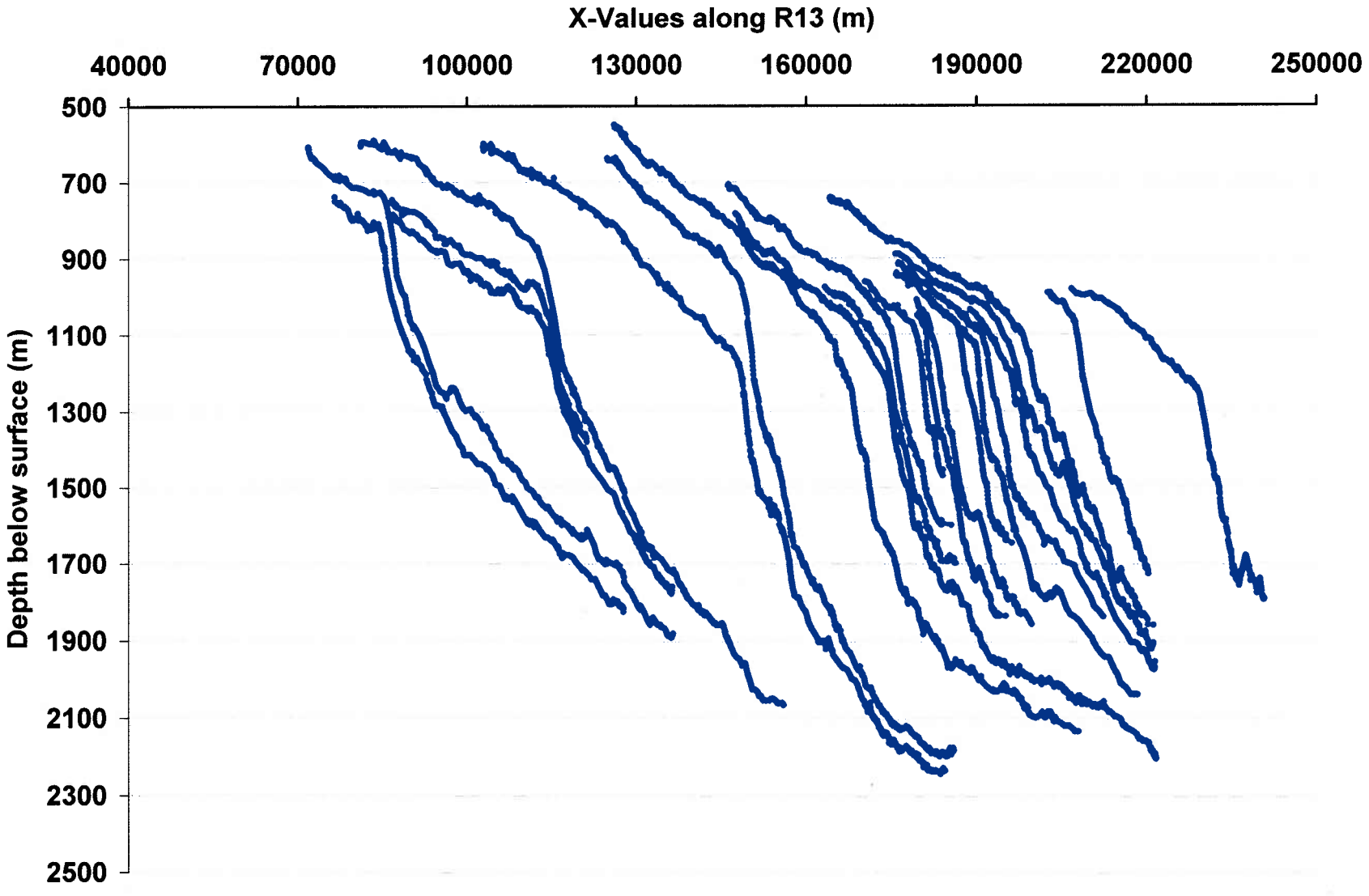


**Figure 16:** Clinoform geometries interpreted along R13. Axes are in original depth-converted seismic scales

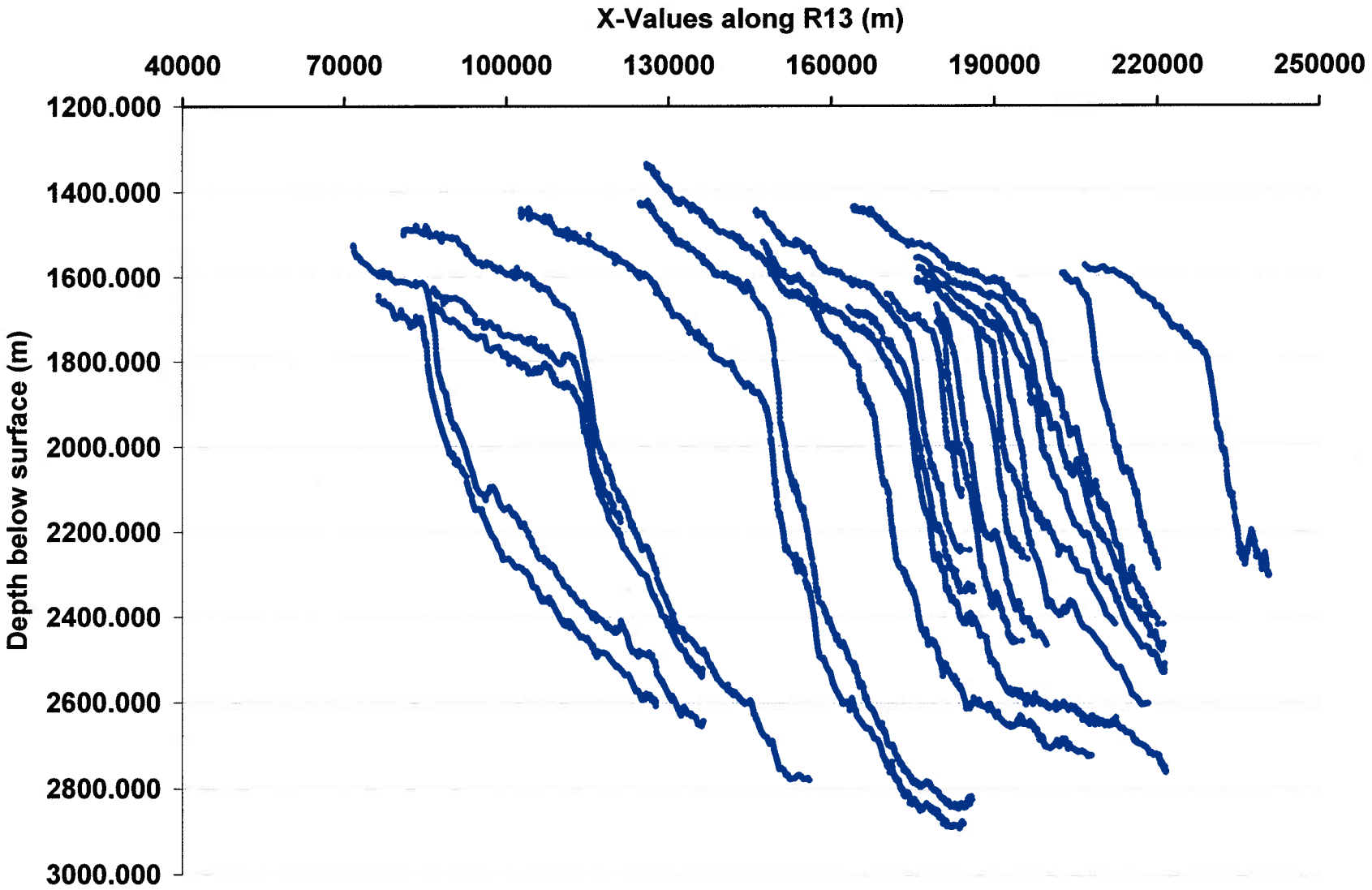


**Figure 17:** Rotated Clinoform geometries interpreted along R13. Axes are in original depth-converted seismic scales

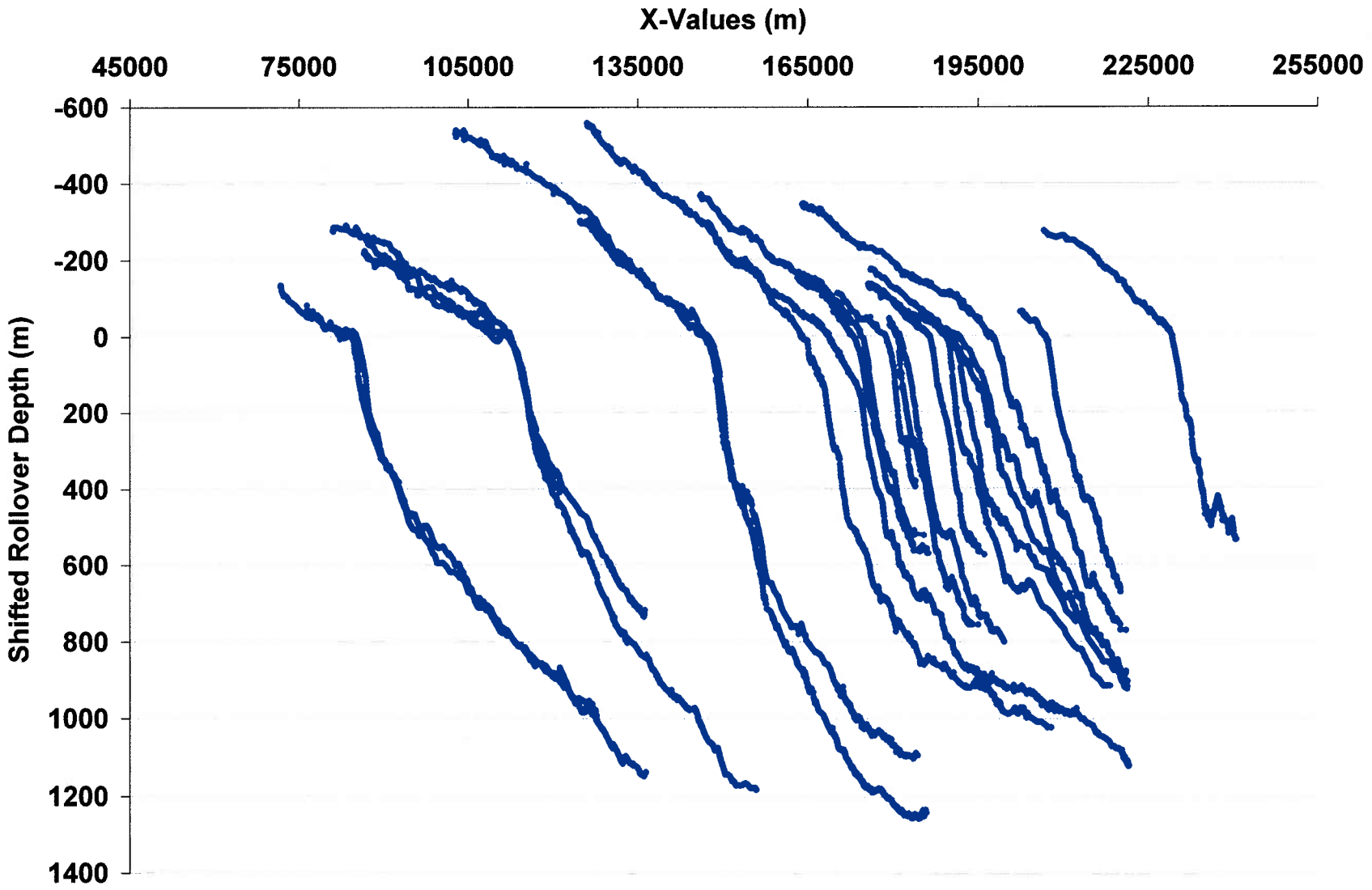


**Figure 18:** All clinoform architectures interpreted on Line R13. X axis is location of clinoform along Line R13. Y-axis is the distance above or below the rollover point of the clinoform surface.

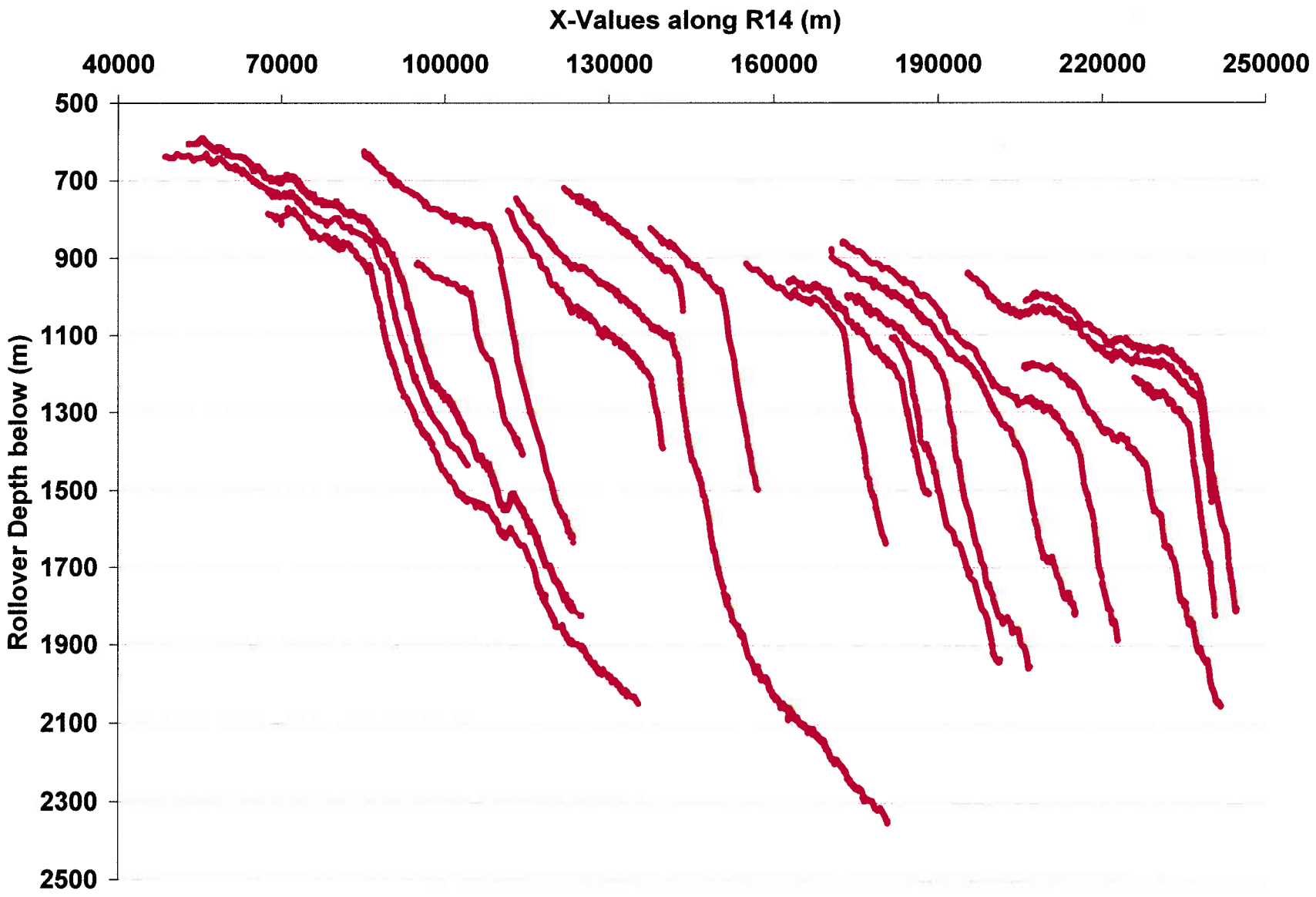


**Figure 19:** Clinoform geometries interpreted along R14. Axes are in original depth-converted seismic scales.

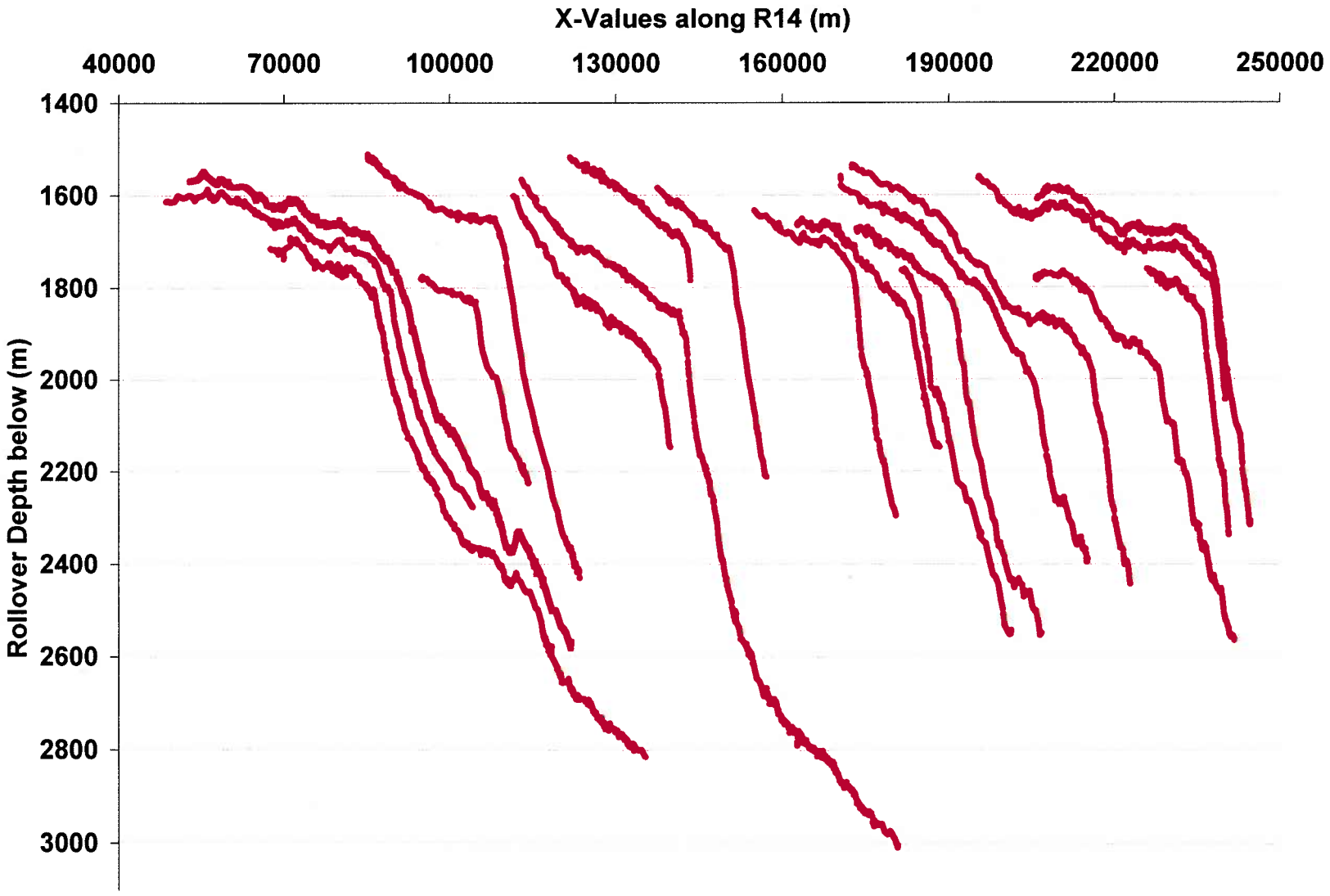


**Figure 20:** Rotated Clinoform geometries interpreted along R14. Axes are in original depth-converted seismic scales.

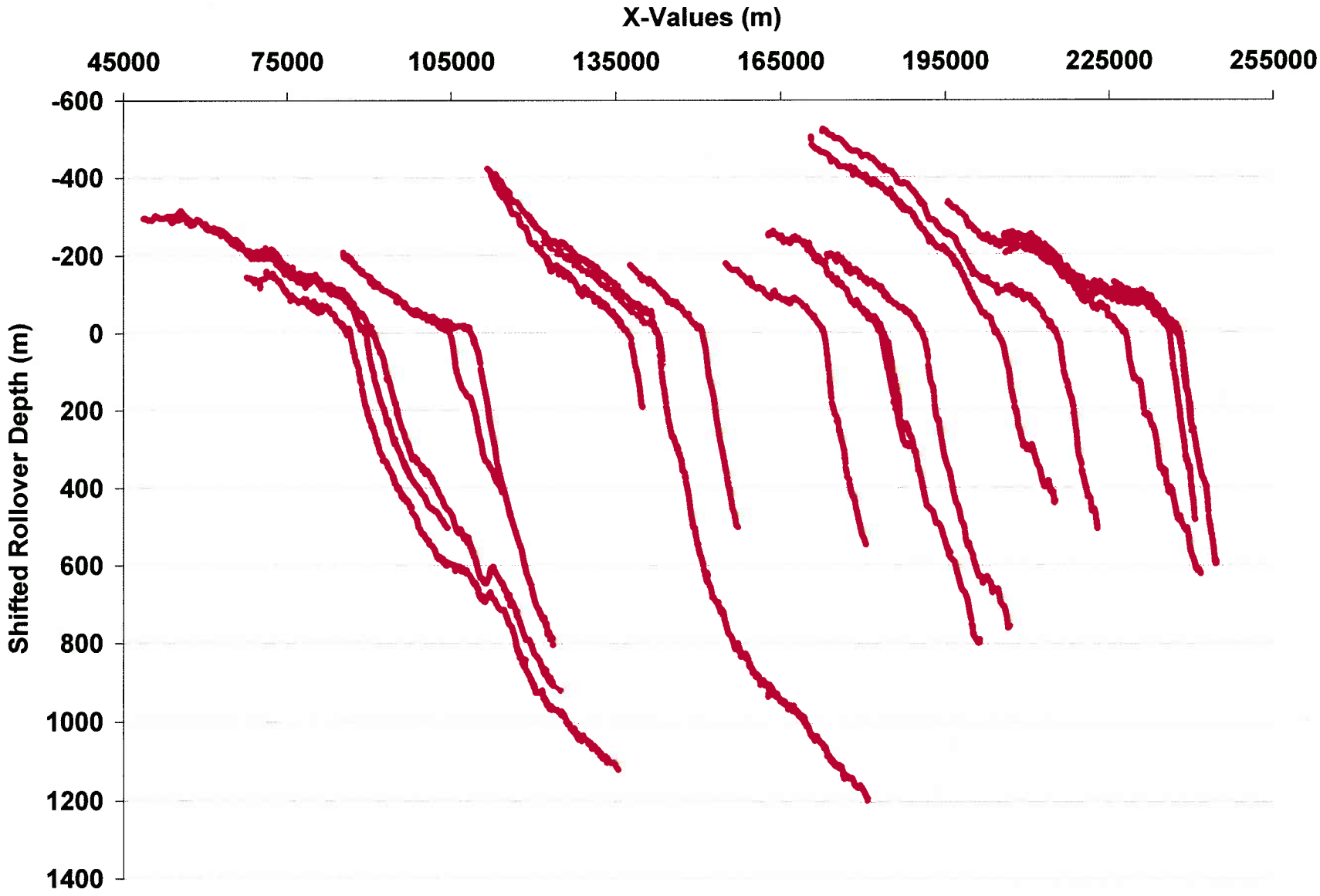


**Figure 21:** All clinoform architectures interpreted on Line R14. X axis is location of clinoform along Line R13. Y-axis is the distance above or below the rollover point of the clinoform surface.

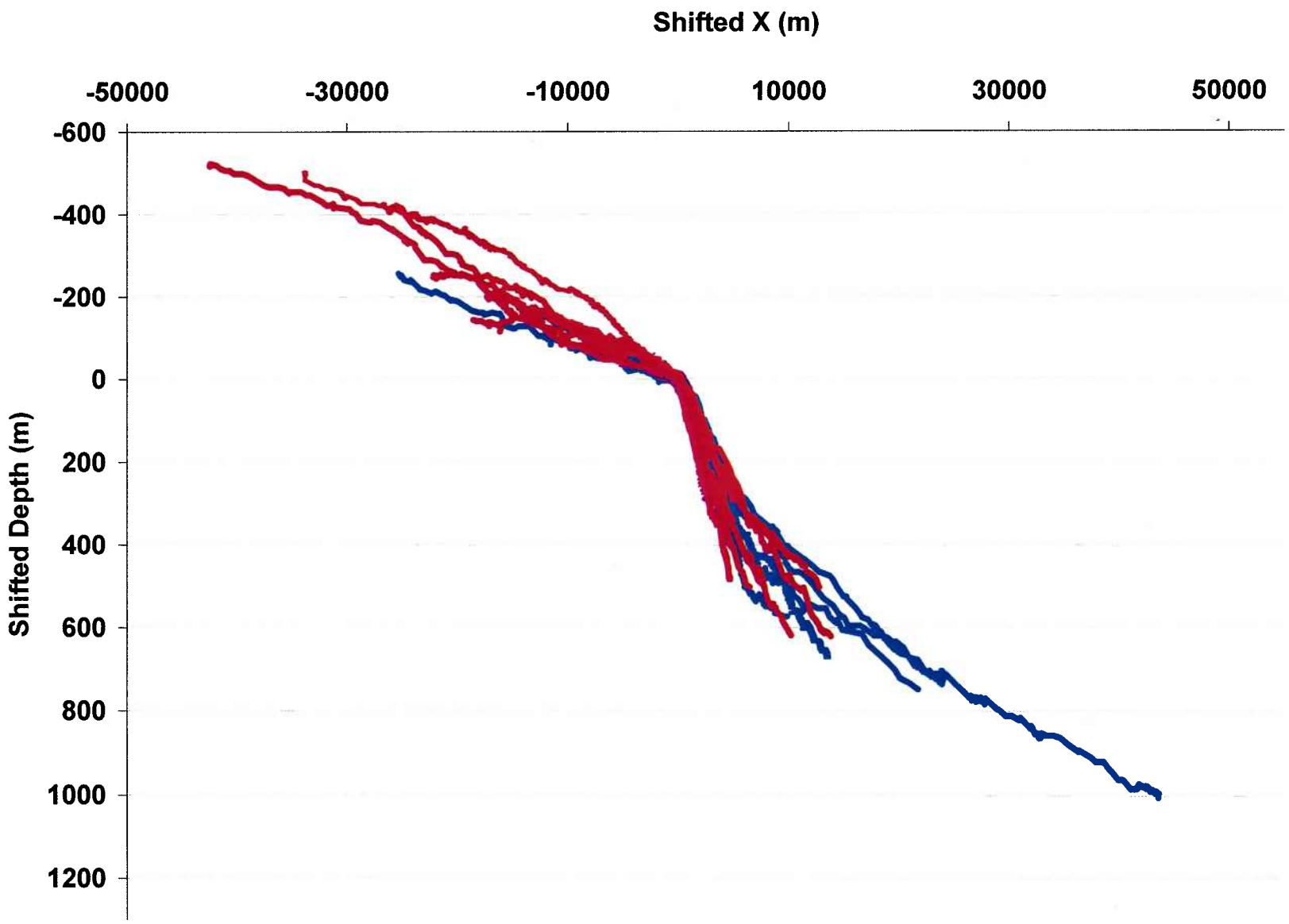


**Figure 22:** Progradational clinoforms normalized in length and height, and stacked to compare geometries

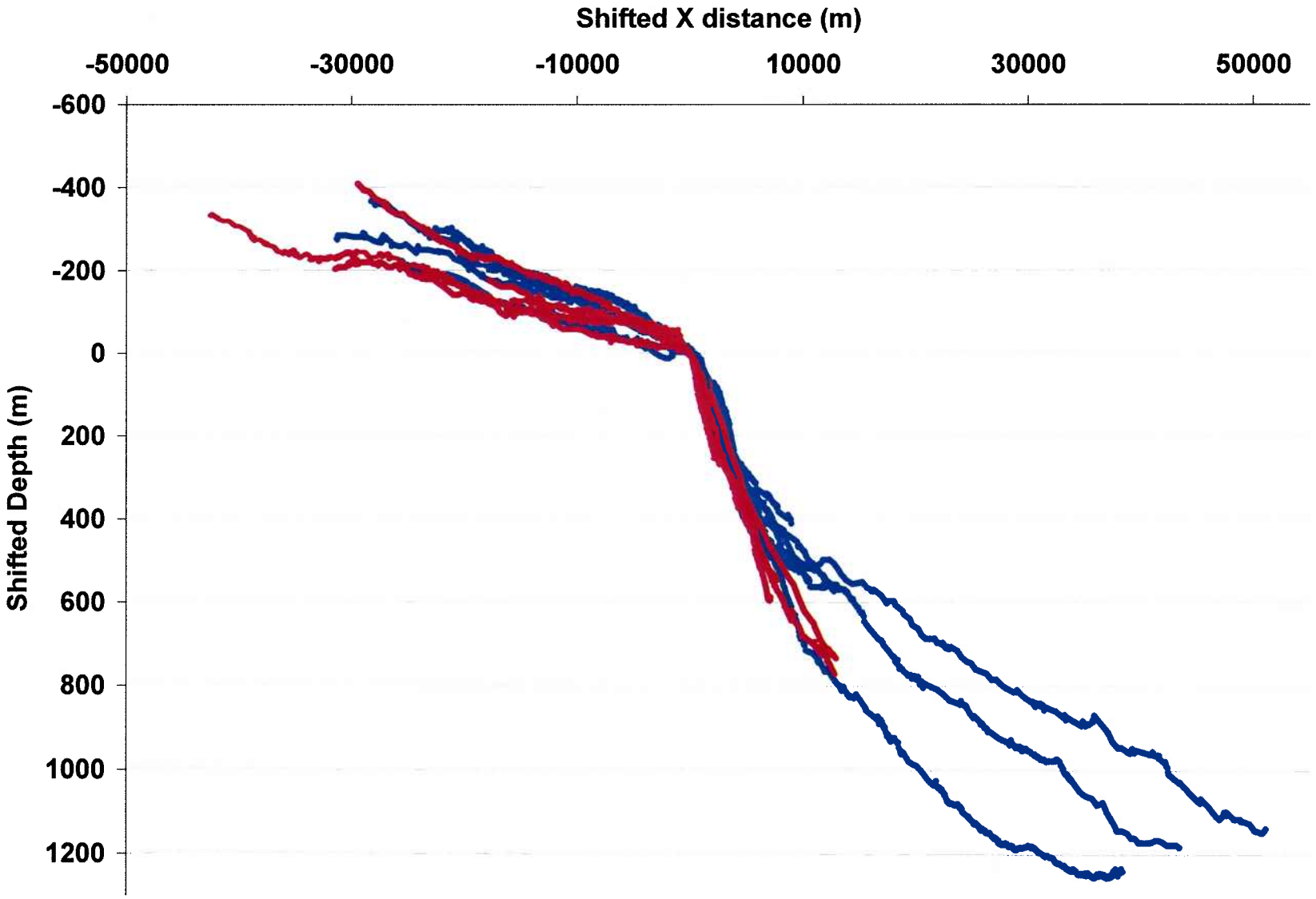


**Figure 23:** Aggradational clinoforms normalized in length and height, and stacked to compare geometries.

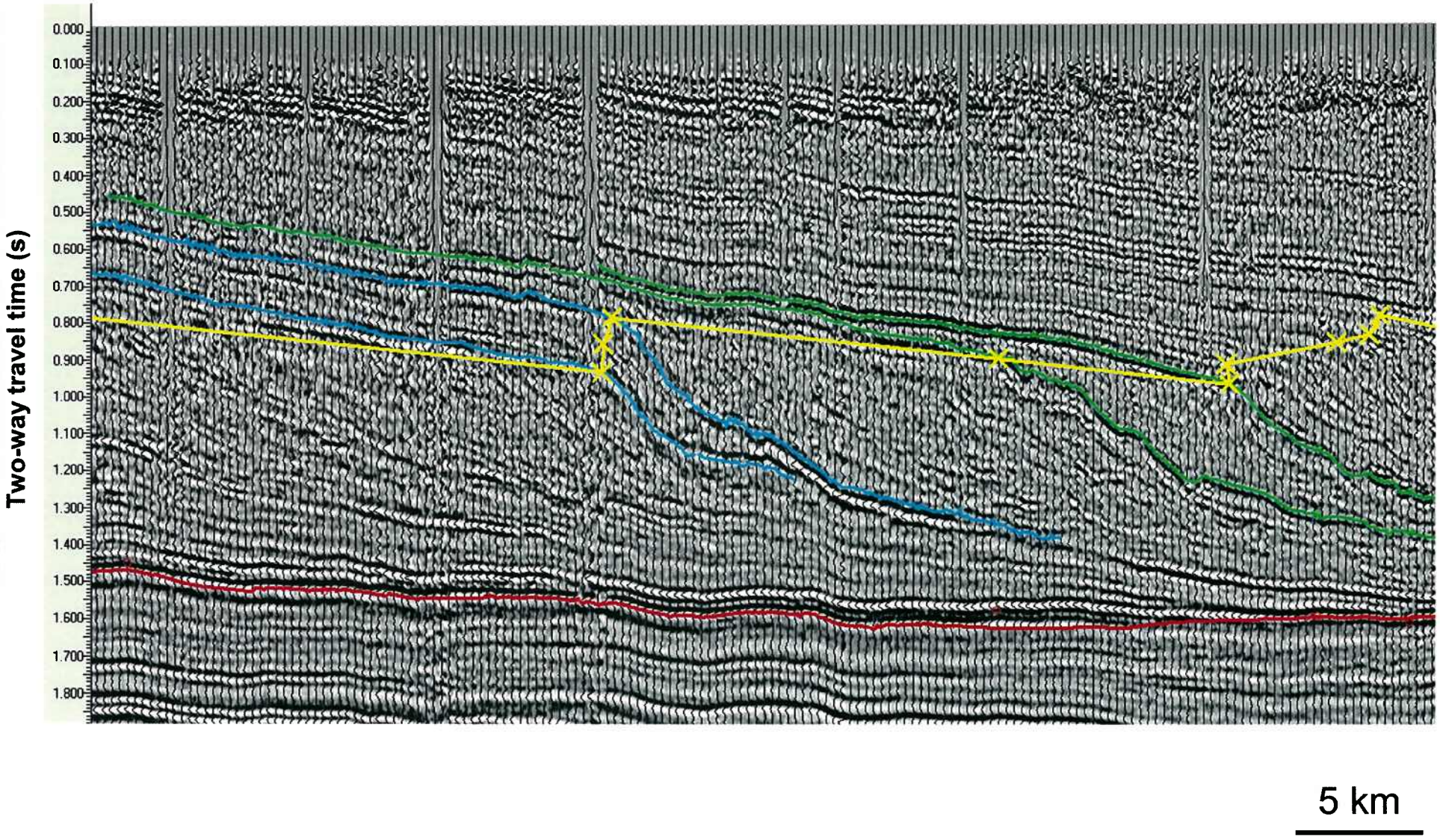


**Figure 24:** Mapping of rollover transition (yellow) across seismic line R13.

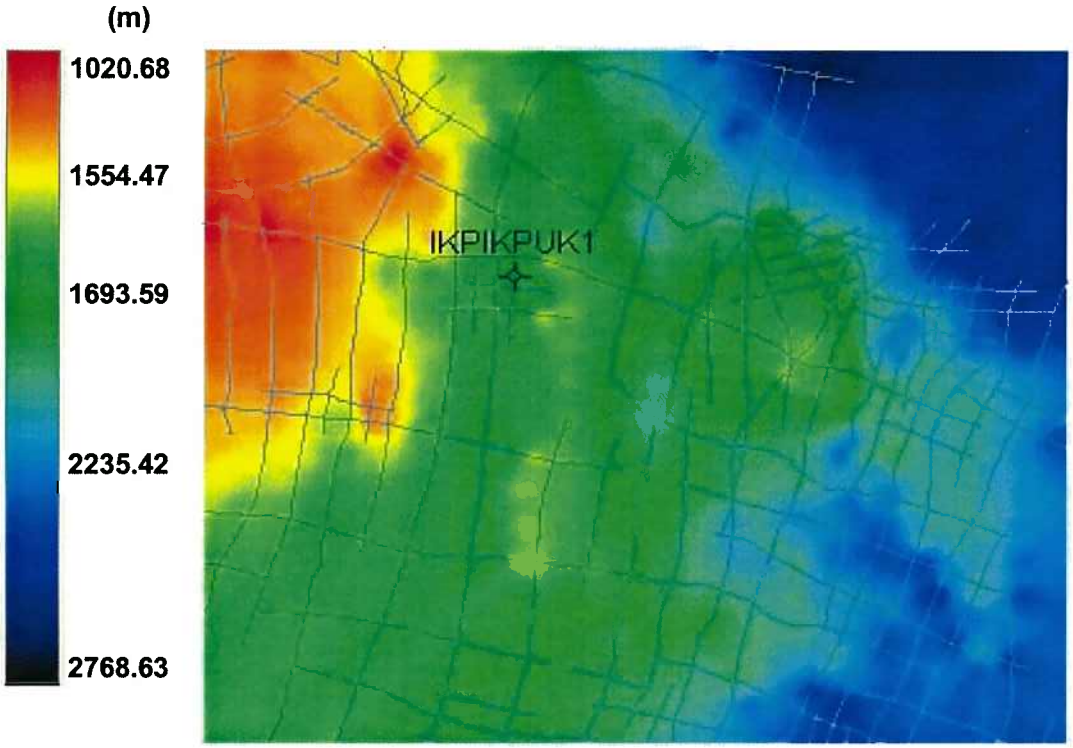


**Figure 25a:** Map of depth to rollover after simple decompaction.

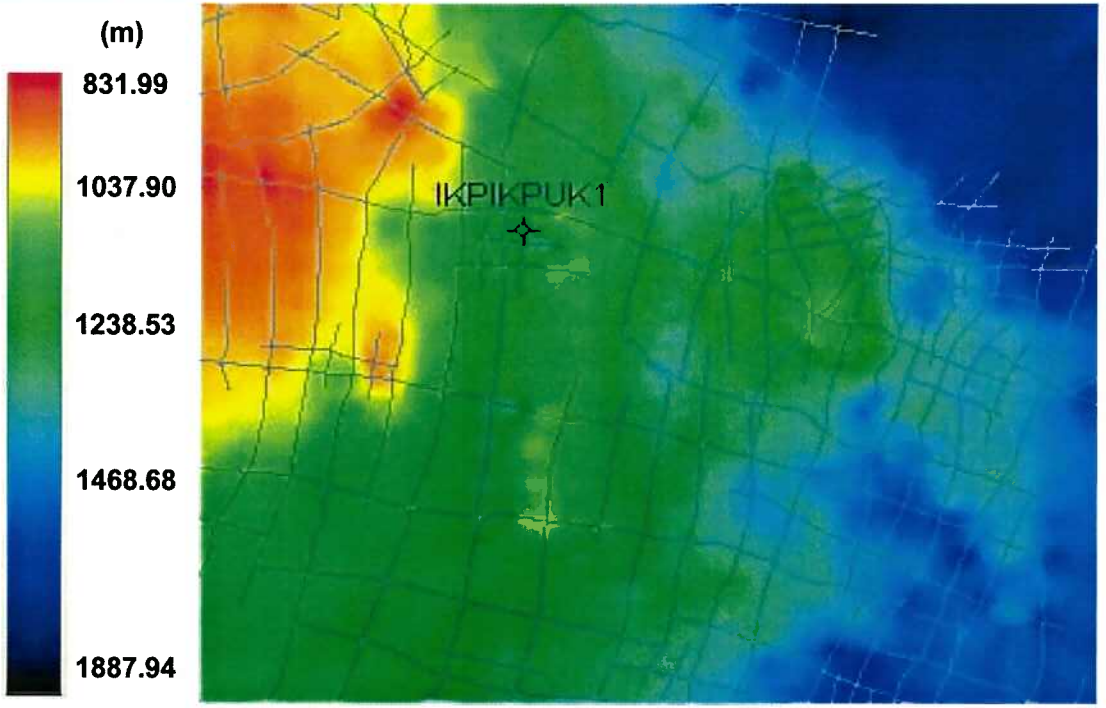


**Figure 25b:** Map of depth to rollover after iterative decompaction.

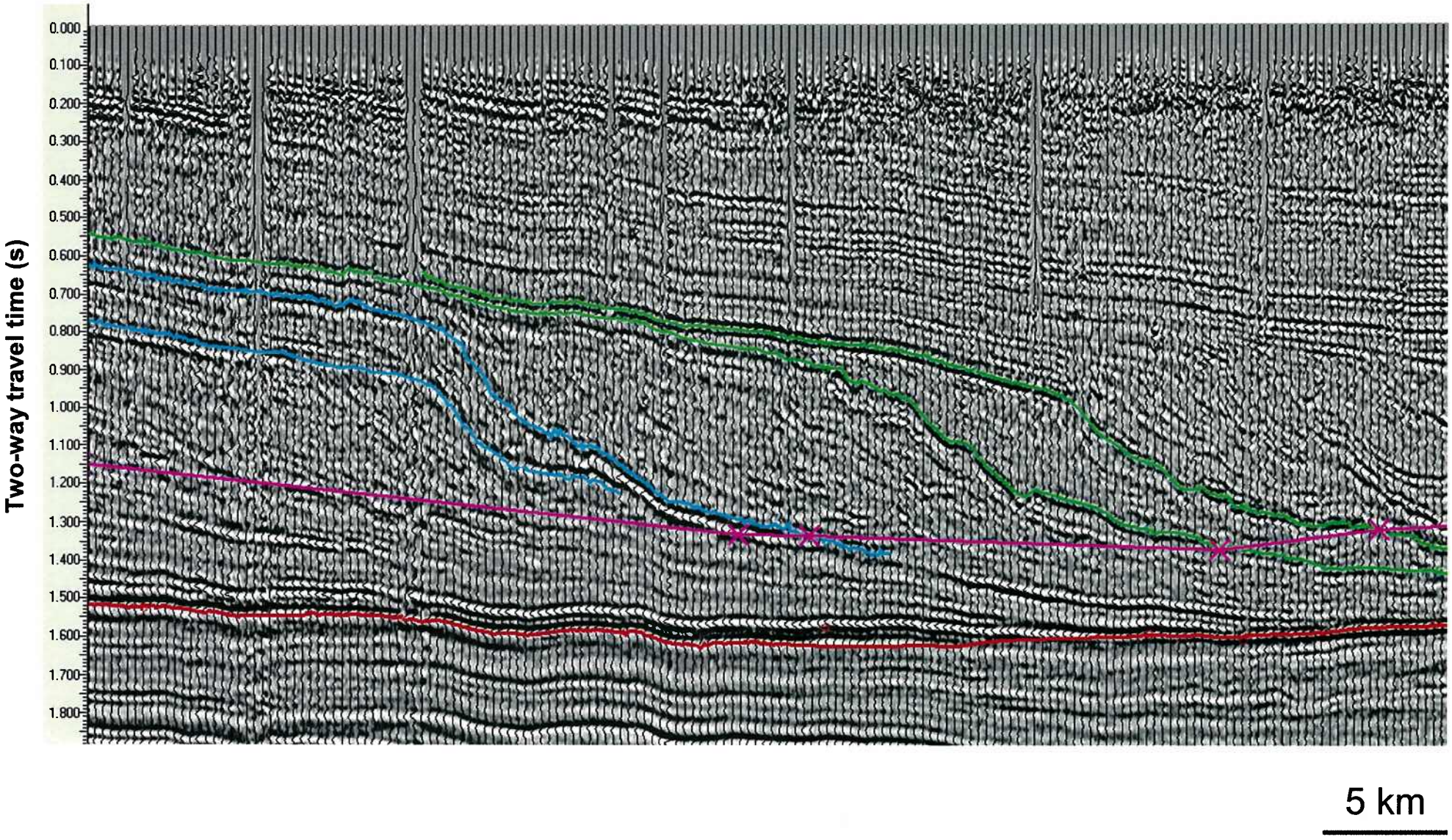


**Figure 26:** Mapping of bottomset transition (pink) across seismic line R13.

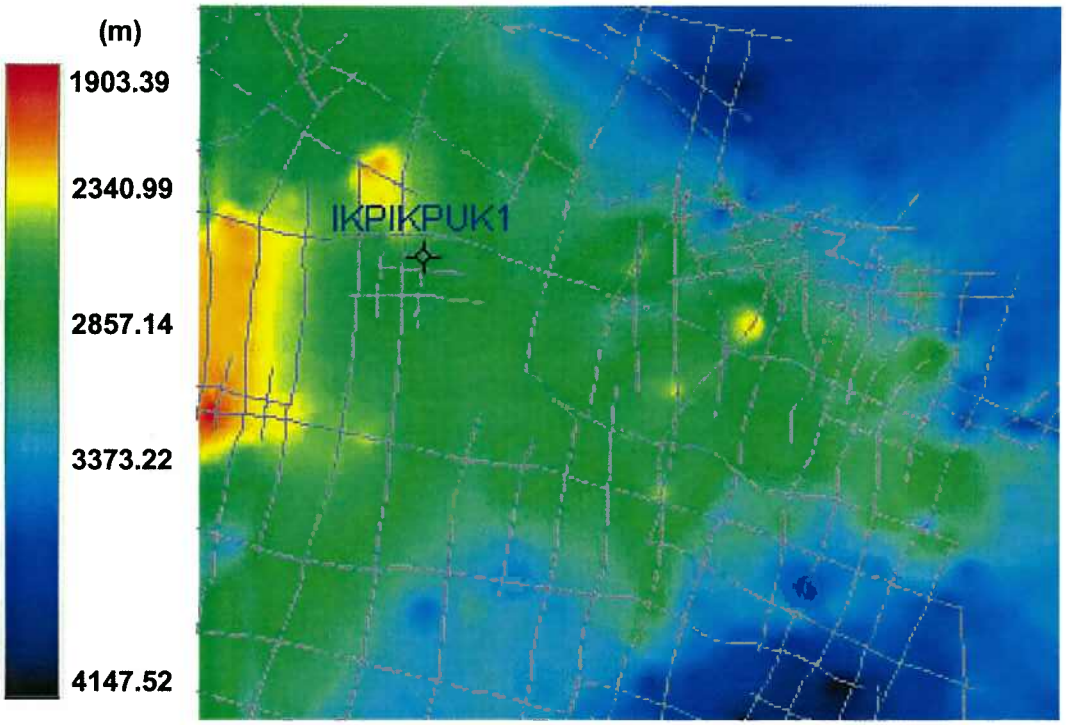


**Figure 27a:** Map of depth to bottomset transition after simple decompaction.

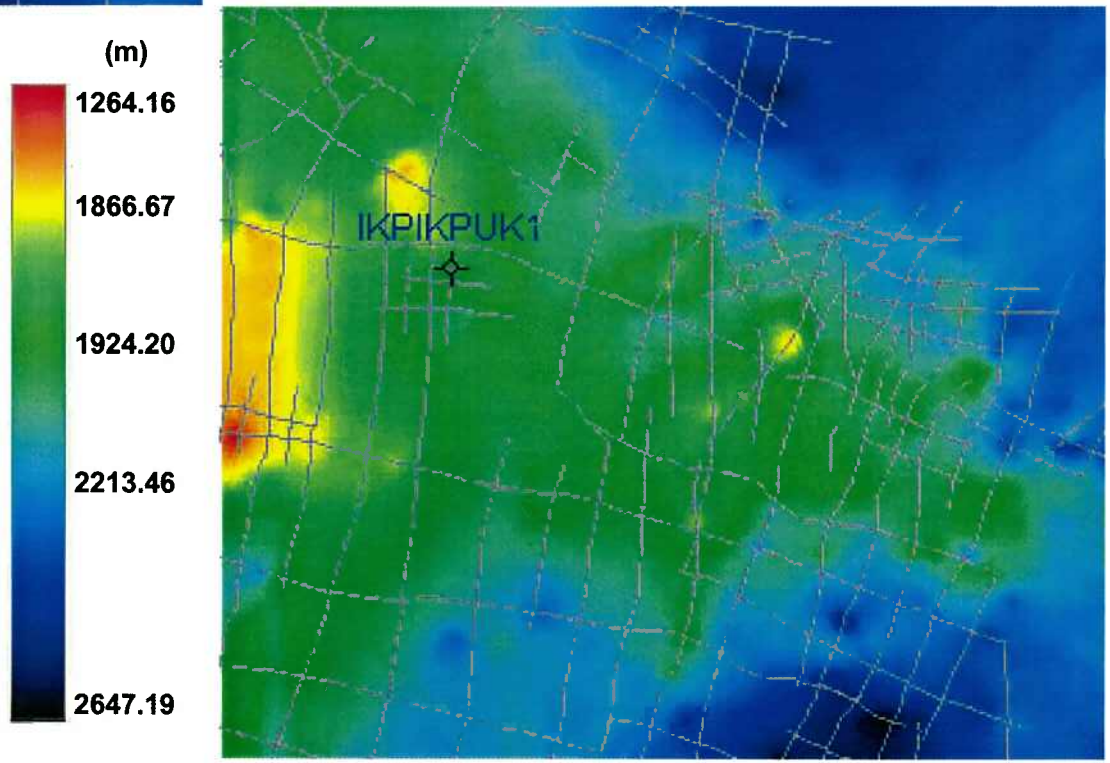


**Figure 27b:** Map of depth to bottomset transition after iterative decompaction.

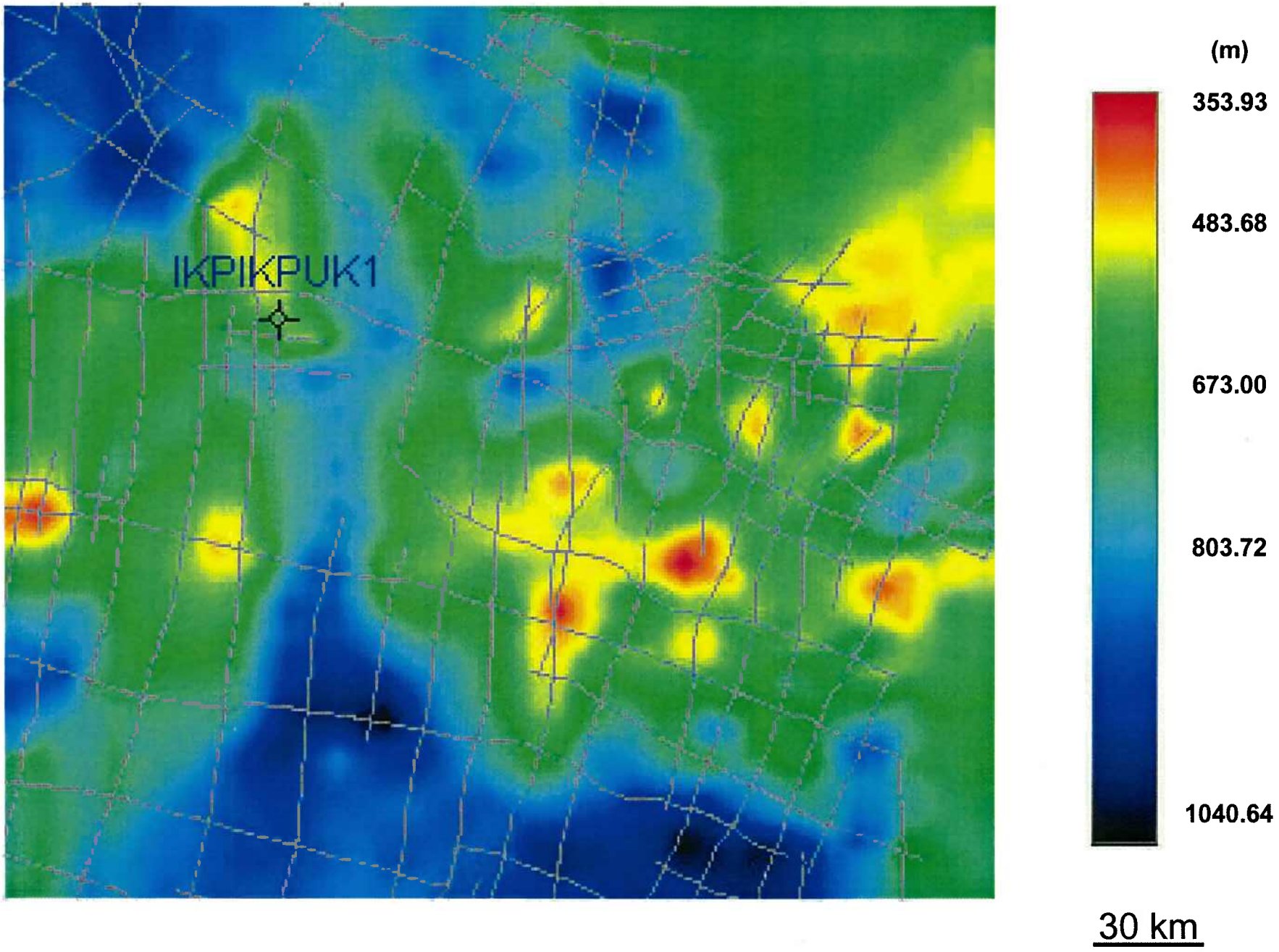


**Figure 28:** Foreset thickness map of focus region created as difference between the iterative decompacted bottomset transition depth map and the iterative decompacted rollover depth map.

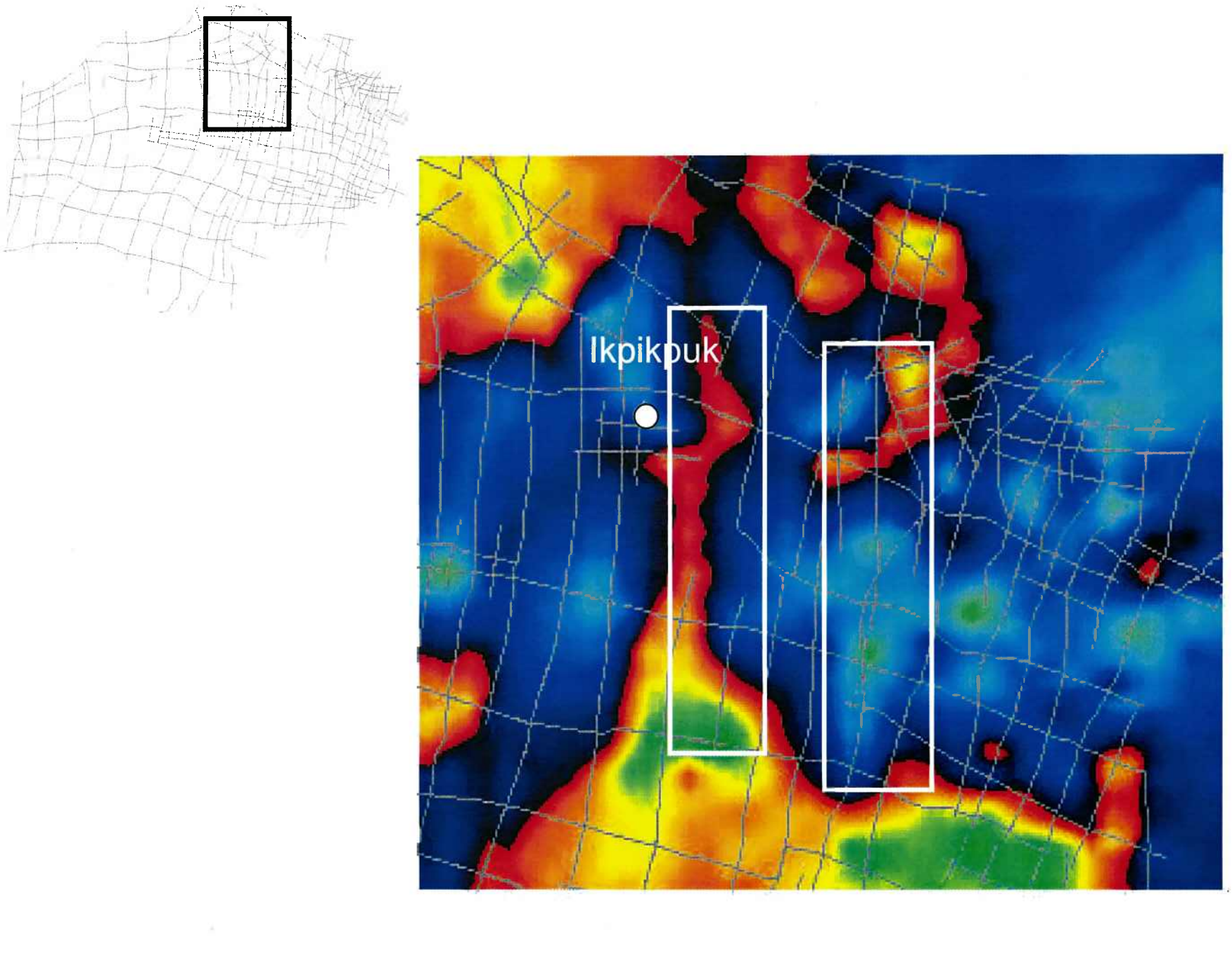


**Figure 29:** Foreset thickness map showing two large depositional events running north-south direction, east of the Ikpikpuk well.

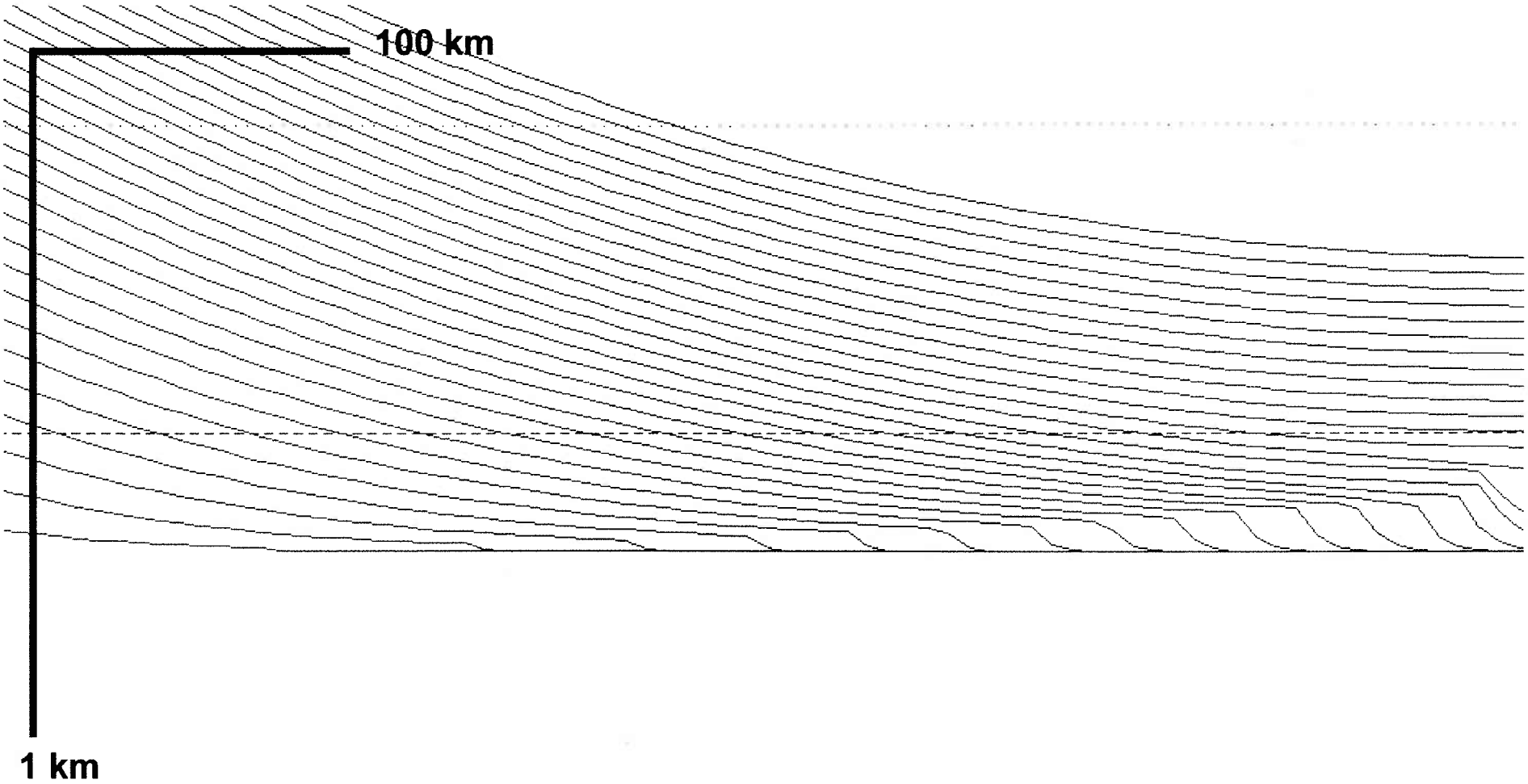


**Figure 30:** Simulation of Line R13 using subsidence rate calculated from seismic data. Accommodation space overwhelms sediment flux giving a continually climbing profile of the rollover point location. Timeline contour is every 300,000 years.

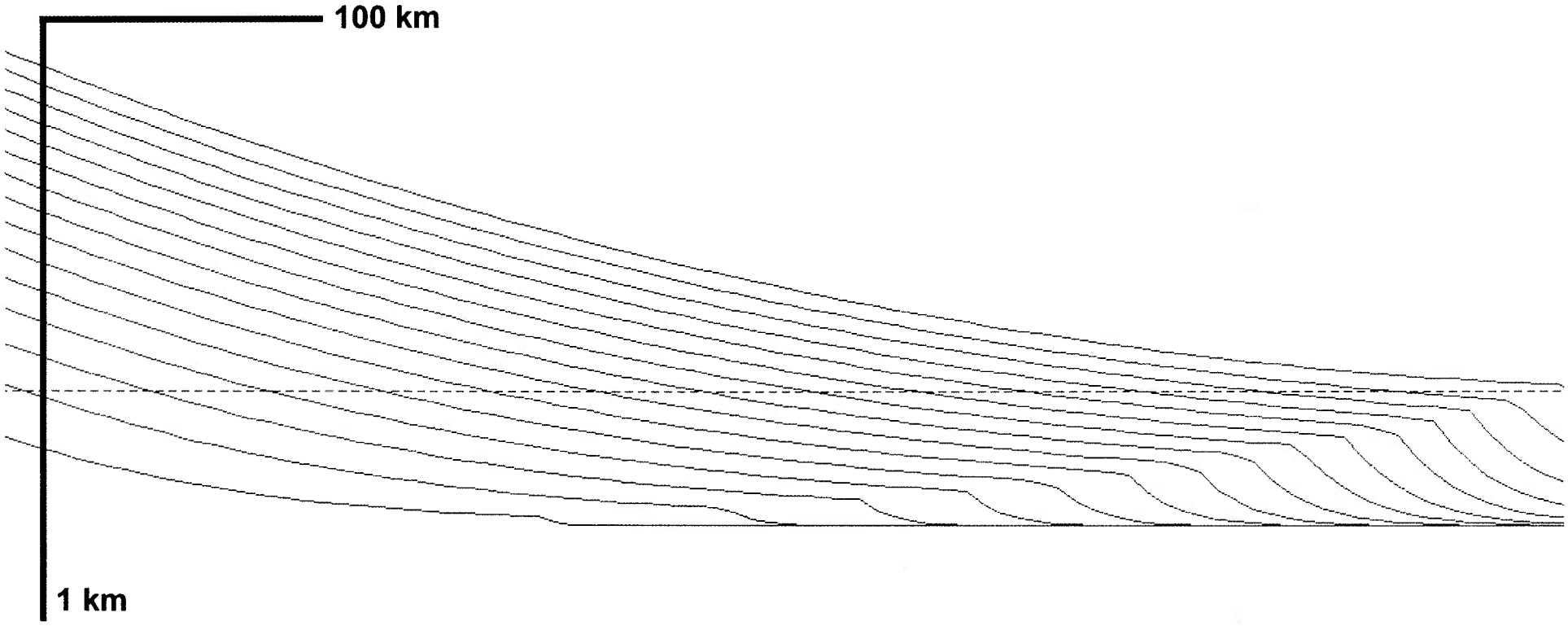


**Figure 31:** Simulation of Line R14 using subsidence rate calculated from seismic data. Accommodation space overwhelms sediment flux giving a continually climbing profile of the rollover point location. Timeline contour is every 300,000 years.

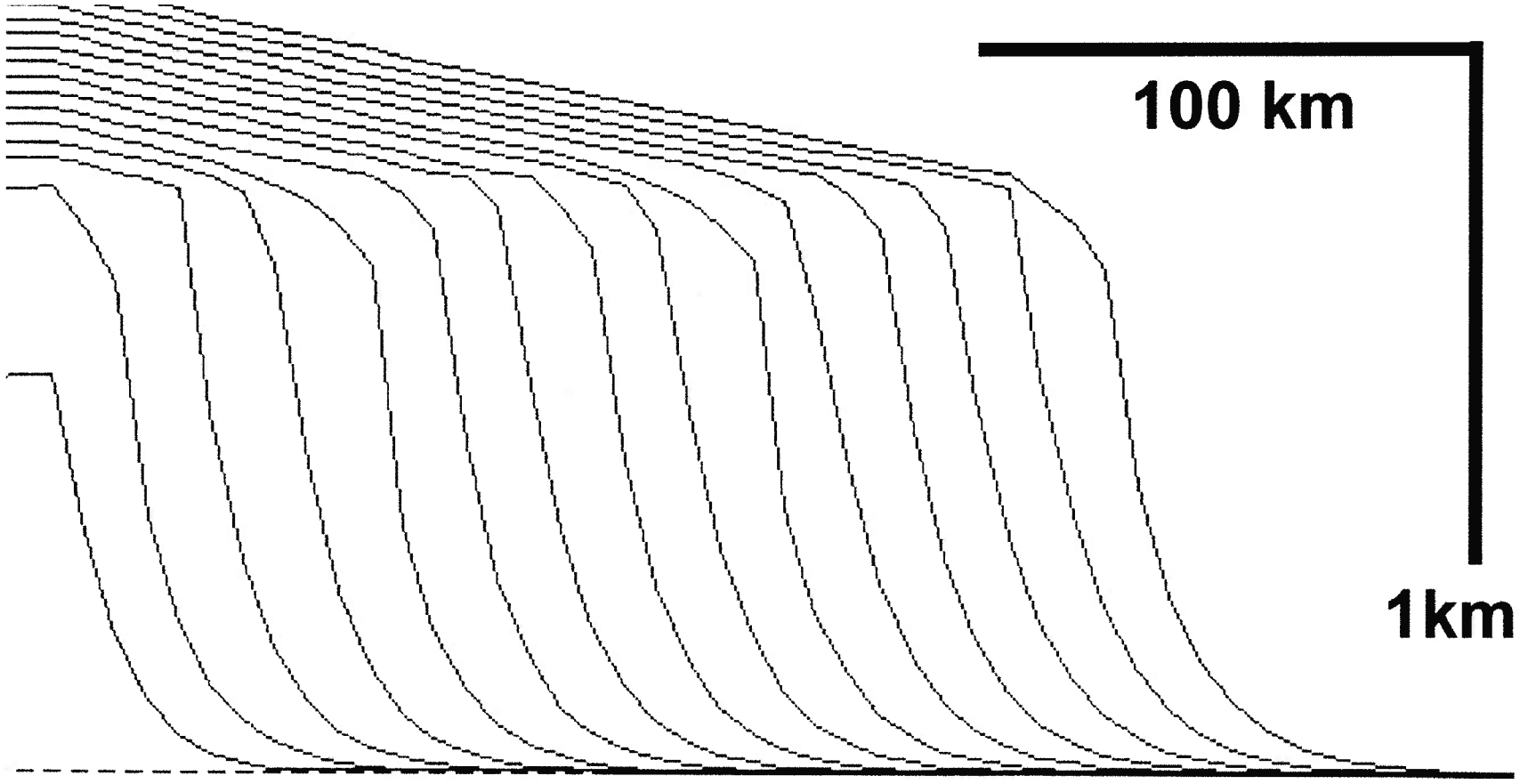


**Figure 32:** Strongly progradational suite on R13 simulation with subsidence set to zero and sea level at 1143 m. Progradation distance is 145.3 km allowing for a minimum sediment flux of 34 $m^2/y$.

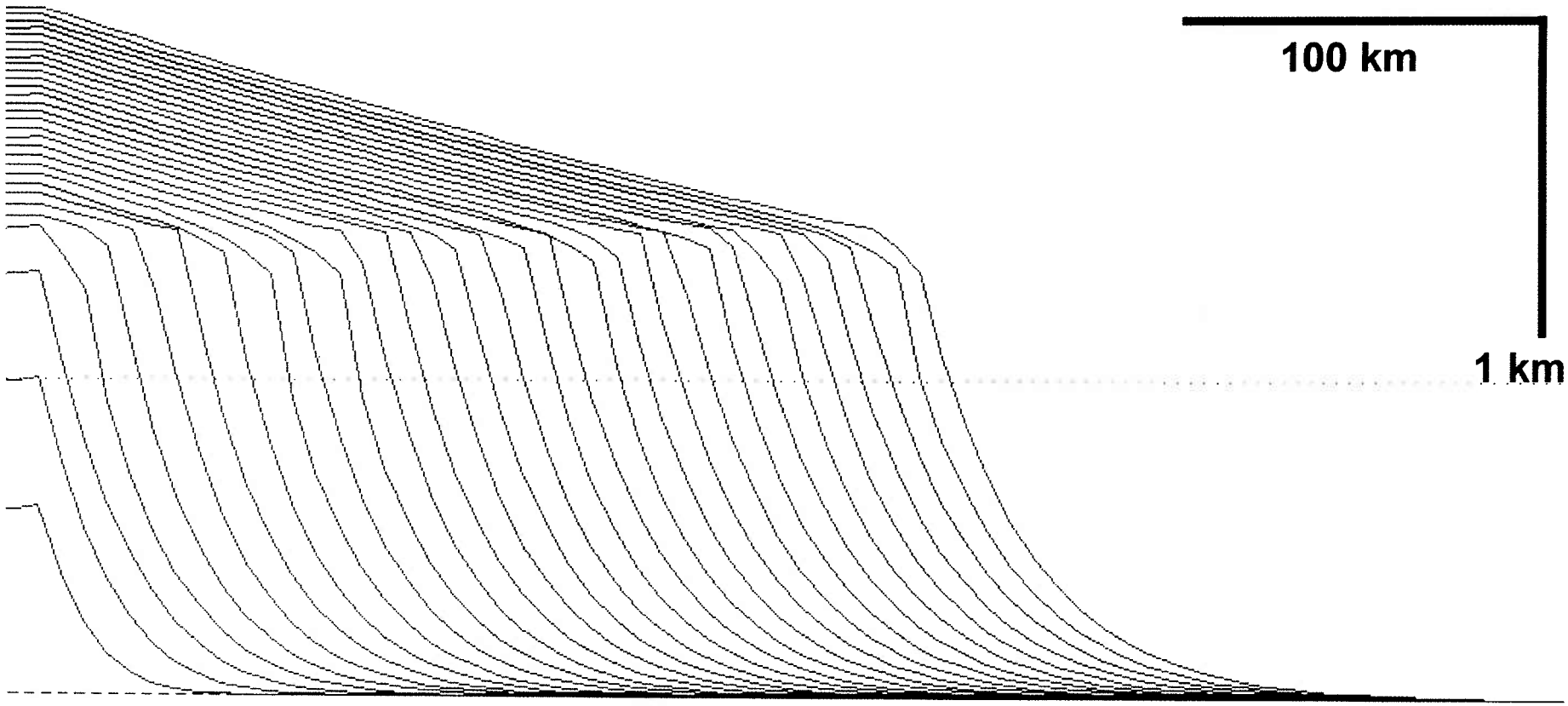


**Figure 33:** Strongly progradational suite on R14 simulation with subsidence set to zero and sea level at 1467 m. Progradation distance is 164.0 km allowing for a minimum sediment flux of 55 $m^2/y$.

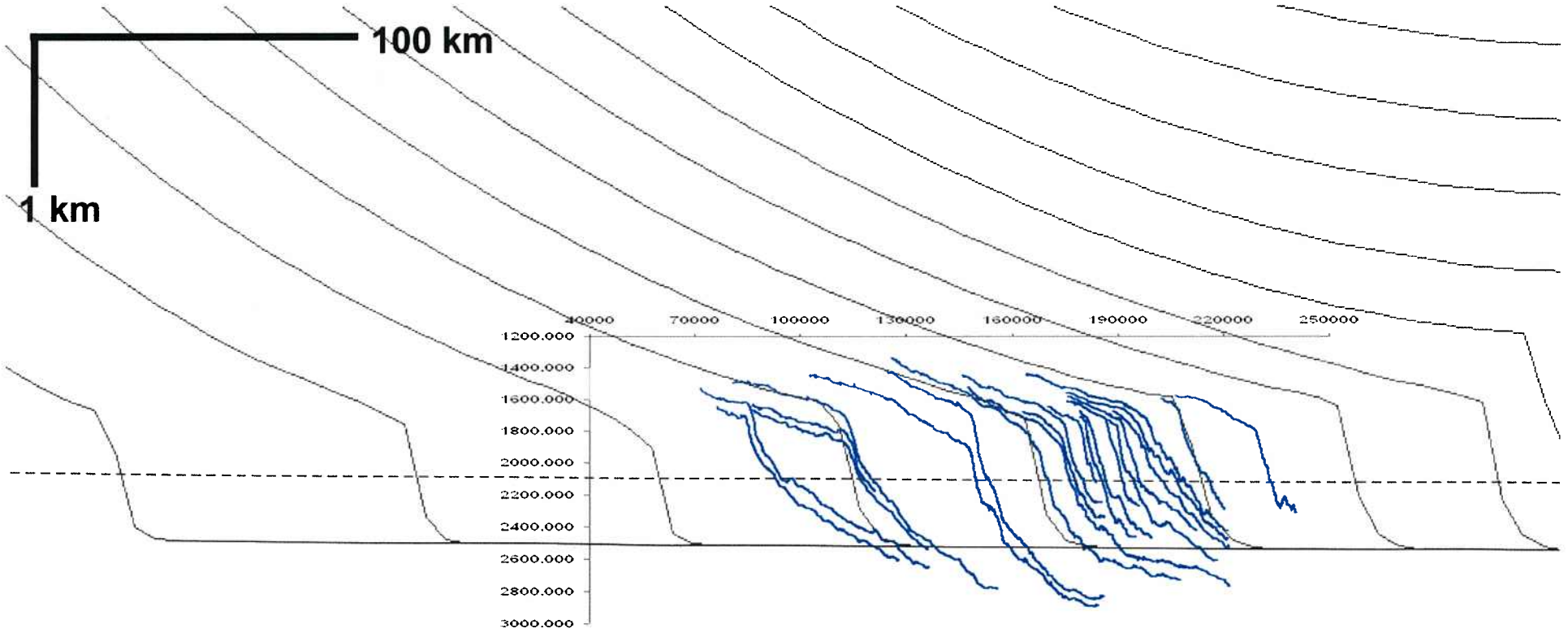


**Figure 34:** Simulated solution match for the Line R13 STRATA model. Reduced subsidence and sea level needed to prograde suite. Overlaid in blue is rotated clinoform geometries from Line R13 in the NPR-A focus region.

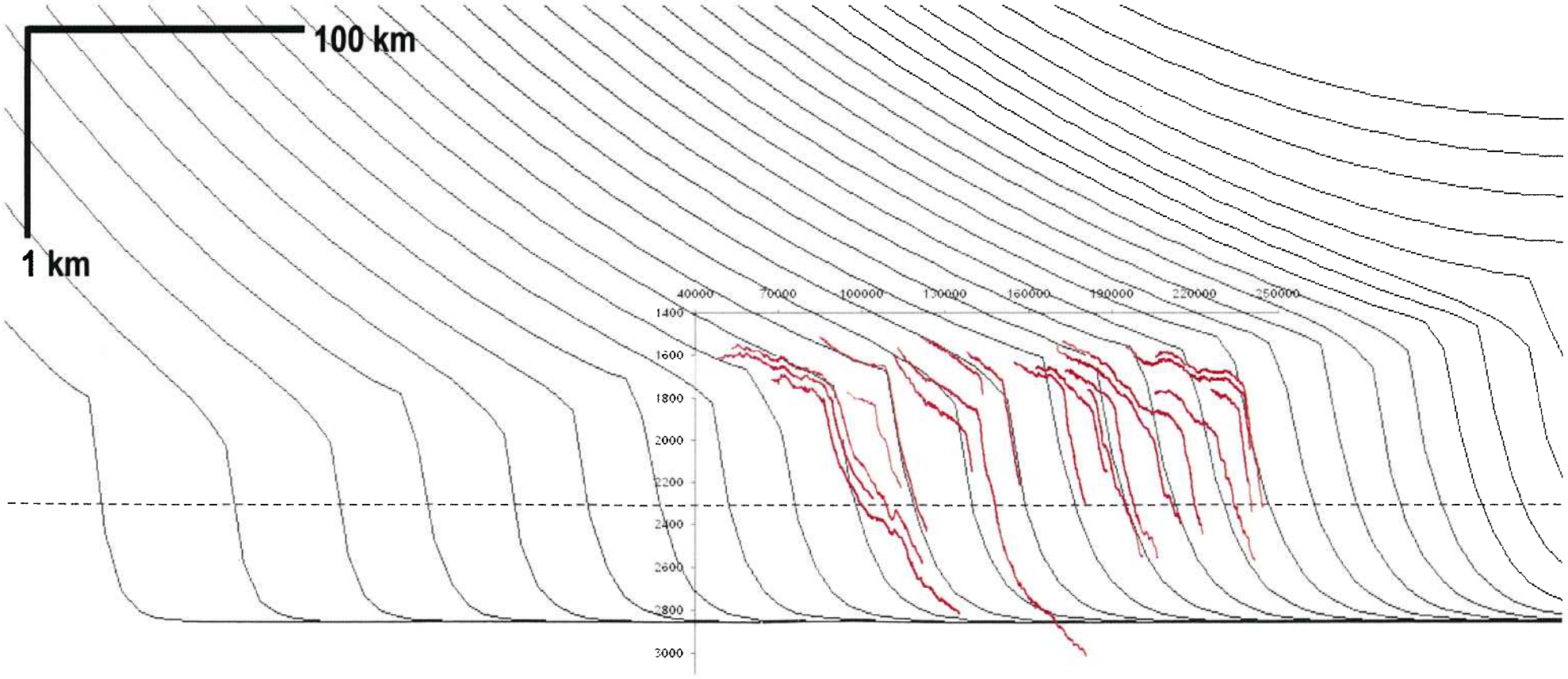


**Figure 35:** Simulated solution match for the Line R14 STRATA model. Reduced subsidence and sea level needed to prograde suite. Overlaid in red is rotated clinoform geometries from Line R14 in the NPR-A focus region.

# Appendix 1: Core Observations

## Drew Point 1

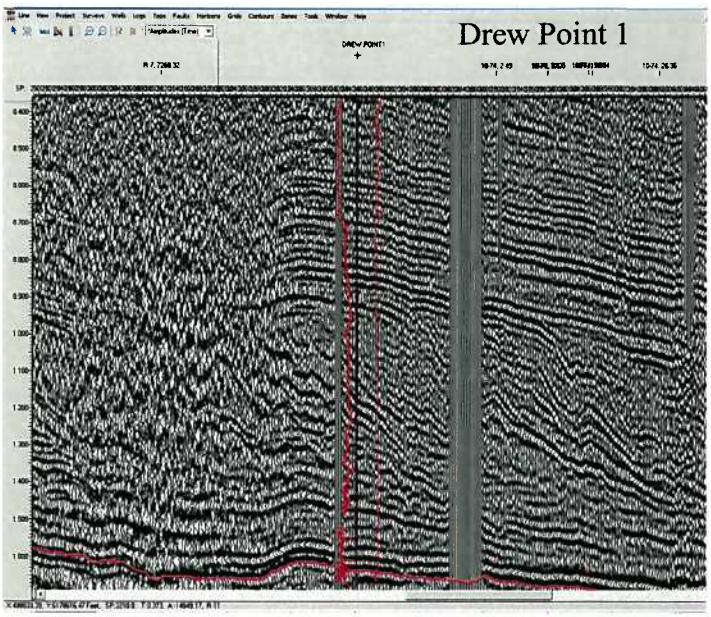


**Core # 1** – 4130 to 3131 ft and 4131 to 4140 ft (1.02 s) in Torok.
Estimated location: Upper foreset/rollover.
Depo environment: Shallow marine, quiet water.
Deposition from south.
Laminations: Planar lamination of sand in mostly silt.
Burrowing: Some in lower portion of core (~ 4131 ft) .
Slumping/Ripples: Small slumps – 1 event (~ 4137 ft).
Dominant lithology: Silty shale.
Sands: Upper bottomset/base of foreset.
Very fine grained laminations and pods.

**Core # 2** – 5537 to 5540 (1.29 s) in Torok.
Estimated location: Mid to lower low angle foreset.
Depo environment: Shallow marine, quiet water.
Deposition from south.
Laminations: more distinct lamination than DP1-1. More fissile.
Burrowing: None observed.
Slumping/Ripples: Possible x-bedding in bottom of core (~ 5539 ft).
Dominant lithology: Silt.
Sands: Very fine to fine grained in laminations.

**Core # 3** –5900 to 5902 ft and 5903 to 5917 ft (1.355 s) in Torok.

Estimated location: Lower foreset of low angle clinoform.
Depo environment: Shallow marine, quiet water. Deposition from south.
Laminations: Top of core is well laminated with many tightly packed laminations. Lower in core is mottled.
Burrowing: None observed due to slumping.
Slumping/Ripples: Bottom of core is slumped and contorted. Loss of lamination and structure.
Dominant lithology: Upper laminated portion is sandstone. Lower 12' shale with sand/siltstone laminae.
Sands: Upper portion has enough sand to be sandstone. Sand is mainly in laminations and slumped fill.

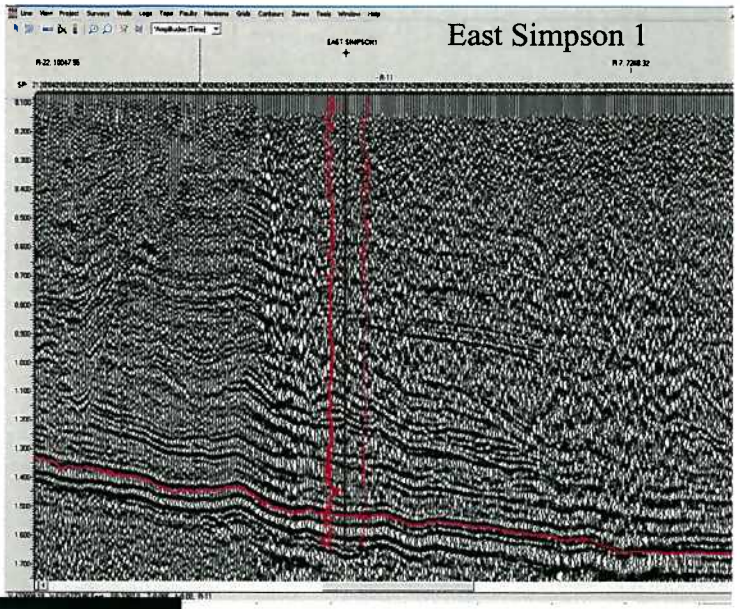


# East Simpson 1

**Core # 4** – 5120 to 5121 and 5121 to 5133 ft (1.215 s) in Torok.
Estimated location: Mid to lower foreset.
Laminations: Slight laminations . Fissile.
Burrowing: Burrowing evident .
Slumping/Ripples: Event near bottom of core brings in sand.
Dominant lithology: Dark grey shale.
Sands: Large sand laminations near bottom (~ 5132 ft).
Overbank deposits. Sands in Torok begin at 5586'.

# Ikpikpuk 1

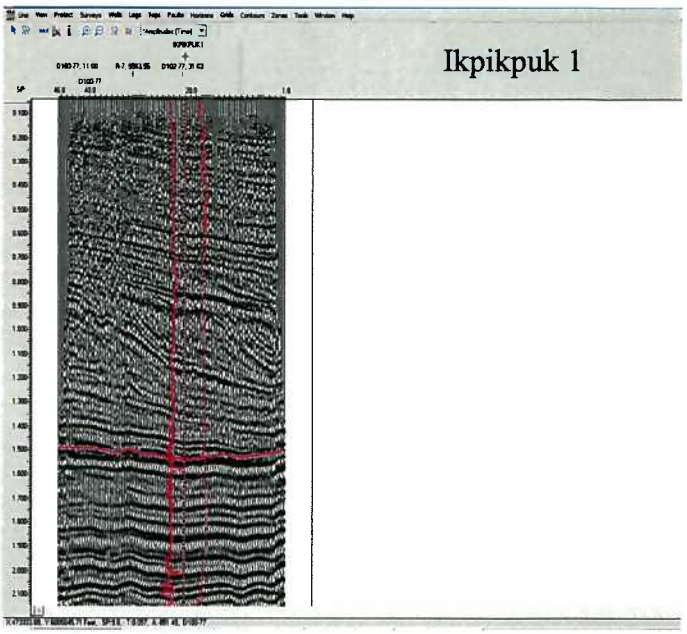


**Core # 2** – 3784 to 3795 ft 3795 to 3810 ft 3810 to 3812 ft (0.95s) in Torok.

Estimated location: Dipping topset.

Laminations: Moderate to few laminations.

Burrowing: Intense burrowing. Pockmarks or watermarks?

Slumping/Ripples: Small evidence of slumping in first column.

Dominant lithology: Shale, fissile with siltstone/sandstone laminations. Pyritic.

Sands: Small amount in thin stingers and small slumped areas.


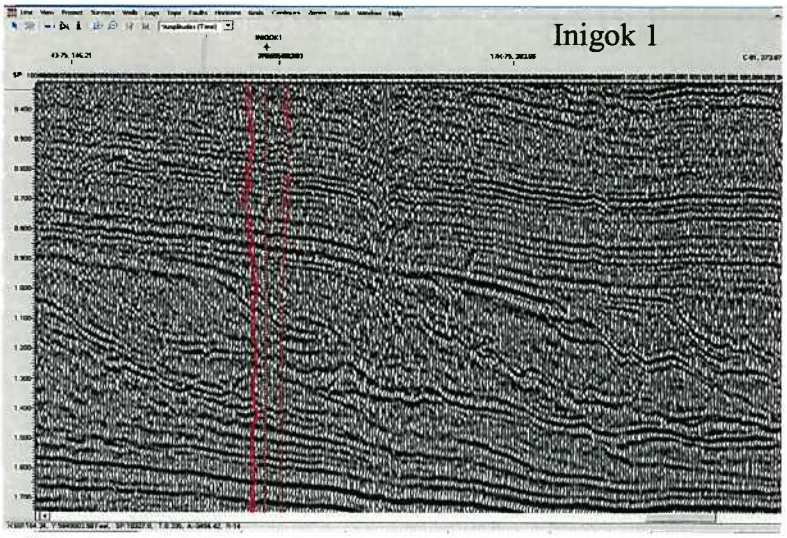


# Inigok 1

**Core # 3** – 4206 to 4216 ft (1.04 s) in Torok.

Estimated location: Upper foreset/rollover.
Laminations: Few sand stingers.
Burrowing: Intense burrowing, few laminations in tact.
Slumping/Ripples: None observed.
Dominant lithology: Shale, Medium grey. Fissile pyritic.
Sands: Very fine grained sandstone.
Thin stringers, calcareous.

# JW Dalton 1

**Core # 2** – 4667 to 4667.3 ft, 4667.3 to 4689 ft, 4689 to 4697.4 ft (1.13 s) Torok.
Estimated location: Progradational surface/rollover contact. Erosional.
Laminations: alternating thin lam of sand and clay.
Burrowing: In bottoms of core.
Slumping/Ripples: Multidirectional x-bedding in sands (3rd column).
Some slumping/burrow observed in bottom of core.
Dominant lithology: Lt brown. Interbedded sandstone. Mod fissility.
Sands: fine grained alternating with claystone.
NOTES: small prograding delta on clinoform edge

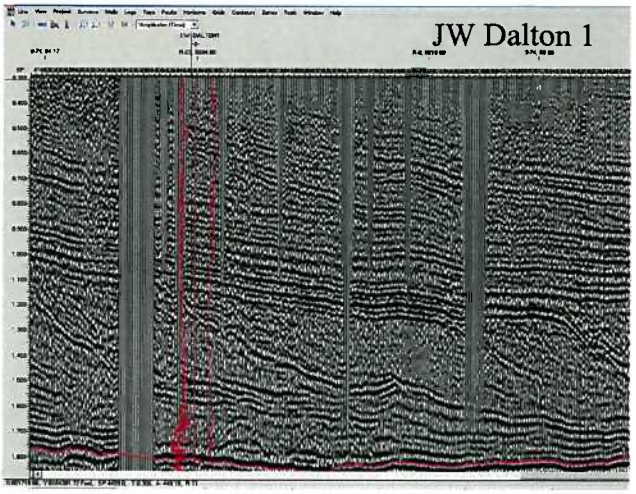


**Core # 3** – 5603 to 5612 ft, 5612 to 5621 ft, 5621 to 5630 ft (1.3s) in Torok
Estimated location: Upper to mid foreset.
Laminations: Less sand laminations
Burrowing: In last pic, some burrowing in core.
Slumping/Ripples: None observed
Dominant lithology: Darker and more fissile than 2. Shale with sand.
Pyritic, interlaminated soft and hard shale bands
Sands: Occasional thin stingers


# North Inigok 1

**Core # 1** – 4022 to 4025 ft, and 4025 to 4036.5 ft (1.0 s) Torok.
Estimated location: Mid foreset.
Laminations: Planar laminations get wider to bottom
Burrowing: None observed.
Slumping/Ripples: low angle dips in sands.
Dominant lithology: Dk grey Claystone,
Fissility increase to bottom.
Sands: Thin stinger interbedded.

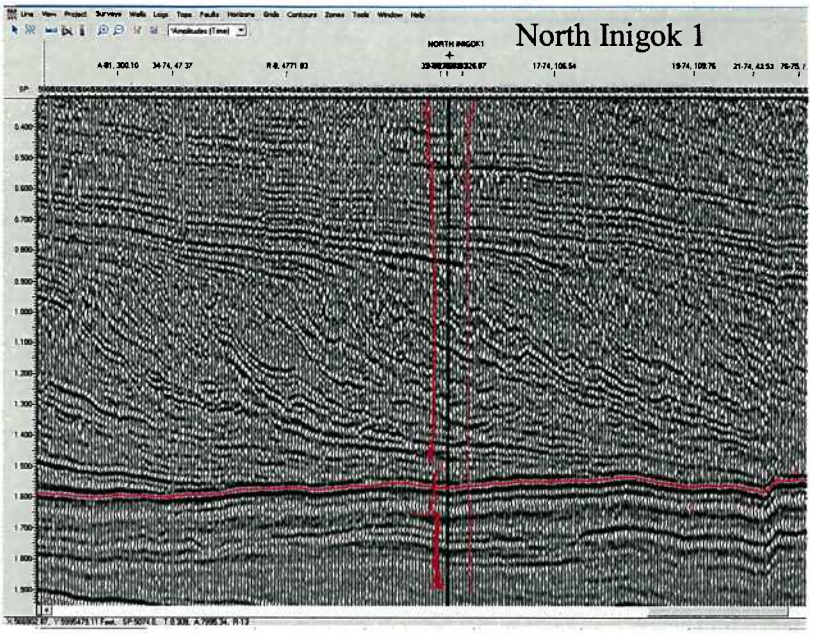



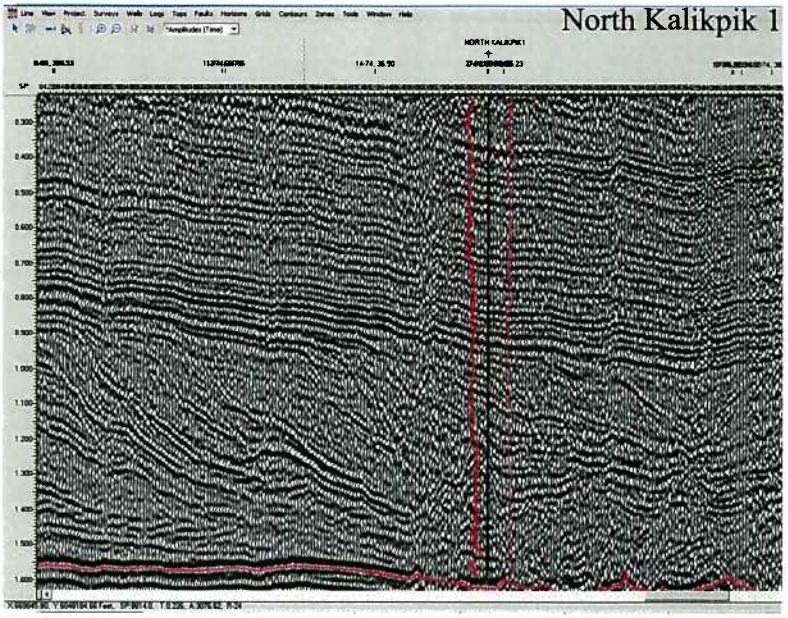


# North Kalikpik 1

**Core # 2** – 4994 to 5004 ft (1.19 s) in Torok.
Estimated location: Lower foreset to bottomset transition
Laminations: Some thin laminations in tact.
Burrowing: Some bioturbation.
Slumping/Ripples: Cross lam cut/fill and small ripple.
Dominant lithology: Very fissile. Dark shale pyritic.
Sands: Fine to v. fine, poor to mod sorted.
Subang to subround

**Core # 3** – 5871 to 5879 ft (1.35 s) in Torok.
Estimated location: Lower foreset to bottomset transition
Laminations: Well laminated, planar
Burrowing: Some.
Slumping/Ripples: Small slumping and ripples
Dominant lithology: Less fissile than above, more sand.
Sands: Common sand stingers. Fine to very fine.



Core observations from photos, Ziblman and Oliver (1999) and Ziblman et al. (2000)

# Appendix 2: Synthetic Seismograms

(taken directly from TKS SynPak help guide, SMT(2003)).

A synthetic seismogram is a simulated seismic response computed from well data, and is most frequently used to correlate geologic information from well logs with seismic data. Whereas seismic data mainly provides time values, synthetics provide time and depth values that are used to verify reflection events.

To generate a synthetic, you must provide a velocity curve and a wavelet. If a velocity or density log is not available, log conversions are available to derive the curves from sonic, resistivity, or density logs. In addition, density may be set to a constant value, such as 1. From this information, SynPAK automatically calculates the Acoustic Impedance (AI) and the Reflection Coefficient (RC) for each sample interval.

Acoustic impedance is the product of rock velocity and density for a given a layer of earth. It is a crucial parameter in modeling how a seismic signal propagates through different layers of earth. The reflection coefficient is a measure of acoustic impedance contrast at a formation bed boundary and is defined as (AI2 – AI1)/ (AI1+ AI2). The reflection coefficient series (RC at each boundary) is convolved with a wavelet, which approximates the seismic signal observed in the field.

The most important objective in generating a synthetic seismogram is to match the synthetic with nearby survey traces so that well log features can be tied to seismic features. With this connection, one can extrapolate lithology using seismic data. Synthetic matching may also be used to deduce the local phase of the wavelet.

The components of a synthetic are a Time-depth Chart, Velocity log, Density log, and Wavelet.

The Time-depth (T-D) Chart, as the name implies, provides the correspondence between depth and time; it is used to position log samples in the seismic section. Once positioned, the seismic expression of the log feature is estimated by computing the synthetic. A log feature may have no distinguishing seismic expression, or it may appear at a zero crossing, as a minor peak/trough, a major peak/trough, or on the shoulder of a peak/trough.

The velocity log records the speed of sound through rock as detected by a logging tool. Direct measurement of velocity is made by a "sonic log", which records travel times from a source point to a receiver on the same tool (typically two receivers, one above and one below the source). Velocity can also be estimated from a density log (Gardner's correlation) or a resistivity log (Faust's correlation). The density log (or a constant density) is combined with the velocity log to compute acoustic impedance as a function of depth.

Acoustic impedance is a rock property, the product of the velocity and the density log value at the same depth sample. A difference in acoustic impedance between two adjacent layers is the physical cause of a seismic echo. Each layer interface produces an echo when the seismic signal arrives. The strength of the echo is proportional to the numerical difference in impedances. The proportionality factor is called the "reflection coefficient." Velocity and density as recorded in well logs typically change from sample to sample, which means that acoustic impedance changes from sample to sample, which implies some degree of reflection from sample to sample. A "reflection coefficient" is computed for each time sample, and this sequence of coefficients is called a "reflection series."

Numerically, acoustic impedance is the product of velocity and density. If Vi is the interval velocity of layer i and ri is the average density of this layer, then the acoustic impedance of layer i is AIi = Viri. The reflection coefficient, or reflectivity, of a compressional wave directly striking the boundary between layers i and i + 1 is computed by the equation RCi = (AIi+1–AIi) / (AIi+1 + AIi).

# Appendix 3: Sample Time-Depth chart from Inigok well

| Depth (feet) | Two-way Time (seconds) |
|---|---|
| 0.00 | 0.00 |
| 346.87 | 0.10 |
| 720.08 | 0.20 |
| 1093.47 | 0.30 |
| 1471.27 | 0.40 |
| 1857.37 | 0.50 |
| 2255.31 | 0.60 |
| 2668.26 | 0.70 |
| 3099.04 | 0.80 |
| 3550.12 | 0.90 |
| 4023.64 | 1.00 |
| 4521.34 | 1.10 |
| 5044.64 | 1.20 |
| 5594.60 | 1.30 |
| 6171.92 | 1.40 |
| 6776.95 | 1.50 |
| 7409.69 | 1.60 |
| 8069.78 | 1.70 |
| 8756.52 | 1.80 |
| 9468.84 | 1.90 |
| 10205.33 | 2.00 |
| 10964.21 | 2.10 |
| 11743.36 | 2.20 |
| 12540.30 | 2.30 |
| 13352.21 | 2.40 |
| 14175.90 | 2.50 |
| 15007.84 | 2.60 |
| 15844.13 | 2.70 |
| 16680.53 | 2.80 |
| 17512.44 | 2.90 |
| 18334.92 | 3.00 |
| 19142.65 | 3.10 |
| 19929.99 | 3.20 |
| 20690.91 | 3.30 |